Studies of Modified Pumice and Titanomagnetite Filtration Media

A Thesis

Submitted in partial fulfilment of the requirements

for the Degree of

Doctor of Philosophy

in Materials and Processing Engineering

at the University of Waikato

by

Zailu Yang

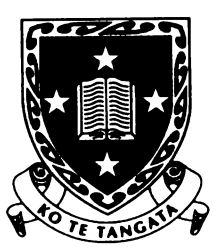

The University of Waikato

2001

Abstract

There is a continuing interest in filtration technologies capable of more efficient filtration, particularly of small microbial particles, but which place less reliance on the use of water treatment chemicals. In order to develop new options for granular filtration systems, two indigenous New Zealand media, titanomagnetite (TM) and pumice were investigated. TM was of interest because its particle size is finer than most filtration media and its magnetic properties allow the possibility of magnetic conditioning of the bed. A modified pumice, marketed as Silicon Sponge (SS), is already finding application in filtration systems where its low effective density and porous structure make it ideally suited for use as the upper layer of dual media filters.

Particle size and surface charge are key parameters influencing the effectiveness of a given filtration medium. Finer medium particle size improves filtration efficiency but at the expense of lower hydraulic conductivity. Magnetic conditioning of fine TM filtration beds was used to improve hydraulic conductivity. Hydraulic conductivity was increased by 140% when a vertically aligned magnetic field 0.018 T was applied. However filtration efficiency was decreased by about 9% in the conditioned (expanded) bed. Adjustment of pH to enhance electrostatic interactions more than compensated for this decrease.

The particulate matter of most waters requiring filtration is negatively charged. Surface treatment to make a filtration medium more electropositive is known to improve the medium's filtration effectiveness. The isoelectric point (IEP) of natural TM, even after rigorous chemical cleaning, was found to be 3.64 ± 0.06 This value was confirmed by the preparation of a synthetic TM and the measurement of its IEP. Attempts to raise the IEP of natural TM by treatment with aluminium and iron polycation solutions were unsuccessful.

Greater success was achieved in the modification of the properties of SS by treatment with aluminium and iron polycation solutions and mixtures of these solutions. IEPs ranging from the 4.10 ± 0.06 of acid rinsed SS to the 8.52 ± 0.06 of aluminium treated SS were achieved. In addition, it was found possible to

impart magnetic properties to fine SS by the use of treatment solutions containing a mixture of ferric and ferrous ions. The presence of aluminium in the treatment solutions allowed higher IEPs to be obtained but the magnetic effect was reduced. In the absence of aluminium, the ferric/ferrous mixture gave a product with a magnetic effect that was 7% of that observed for pure magnetite.

Filtration studies using 1.7 μm negatively charged kaolin as a model negative colloid showed that significant increases in filtration efficiency were achieved by medium pre-treatments with the aluminium and iron solutions. For example, turbidity removal for 710-1000 μm SS was increased from 22% to 94% by aluminium pre-treatment.

The information on the performance of magnetically conditioned beds and the ability to enhance filtration efficiency by surface modification using iron and aluminium has potential applications in the design of novel systems for water and wastewater treatment. A small-scale system based upon the use of a permanent magnet has been proposed and work in this area is continuing.

Acknowledgements

Firstly, I would like to give a special thanks to my chief supervisor, Associate Professor Alan Langdon, for introducing me to this exciting field of research, and for his great patience and encouragement throughout this research, for his effective directions and constructive suggestions during our discussions, and for his accurate correction throughout this report.

I would like to gratefully acknowledge to my second supervisor, Dr. De Liang Zhang, for his knowledge, support and advice throughout this thesis.

I would like to thank the laboratory staff, in the Chemistry and Materials and Processing Engineering Departments especially Jijian Lu, Yuanji Zhang and Annie Barker for their assistance.

I would also like to thank my friends and colleagues, especially Anna, Gune, Marion, Ratsamee, Rachna and Zhihong, for their support and feedback on my work.

Special thanks to my mother, Mrs. Yaqin Li, for her love, support and delicious foods; to my father, Professor Xinghua Yang, for his love, knowledge, advice and help during the long and challenging experimental programme.

No words can express my deepest gratitude to my husband He Yuan and my son Bo Yuan, for their love and support.

Contents

List of Figures

List of Tables

Abbreviations

AFF	Al(III)/Fe(III)/Fe(II) hydrous oxide precursor solutions
ARSS	Acid-rinsed Silicon Sponge
ARTM	Acid-rinsed titanomagnetite
$ARTM_{Al\text{-}n}$	Aluminium treated ARTM
$ARTM_{Fe\text{-}n}$	Iron treated ARTM
BET	Brunauer-Emmett-Teller
EDAX	Energy dispersive analysis of X-rays
HGMF	High gradient magnetic filtration
HM	Heavy metals
ICP	Inductively coupled plasma
IEP	Isoelectric point
JCPDS	International centre for diffraction data
KSS	Kaolin stock solution
MPS	Magnetite precursor solution
MSFB	Magnetically stabilised fluidised beds
NTU	Nephelometric Turbidity Unit
PCDM	Porous ceramic dual media
$S_{al\text{-}n}$	Aluminium multiple treated ARSS
$S_{Al\text{-}pH\text{-}n}$	Aluminium treated ARSS at various pHs
SEM	Scanning electron microscopy
S_{Fe}	Iron treated ARSS

$S_{mag\text{-}n}$	Magnetite treated ARSS at various concentrations
$S_{nAl(III)nFe(III)}$	Al(III)/Fe(III) in various mole ratios treated ARSS
$S_{nAl(III)nFe(III)(2)}$	Al(III)/Fe(III) in various mole ratios twice treated ARSS
$S_{nAl(III)nFe(III)nFe(II)}$	Al(III)/Fe(III)/Fe(II) in various mole ratios treated ARSS
SS	Silicon Sponge
TM	Titanomagnetite
UC	Uniformity coefficient
WRTM	Water-rinsed titanomagnetite
XRD	X-ray diffraction

Chapter One: Introduction

1.1 General introduction

Efficient filtration is an essential aspect of water treatment. Continuing concerns about microbiological quality of potable water maintains an interest in the development of improved media that are able to remove fine suspended impurities from natural and wastewater. Titanomagnetite (TM) and pumice are two volcanic minerals, indigenous to New Zealand that may be useful filtration media. TM is volcanic iron sand having fine particle size, high density and strong magnetic properties. These features may allow it to be used in magnetically conditioned filter beds. Pumice in contrast generally has coarse particles of low density, a porous structure and large surface area. Pumice has already found application in filtration technology (Moergeli and Ives, 1979; Matsumoto, *et al.,* 1984; Hill and Langdon, 1993; Langdon, *et al.,* 1995) and its usefulness may be increased by surface modification.

In mechanical filtration systems the most important medium characteristic in determining performance is medium particle size. When the suspended particle diameter is larger than the constriction through which the fluid flows, a straining mechanism occurs. The finer the medium particle sizes the narrower the passages and the more efficient the filter becomes. However the restricted flow through fine media causes high head loss and slow filtration rates. It may be possible to increase hydraulic conductivity of a fine bed, for example, TM, by magnetic conditioning. Magnetic conditioning may also be useful during backwashing of fine media.

Natural waters, domestic and industrial effluents are complex colloidal systems, which include microorganisms such as bacteria and viruses, natural organic matter (mainly humic substances) and clay-metal complexes. These suspended particles are generally negatively charged and are stabilised by electrostatic repulsion.

Removing such particles by unaided filtration may be difficult, since the suspended particles carry a negative surface charge at the pH of natural waters and most filter media (e.g. sand, diatomaceous earth and pumice) are also negatively charged in this pH range. Surface treatment of filter media to form coatings of metallic hydroxides and oxides can modify the surface charge making it more electropositive (Lo, *et al.,* 1997a; Ahammed and Chaudhuri, 1996). It has been suggested that adsorptive filtration using coated sand is a useful approach to water treatment (Benjamin and Leckie, 1981; Edwards and Benjamin, 1989a; Schultz, *et al.,* 1987).

The overall aim of the present investigation was to examine the usefulness of New Zealand TM and pumice in filtration applications. We wished to determine whether magnetic conditioning would allow the use of fine TM at useful filtration and backwash flow velocities. Control of surface charge to render the media positive, offered a means of removing negative colloidal particles without the use of flocculating agents. By the use of these media in natural and modified forms it may be possible to develop filtration systems that place less reliance on the use of chemicals in, for example, flocculation and clarification steps.

The thesis has eight chapters. It begins with an overview of filtration technologies and filtration media in Chapter One. Chapter Two describes the experimental methods used in the work. Chapter Three presents and discusses the characterisation of natural and synthetic TM as well as attempts to modify natural TM by surface coatings of hydrous oxides. Chapter Four describes the use of TM as a filtration medium in magnetically conditioned beds. The effect of filtration pH on the filtration efficiency is discussed. The effectiveness of magnetic conditioning on backwashing is also included. Chapters Five and Six deal with modification of pumice by surface coatings of aluminium and iron hydrous oxides. These render the media surface more electropositive (Chapter Five). In Chapter Six mixed Al(III), Fe(III) and Fe(II) systems were investigated in attempts prepare magnetic media with high isoelectric points. Chapter Seven presents and discusses the results of a study of filtration using modified pumice.

Finally, in Chapter eight a number of conclusions are drawn and recommendations are made for the future work.

1.2 Review

1.2.1 Particles and impurities in surface water

Impurities present in raw water sources can be of many types and origins, but broadly they can be classified as microorganisms (e.g. bacteria, viruses and protozoa), clay and silt, inorganic species (e.g. metal hydrous oxides) and organic substances (e.g. natural organic matter, synthetic organic chemicals and disinfection by-products). Pollutants from human activities include:

- Nutrients from fertilizers and sewage effluents i.e. nitrogen and phosphorus compounds.
- Carbonaceous impurities from sewage effluents, intensive livestock enterprises and food processing.
- Toxic chemicals from agricultural areas, mining sites and industry.
- Suspended matter and salinity from land clearing and over-irrigation.

Most of these impurities, including pathogenic organisms and natural organic matter, lie in the general colloid size range (1 nm-10 μm). Figure 1.1 shows a size spectrum of waterborne particles (Stumm, 1977). Bacteria and algae have sizes in the upper colloid range, whereas viruses are in the middle of the range. Colloids with diameters less than about 1 μm remain suspended in water because their sedimentation velocity is less than 10^{-4} m/s. These small particles, at the pH of natural water, are generally negatively charged (Hunter and Liss,1982; van der Mei, *et al.,* 1993).

- Viruses & bacteria

Bacteria range in size from about 0.2 μm to 2.0 μm or more in length or diameter, but most bacteria in natural habitats tend towards the smaller end of this scale (Michael, *et al.*, 1997).

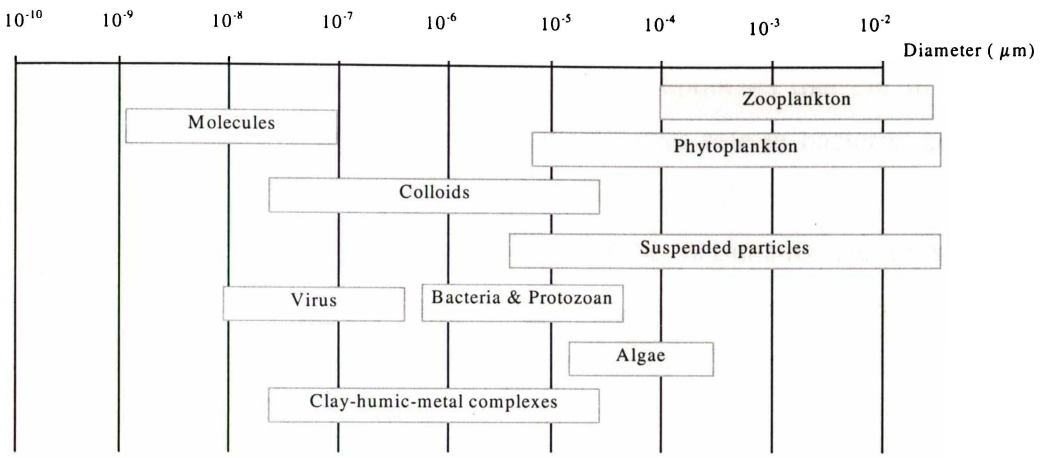

Figure 1.1 Particles and dissolved impurities in natural and wastewater

Generally, bacteria form stable colloidal suspensions in water despite the fact that the size of the cells exceeds the normal upper limit assigned to colloidal particles. This results partly from mutual electrostatic repulsion between the negatively charged bacteria and partly from the fact that the density of the bacterial cells is only slightly greater than that of water. The electrokinetic properties of bacteria may be determined by microelectrophoresis of cells suspended in buffers of different pH. Despite the presence of positively charged surface ionogenic groups on many bacteria, the net charge on bacterial cells at neutral pH values is strongly negative (Marshall, 1976). The surface ionogenic properties of bacteria result from the particular chemical constitution of the cell envelope (wall) of the bacterium in question as well as the properties of exopolysaccharides (EPS) produced by the organism.

Different bacteria exhibit varying degrees of cell surface hydrophobicity, and it is believed that this characteristic is important in determining the extent of adhesion of bacteria to solid surfaces (Rosenberg and Kjelleberg, 1986). The overall colloidal nature of bacterial cells provides some insights as to why they readily adhere to so-called inert surfaces.

Although most metabolic functions of bacteria are localised within the plasma membrane, it is the cell wall and extra-cellular components that are in contact with the external environment and, hence, play a vital role in bacterial adhesion and biofilm properties. Bacteria have the simplest of cellular structures (termed prokaryotic cells) yet the cell envelopes of these organisms are remarkably complex. Most bacterial cells possess a rigid cell wall that is responsible for the characteristic morphology of the cell and for its structural integrity under variable osmotic conditions.

- Protozoan parasites

Giardia and *Cryptosporidium* are protozoan parasites that can be found in contaminated water. If water treatment is inadequate, drinking water may contain sufficient numbers of these parasites to cause illness. Low levels of both parasites, especially *Giardia* can cause an intestinal illness called giardiasis or "beaver fever". *Cryptosporidium* is responsible for a similar illness called cryptosporidiosis. Research has shown that both *Giardia* and *Cryptosporidium* are highly resistant to chlorine, a commonly used water disinfectant (Smith, *et al.,* 1991). Membrane filtration or flocculation followed by granular filtration is currently the principal means of removing these organisms during the water. The development of filtration media capable of removing these organisms without the need for the flocculation step was one of the central ideas of the current work.

- Algae

Algae are large and diverse assemblages of eukaryotic organisms that contain chlorophyll and carry out oxygenic photosynthesis. While most algae are of microscopic size and hence are clearly microorganisms, a number of forms are

macroscopic, e.g. some seaweeds which grow to over 30 m in length (Michael, *et al.,* 1997). Algae abound in nature in aquatic habitats, both freshwater and marine. Algae are also found in moist soils and artificial aquatic habitats like fish tanks and swimming pools, and in temporary pools of water formed from rainwater runoff. Taste and odour usually arise from algae and decaying vegetable matter. Algae growth can be prevented by limiting the nutrients present in effluents discharged to sensitive receiving waters. This is difficult if sources are diffuse. Copper sulphate may be added to reservoirs to minimise algae production. Dissolved air flotation can be used to remove algae from drinking water.

- Inorganic colloids < 1 μm

Inorganic colloids have the potential to contaminate water with trace elements. Among the industries regulated for potential trace element pollution of water are the chlor-alkali, hydrofluoric acid, sodium dichromate (sulfate process and chloride ilmenite process), aluminium fluoride, chrome pigments, copper sulfate, nickel sulfate, sodium bisulfate, sodium hydrosulfate, sodium bisulfate, titanium dioxide, and hydrogen cyanide industries.

- Organic colloids & polymers

Sewage from domestic, commercial, food-processing, and industrial sources contains a wide variety of organic pollutants. Some of these pollutants, particularly oxygen-demanding substances, oil, grease, and solids, are removed by primary and secondary sewage-treatment processes. Others, such as salts, heavy metals, detergents, phosphates and refractory organics, are not efficiently removed (Manahan, 1994).

Studies have found that in addition to the microorganisms, other small particles in natural water at neutral pH are almost always negatively charged (Hunter and Liss, 1982; van der Mei, *et al.,* 1993). This result suggests that all particles be covered with a common coating. While silica, clays, feldspars would be expected to be negatively charged, particles of iron and aluminium oxides should be positively charged at natural pHs (Stumm and Morgan, 1996). Coatings of

hydrous oxides of iron, aluminium and perhaps manganese would not be consistent with the high negative charge observed. A more consistent explanation is that the particles are coated with humic substances whose hydrolysable acidic functional groups could easily give rise to negative charge (Neihof and Loeb, 1972; Hunter, 1980; Tipping, 1981; Loder and Liss, 1985).

1.2.2 Filtration technologies

The stages of the classical scheme of a full-scale physico-chemical purification process are shown in Figure 1.2. Flocculating agents are introduced to transform suspended impurities into settable solids. Some dissolved species may also be removed. Products of coagulation are removed by sedimentation or flotation, depending on the charge and hydrophobicity of suspended particles. Additional reagents (poly-electrolyte) are introduced to intensify these processes. Only parts of the dissolved contaminants are removed in this way. The remainder can be removed by ion exchange or adsorption. While most of the flocculated material can be removed by sedimentation or flotation, filtration is needed to remove residual particles.

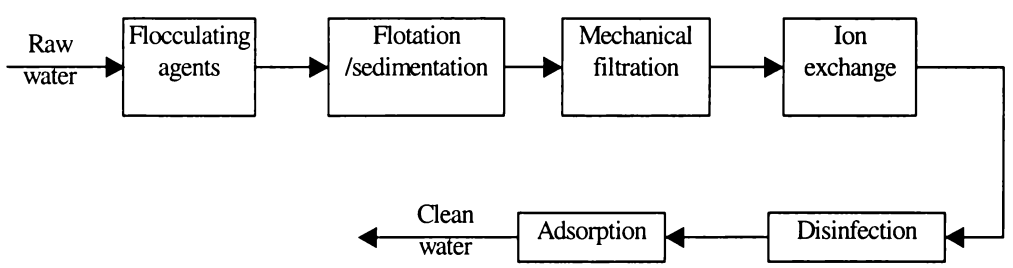

Figure 1.2 Typical scheme of full-scale physico-chemical water treatment

Ion exchange and adsorption stages utilise synthetic sorbents and ion exchange matrices to remove dissolved materials. Depending on the raw water quality and the required level of purification, some or these stages may be omitted. A problem associated with the use of chemical reagents in water treatment process is the possibility of formation of chemical residuals and by-products. Regeneration of ion-exchange resin by backwashing with brines results in secondary pollution due

to spent solutions. Activated carbons, which are known as the best sorbents of organic materials, are expensive and have a low efficiency for the removal of many polar or hydrated molecules (Smith, *et al.,* 1991). These factors have led to a continuing interest in the development of more efficient and more ecologically clean processes for water and wastewater treatment.

Water filtration is a physical process for separating suspended and colloidal impurities from water by passage through a porous medium. It is a very important unit operation in the treatment process and many technical papers have been written on the subject. A wide variety of filtration technologies have been developed to deal with a large number of industrial and municipal water treatment problems. Filters can be classified by filtration rate (slow, rapid and high rate), pressure (gravity, vacuum and pressure filters), direction of flow (down-flow, up-flow, bi-flow and cross-flow filters) and medium (granular and membrane filters).

Many different types of granular filters have been designed. They are all based on the fundamentals of sand bed filtration (Degner, 1990; Apelian, *et al.,* 1985). They differ in method of media placement, influent flow direction, method of operation and facilities for backwashing. The use of modified media has improved filtration efficiency. For example organically modified clay or organically filter media have a capacity for removal of oil that is seven times greater than conventional activated carbon (Alther and Biomin, 1999).

A porous ceramic dual media (PCDM) filtration system using porous ceramic nozzles (tiles) as a support and underdrain system and a modified pumice (Silicon Sponge) with high surface charge and large surface area upper layer has allowed filtration rates to be increased (Hill and Langdon, 1993). Yong (1997) reported that this filtration system allowed higher filtration rates, longer running time and slower headloss development than a conventional filter. Andrews (1993) reported that the use of the PCDM system in conjunction with micro-filtration was successful in the removal of *Cryptosporidium* and *Giardia* from a municipal drinking water. It is possible that advanced granular media will eliminate the need for membrane filtration.

Membrane filtration technology for water purification has been applied for a long time. Membrane filters are classified as surface or screen filters. Particles are retained on the surface of the filter or within a depth of 10-15 μm. It is this characteristic that distinguishes membrane filters from deep bed filters, which trap particles within the filter matrix. Membrane filters are capable of retaining microorganisms and particles by mechanisms other than a simple sieving action. Microbes and particles may be adsorbed by the filter, react with the membrane itself, or may be retained on the membrane by coagulation. Membrane filters can be used to filter large volumes of drinking water containing low concentrations of microorganisms (Onitsuka, 1996; Yagi, 1999; Kunikane, *et al.,* 1996). Membrane filters are widely applied for treatment of dye industry effluent (Crossley, 1998). In the semiconductor industry, membrane filters are used to prepare ultra-pure water (Ulieru, 1998).

Magnetic filtration is another kind of filtration technique used in water treatment and magnetic separation processes. Because of their magnetic and heat-resistant properties, magnetic filters are capable of operating in hostile environments with high temperatures and high pressures. Algae and heavy metals have been removed by high gradient magnetic filtration (HGMF). Yadidia, *et al.* (1977) reported that laboratory HGMF algae removals above 90% were obtained. Terashima, *et al.* (1986) reported removal of heavy metals, including mercury, from gas scrubbing wastewater from a municipal solid waste incineration plant. About 70% of heavy metals were removed (Terashima, *et al.,* 1986).

Another magnetic technique for water and wastewater treatment is the SIROFLOC process (Bolto, *et al.,* 1975). The SIROFLOC process relies on the ability of surface activated magnetite particles to destabilise and coagulate colloids and to adsorb impurities from the water. This process for water clarification possesses a number of advantages over conventional water treatment methods. It replaces the conventional water treatment by means of the classic coagulants [$FeCl_3$, $Al_2(SO)_4$], with a suspension of finely milled and sorted natural magnetite (size 5-10 μm) (Anderson, *et al.,* 1982b; 1983; Kolarik, 1983). A positive charge appears on the surface of magnetite in acidic media and as a

result, negatively charged particles of impurities contained in untreated water are attracted to the surface of the magnetite grains. In alkaline media the surface of magnetite is negatively charged and therefore the negatively charged impurities are repelled from the surface of the magnetite. In acidic media magnetite acts as an adsorbent of impurities, which desorb in alkaline media. In this way it is possible to regenerate and re-use the surface of magnetite indefinitely.

The formation of charges on the surface of magnetite can be described schematically as follows:

In acid medium: $= Fe - OH + H^+ \Leftrightarrow = Fe - OH_2^+$

In alkaline medium: $= Fe - OH + OH^- \Leftrightarrow = Fe - O^- + H_2O$

The SIROFLOC process offers greatly improved kinetics of clarification and sedimentation, which translates into capital cost savings and most importantly avoids problems of sludge disposal. The highly concentrated effluent produced by regenerating the magnetite, is of low volume and its disposal is much easier than that of the highly gelatinous sludge from conventional plants (Bolto, *et al.,* 1975; 1990; Anderson, *et al.,* 1980).

Other filtration techniques such as pressure filtration and capillary filtration have also found unique advantages in some applications. Pressure filtration has been successfully used in the treatment of cyanide-bearing tailing pulp and gold recovery (Chen, *et al.,* 1998). Recycling of filter liquor decreased the water consumption and investment in tailing pool facilities as well as providing better safety conditions. The use of capillary filtration with ceramic filters in mineral processing is an efficient liquid-solid separation method (Rantala, 1994). Other new filter systems such as membrane-stack cloth filters, magnetic filters, and bio-filters require careful studies to ensure technical feasibility under long-term conditions. The trend toward the use of less chemicals may lead to a return to slow sand filter applications (Boller, 1994). In the future, membrane filtration, particularly ultra-filters, will also have to be considered as an alternative to

conventional multistage schemes for the treatment of drinking water and industrial effluents.

1.2.3 Theory of filtration

Filtration with granular media has long been applied in treatment of municipal and industrial waters, as well as in wastewater treatment. This process has been widely employed, thoroughly investigated and greatly improved. A number of papers have rationalised the various theoretical concepts developed during last quarter of a century and have provided a better understanding of filtration technology (Maroudas, 1965; Mintz, 1960; Yao, 1971. Beckett, 1990). Development of a clear understanding of the filtration process is useful in the evaluation and control of the performance of existing facilities. It also helps the design engineer cope with increasing variation in raw water characteristics and to obtain maximum benefits from new filtration technologies and equipment.

There are a variety of parameters that affect the performance of filters. These include filtration rate, media, headloss, backwashing, temperature, particle size, hardness, pH and other influent characteristics. The relationships of these parameters to filter performance are extremely complex. To understand these complex factors, the retention force between media and particle and the filtration mechanisms are required.

Retention forces

When particles pass through the filer medium, retention forces will act on them. These forces can be classified into five broad categories: axial pressure of the fluid (the fluid pressure may hold a particle against the opening at a constriction), friction forces (a particle wedged in a crevice may have been slightly deformed when stopped and may remain in place by friction), surface forces (these include the van der Waals forces, which are always attractive), electrical forces (which are either attractive or repulsive according to the physicochemical conditions of the suspension) and chemical forces (in the case of colloidal particles) or in other cases, actual chemical bonding may occur.

Sites

Under retention forces, the particles may become immobilised at the sites. Figure 1.3 shows several types of retention site (Nunge, 1970). These include, surface sites (Figure 1.3 a), where a the particle is retained on the surface of a porous bed grain; crevice sites (Figure 1.3 b), where the particle becomes wedged between the two convex surfaces of two grains; constriction sites (Figure 1.3 c), where the particle is too large to penetrate into a pore (a diameter limit exists above which no particle can penetrate the constriction); cavern sites (Figure 1.3 d), where the particle is retained in a sheltered area or small pocket formed by several grains.

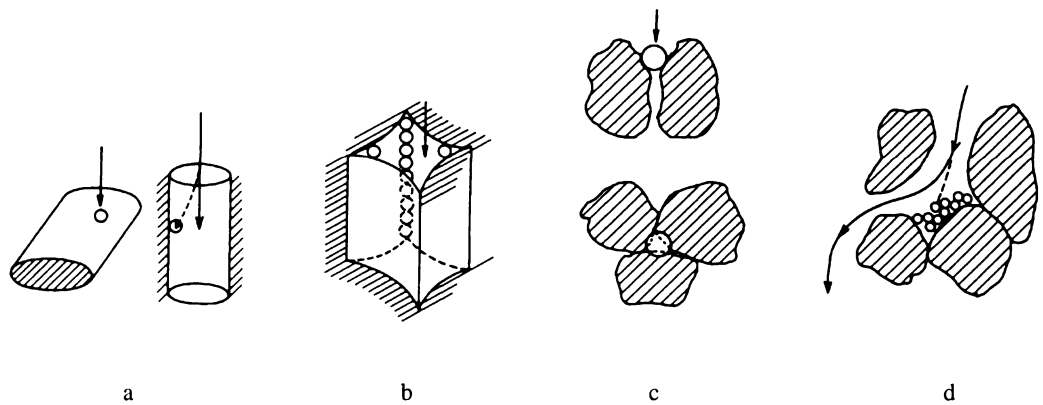

Figure 1.3 Retention sites. a) Surface sites. b) Crevice sites. c) Constriction sites. d) Cavern sites.

Transport steps

Transport steps are a combination of factors including: straining and interception, sedimentation, inertial impacting, hydrodynamic interaction and diffusion, which bring particles into contact with grain surfaces where they are immobilised. Generally these mechanisms are additive and depend on the particle size. (Mackie and Bai, 1993; Rushton, *et al.*, 1996).

Straining or interception. Straining is the simplest of the collection mechanisms and occurs when the particle diameter is larger than the constriction through which the fluids flow streamlines pass. The grain size plays an important role in this mechanism as narrower passages are found with smaller grained media.

Sedimentation. When the fluid flow is directed downwards through a filter, gravitational sedimentation effects will cause particles to settle vertically as the flow distorts around the grain.

Inertial impacting. The particles do not follow the same trajectories as the fluid. They deviate from the streamlines, when the direction of the trajectories changes suddenly. They can be brought into contact with the bed grains.

Hydrodynamic interaction. Because of the non-uniform shear field and the non-spherical shape of the particles, hydrodynamic effects may occur. These effects can cause a lateral migration of suspended particles bringing them into contact with retention sites.

Diffusion. Particle diffusion allows particles to reach sites, which are not normally irrigated by fluid flow. It is generally accepted that particle diffusion is only applicable for particles of diameter less than 1 μm (Rushton, *et al.,* 1996)

For any given filter bed, it is often difficult to assess which are the most important mechanisms. For large particles ($d >= 30$ μm), volume phenomena, i.e., friction and fluid pressures prevail over surface phenomena, and capture mechanisms may involve sedimentation and direct interception. Maroudas (1965) found the important parameter to be the ratio d/d_g (d particle diameter, d_g medium diameter). For $d/d_g > 0.15$, the medium is irreversibly blocked and a filter cake is formed. For $d/d_g < 0.0065$, the retention is always low. For intermediate values of d/d_g, a partial blocking of the porous bed may occur. This depends on particle shape and bed porosity.

For mean grain size of $3 < d < 30$ μm, it was found that volume phenomena and surface phenomena often were of the same order of magnitude. Generally retained particles are considered to occupy only surface sites but some investigators

suggest that the particles can be wedged between the grains in crevices or constrictions. Surface effects may be neglected when d >10 μm. van der Waals forces, in spite of their low range, are sufficient to explain the contacting of small particles with bed grains.

For particles of diameter of the order of 1 μm, surface phenomena prevail. The specific surface area of the bed is important. Particles occupy surface sites and are retained by van der Waals forces and electrostatic forces.

Colloidal particles (d < 0.1 μm) are retained solely by adsorption process e.g. van der Waals forces and electrostatic forces.

Yao (1971) found that the interception and sedimentation played the most significant part in the capture of relatively large particles (> 5 μm). The minimum particle size for efficient mechanical removal was about 1 μm. In contrast, for submicroscopic particles (< 1 μm), diffusion intervenes. Intermediate particles (1 to 5 μm) diffuse slowly and are also inefficiently removed by mechanical mechanisms.

In water and wastewater treatment, many suspended particles are 1 μm or smaller (viruses, bacteria, a large portion of the clays, and a significant fraction of the organic colloids). Removing such particles by filtration is difficult, since they carry a negative surface charge at the pH value of natural waters and most filter media (e.g. sand, diatomaceous earth and pumice) are also negatively charged in this pH value range. Furthermore, the pores formed in granular filtration beds are generally much larger than 1 μm. A key to improving removal of these colloid impurities from water is to make the media surface more electropositive in the natural water pH range. This will enhance electrostatic interactions.

When a solid particle is immersed in a polar solvent such as water, it usually acquires a surface charge by adsorbing or desorbing ions according to some chemical equilibrium. For example, hydrous oxide surfaces have surface groups that undergo proton association–dissociation reactions of the type:

$$-M-OH_2^+ \xleftarrow{H^+} -M-OH \xrightarrow{OH^-} -M-O^- + H_2O$$

where –M represents the metal atom. Thus, the surface is positively charged at low pH and becomes negatively charged at high pH (Figure 1.4). At the IEP the total charge on the surface is zero and the electrical repulsion between two such surfaces is diminished.

Commonly used filter media, which have low isoelectric points (IEPs) (e.g. sand and diatomaceous earth) are effective against positively charged flocs but are less effective against unflocculated negative turbidity particles. For the negatively charged particles of unflocculated water, filtration relies on mechanical mechanisms such as straining, interception and sedimentation for particle removal. Modification of the media surface chemistry to increase IEP should improve filtration efficiency.

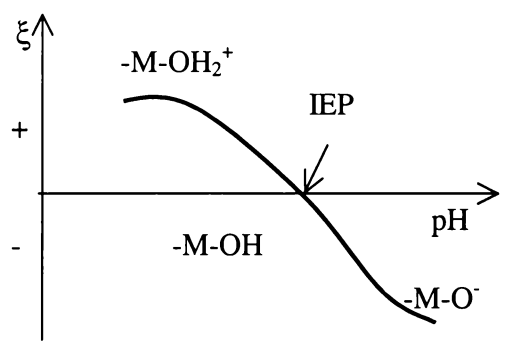

Figure 1.4 Typical variation of surface potential, ξ, with pH for a metal oxide surface. Surface charge has the same sign as surface potential. At the IEP, the surface has no net charge.

1.2.4 Filtration media

Over last fifty years, there have been many studies of the performance of the various media. Examples include granular media, weave media, filter cloth, filter paper, wire mesh, cotton, wool, linen, glass fibre and rayon. The optimum type often depends on the properties of the suspension and specific process conditions.

The filtration medium is the most important part of a filter and the successful performance of a filter is largely dependent on the use of a suitable filtration medium (Rushton, *et al.,* 1996). It takes on the main functions of the filter. The principal role of the filtration medium is to separate particulate solids from a flowing fluid with minimum consumption of energy.

A good filtration medium should:

- be able to remove a wide size distribution of solid particles from the suspension.
- offer minimum hydraulic resistance to the filtrate flow.
- allow easy discharge of cake.
- be resistant to chemical attack.
- not undergo swelling when in contact with filtrate and washing liquid.
- be heat-resistant within the temperature ranges of filtration.
- have sufficient strength to withstand filtering pressure and mechanical wear.
- be capable of avoiding wedging of particles into its pores.

In recent decades there have been numerous developments in the field of water processing involving low cost, natural, granular materials. The behaviour of granular filtration medium is complex. The factors that affect the performance of the filter medium include composition, particle size, uniformity coefficient, shape, porosity, specific gravity and bed depth. The most important medium characteristics that determine performance are medium composition, medium surface properties, medium size and medium depth. Examples of novel media include minerals such as zeolites, clay minerals, micas, pumice, TM and iron and

manganese oxides, hydroxides and oxyhydroxides present in various geological environments and soil formations. Properties such as crystal structures characterised by intracrystal micropores (channels or interlayer void spaces) providing high microporosity/surface area and other physico-chemical properties such as catalytic activity and sorptive/ion-exchange capacity, contribute to the usefulness of these materials as filtration media (Misaelides, 1999).

The possibility of applying mineral media to remove organic substances, heavy metals (HM) and inorganic ions from wastewater has been extensively investigated (Spevakova, 1994). Many natural minerals display ion exchange properties due to their composition and crystallographic structure. Their utilisation for removing HM is a promising alternative to the use of very expensive ion-exchange resins and chemical treatment technologies (Zorpas, *et al.,* 1999; Ouki and Kavannagh, 1999). They produce no toxic by-products in the treated water, the sludge is easily dewatered and the metals can be regenerated and reused. Natural minerals can be used to enhance the traditional purification processes of coagulation, sedimentation, flotation and filtration. Application in drinking water treatment is favoured due to their non-toxicity and ability to remove microorganisms. For similar reasons they are widely used in the food industry and medicine. Some minerals, such as TM sand and pumice exist in vast quantities. TM possesses high density, fine particle size and strong magnetic properties; pumice has a highly porous structure and a large surface area.

Below are some examples of the use of natural minerals in water treatment.

- Silica sand is the cheapest and most commonly used medium for mechanical filtration of solutions containing suspended solids. Determining characteristics are the grain shape and size, mechanical strength and chemical inertness. There have been many studies of the evolution and effectiveness of silica sand filtration (Trussell and Chang, 1999; Marin, *et al.,* 1992). Silica sand also shows very good results for the removal of certain ions (Dudeney, *et al.,* 1999; Brodsky, *et al.,* 1978). Coating silica sand with various metal oxides and hydroxides has

improved filtration efficiency. Sansalone (1999) reported good results for the treatment of urban acid rainfall. Janda and Rudovsky (1994) investigated silica sand covered with manganese for the removal of ammonia from drinking water. The efficiency of ammonia removal was large than 90%.

- Garnet and magnetite have densities approximately twice that of silica sand are often used as a fine layer at the bottom of a filter. A fine dense madium at the base of a filter acts as a polishing step removing fine suspended particles in triple media filters. Watson (1989) compared four types of filter media for water purification and found that the anthracite/sand/garnet filter provides excellent removal of algae, particulate organic C, Fe and turbidity. Multimedia filtration generally produces a higher quality drinking water (Brown, *et al.,* 1996; Barnett, *et al.,* 1990; Xia, 1989).

- Precoated diatomite or perlite filters are effective for removal suspended particles < 1 μm. Perlite is a water-containing glassy volcanic rock. On rapid heating, internal water transforms rapidly into steam, which expands and modifies the material's structure. Ostreicher (1977) investigated the efficiency of the negatively charged, high surface area filter media diatomaceous earth and perlite, for removal of suspended solids < 0.7 μm from water. They found that the media when modified with a melamine-formaldehyde cationic colloid, had higher efficiencies than untreated materials. Expanded perlite is characterised by a fine network of spheroidal fractures and its filtration characteristics are very similar to those of diatomite. Due to their extremely low densities, the materials are used for intensification of flotation processes, and as a replacement for flocculants and surfactants (Martin, *et al.,* 1993). The porous and intricate structures of diatomite and expanded perlite have been used to make a composite filtration medium (Palm, *et al.,* 1997). The composite medium offered unique properties such as increased permeability, low speed

centrifugal wet dewatering, low cristobalite content, and uniquely shaped particles.

- Zeolites such as clinoptilolite and mordenite are abundant minerals. They have a skeleton structure that allows ions and molecules to reside and move within the overall framework. The structure contains open channels that allow water and ions to travel into and out of the crystal structure. The size of these channels controls the size of the molecules or ions and therefore a zeolite like mordenite can act as a molecular sieve, allowing some ions to pass through while excluding others. Due to these distinct properties they are widely used in water and sewage purification, ammonia and HM removal, ion exchange in radioactive wastewater treatment, removal of oil pollution from water and adsorption of other components from liquid and gaseous phases (Colella, 1999; Piaskowski and Anielak, 2000). The effectiveness of certain zeolites for extracting HM, Pb, Zn, Cu, Cd, Fe Mn, Ni, Cr from water has been demonstrated as meeting required quality standards (Zorpas, *et al.,* 1999; Ouki and Kavannagh, 1999); Clinoptilolite has been used to remove cesium and strontium from radioactive wastes produced in reprocessing nuclear fuels (Sikalidis, *et al.,* 1989); and to remove ammonia and coliforms from sewage streams (Abdullaev, *et al.,* 1981; Reyes, *et al.,* 1997). Reyes found that turbidity removal was similar to that of sand. A filter packed with zeolite had lower pressure losses and better hydraulic behaviour. A maximum ammonia N removal of 95% was obtained and the total coliform removal was approximately 100% when using particle sizes of 0.35-1 mm. The mineral is also used as a filler and bulking agent in the manufacture of paper.

- Clay minerals. Chemically, almost all clays are hydrous silicates (principally of Al or Mg), which on heating lose adsorbed and constitutional water. Their structures are with a few minor exceptions, based on composite layers. Most occur as plate particles in fine-grained aggregates, which when mixed with water yield materials with varying degrees of plasticity. The particles of clay minerals may vary from colloid

dimensions to above 1 μm, which can be seen in an ordinary microscope. They are used in water purification processes mainly as an additive during coagulation and flocculation. Many clay minerals show marked ion exchange and sorption properties. Kaolinite and hydromica show lower cation exchange, but their anion exchange is higher and may be attributed to the presence of replaceable OH^- ions on the outside of the structural sheets. Kaolinite and alumina (Al_2O_3), are used as additives to intensify the coagulation process and to allow better dewatering of sludge. The ability of kaolinite to fix phosphate ions, which cause eutrophication, is also of importance (Iwamoto, *et al.,* 1977).

- Montmorillonite is the main representative of bentonites, which are mixtures of more than one clay mineral. Bentonites are known as "swelling" clay minerals in that they can take up water or organic liquids between their structural layers. Cation exchange involves inter-layer exchange cations, usually Na^+ or Ca^{2+} and Mg^{2+}. Montmorillonite was found to be effective in removing cationic dyes, such are highly oxidised organic substances for which abatement by all other techniques had failed (Sethuraman and Raymahashay, 1975; Subbotina, *et al.,* 1985). Introduction of bentonite clay together with coagulant and flocculant intensifies coagulation by up to six times, enhances microorganism removal by up to 99.9%, gives better colour reduction and higher extraction of HM (Zn, Cu, Cd, Cr, Hg) (Iwamoto, *et al.,* 1977) and ammonium ions (Polyakov, *et al.,* 1977). The ability of bentonites to remove microorganisms is of importance as it involves a low cost and simple technology. Fine clay particles form aggregates with microorganisms, which causes destabilization of microorganism dispersions. Similarly, theoretical and experimental studies indicate that dispersed sheet silicates, due to their exchange and sorption properties are more effective sorbents of nonionic surfactants and water-soluble polymers than activated carbon.

- Vermiculite possesses the highest cation exchange capacity and surface charge among clay minerals. The crystallographic structure of vermiculite includes inter-layer water molecules. When vermiculite is heated rapidly, steam generated escapes separating the layers by a phenomenon called exfoliation. Vermiculite generally has a larger grain size and when exfoliated it provides a low-density material (similar to perlite) for use in filter beds, flotation processes and water surface cleaning (Martins and Fernandes, 1992). Vermiculite has found increasing application in the field of pollution abatement. It is being used for the removal of *Cs-137* from radioactive wastewater (Sikalidis, *et al.,* 1989); recovery of HM (Pb, Cu, Zn, Cd) and ammonium ions from rinse water of a plating plant (Hiromi, *et al.,* 1984). Vermiculite also shows the property of absorbing organic liquids between its layers.

- Magnetite has a high density and magnetic properties. It may be used in the bottom layers of a multimedia filters and can also be used in magnetic seeding processes. One application is the SIROFLOC process (Dixon, 1991; Anderson, *et al.,* 1980). The SIROFLOC process is a technique for potable and technological water conditioning (colour, turbidity removal). Magnetite particles of size 1-10 μm are employed at pH 5-6. A 1% slurry in the raw water at this pH will remove about half the turbidity and colour through electrostatic interaction involving the positive surface charge of the magnetite (Anderson, *et al.,* 1980; Kolarik, 1983). Other potential applications are removal HM, phosphates, nitrates, dyes and organic compounds from industrial sewage and in the remediation of contaminated ground water. Also, valuable components from process solutions and slurries of pharmaceutical and food processing industries can be selectively adsorbed and separated. (Gusev, *et al.,* 1991; Bryan, *et al.,* 1990; Drakhlin, *et al.,* 1983; De Latour, 1975; Yadidia, *et al.,* 1977).

- Ignimbrite and pumice are light, relatively soft, porous rocks formed by the compaction and cementation of volcanic ash or dust (Beresford, 1997). They cover vast areas in New Zealand, Guatemala, Peru and Yellowstone

National Park in the United States. Natural pumice, which has essentially the same composition as ignimbrite, is formed by explosive release of gas from molten volcanic glass during eruptions. It possesses a porous structure and relatively large surface area. It has proven to be a useful media in filtration applications allowing more vigorous backwashing (Moergeli and Ives, 1979; Matsumoto, *et al.,* 1984). The large proportion of free silica sites at the grain surfaces leads to a reaction with water to form hydroxyl groups, resulting in a negatively charged surface (Hill and Langdon, 1993). Positively charged flocs from secondary treatment processes are therefore readily removed. A thermally modified pumice (marketed as Silicon Sponge (SS) by Works Filter Systems, Hamilton, New Zealand), allowed greater filtration rates, longer running times and slower headloss build-up compared with conventional filter sand (Yong, 1997). In order to extend the usefulness of pumice, some studies have modified its surface properties with coatings of iron oxide and manganese dioxide (Sharma, *et al.,* 1999; Sims, 1993). It was found that the capacity for adsorption Fe^{2+} from ground water was much higher than untreated pumice.

- Titanomagnetite (TM). Natural TM is derived from erosion of andesite and rhyolite volcanoes and is concentrated by longshore currents and wave and wind action (Draham, 1980). New Zealand TM, being magnetic, shares some of the characteristics of the magnetite used in the SIROFLOC process. Its magnetic properties and high density may allow it to find application as a filtration medium. The IEP of TM has not been reported. Because of it magnetite content, it is possible that the value will be higher than conventional filtration media. A novel application of TM has been the development of a porous ceramic material (Silicon Suppliers, 1994). This material has found application in porous ceramic filtration nozzles (Hill and Langdon, 1991). To date however, TM has not been exploited in the treatment of waters.

1.2.5 Surface coatings

Natural sand has long been used as a filter medium in water treatment. However, to be effective for the removal of contaminants such as bacteria and viruses, rapid filtration needs to be preceded by pre-treatment such as coagulation. Coagulants such as aluminium or iron salts form polycations, which cause negative particles to stick together. Pre-polymerised Al(III)/Fe(III) coagulants are currently used extensively in Japan, many European Community countries, the USA and China for drinking water and wastewater treatment. It is claimed that pre-polymerised coagulants have the following advantages over conventional metal salt coagulants (Leprince, *et al.,* 1984; Tenny and Derka, 1992):

- Better overall purification efficiency.
- Better floc-separation.
- Wider working pH range
- Less sensitivity to low temperature
- Low residual Al or Fe concentrations in the treated water.

According to Stummn and O'Melia (1968), the main function of Al(III)/Fe(III) chemicals used to treat water is to form a series of Fe(III) or Al(III) hydrolysis products with cationic potentials which can be strongly adsorbed on to negatively charged particles, reducing their charge and consequently reducing the double layer electrical repulsion energy.

Precipitates of metal hydroxides are known to be good adsorbents for bacteria and viruses, and have been used in the concentration of viruses by many workers (Walter, *et al.,* 1985; Vilangines, *et al.,* 1982). Some attempts have been made to improve filtration media by coating with hydroxides of iron, aluminium and magnesium (Merkle, *et al.,* 1994, 1996).

Iron oxide coated media

Iron oxide, which commonly presents as amorphous ferrihydrite, has proven to be an excellent, regenerable adsorbent for removing metals from solution over a wide pH range (Edwards and Benjamin, 1989a; Stenkamp and Benjamin, 1992) and from low concentrations (Bailey, *et al.,* 1992). A process of coating iron oxide onto the surface of sand was developed to allow the medium to be used in a packed column reducing the cost of sludge disposal (Edwards and Benjamin, 1989b). Numerous studies of iron oxide coated sand have been carried out for the removal of natural organic matter (NOM) (Chang, *et al.,* 1997), Cr(VI) (Bailey, *et al.,* 1992; Liu and Huang, 1998), arsenic (Joshi and Chaudhuri, 1996), Se(IV) and Se(VI) (Lo and Chen, 1997b), zinc (Stahl and James, 1991a), copper and lead (Lai, *et al.,* 1994, 2000), cadmium, chromium (Satpathy and Chaudhuri, 1995) and other heavy metals (Benjamin, *et al.,* 1996 and Lo, *et al.,* 1997a). It was reported that pH during the coating process played a very important role in iron oxide formation and subsequent heavy metal removal. The species of iron oxide prepared at higher pH tended to be goethite, which had better adsorption efficiencies, but had poorer acid resistance. Coated sand produced at higher temperature had enhanced metal adsorption efficiency and greater stability (Lo, *et al.,* 1997a).

Aluminium coated media.

A number of aluminium hydroxides, oxyhydroxides, and oxides are found in nature and can be prepared in the laboratory. This group of materials generally has high zeta potential and high isoelectric point compared with other materials (Parks, 1965). This particular feature renders them more positively charged in water and able to adsorb negatively charged particles. The primary function of the coating of $Al(OH)_3$ on filter media is to make the surface of the filter media more electropositive, thus facilitating colloidal attachment. Gao, *et al.* (1999) studied the removal of effluent turbidity, total organic carbon (TOC), chemical oxygen demand (COD) and manganese by sand and Al coated sand. They found the absorbance at 254 nm of effluent treated by Al coated medium was much lower

than that of water treated by untreated sand. Chen, *et al.* (1998) used aluminium hydroxide coated sand for removal of bacteria from wastewater. They found that over a 4-month period following an initial conditioning effect giving, an increase in bacterial removal capacity, bacterial removal capacity gradually decreased to that of uncoated sand. Biogrowth on the sand accelerated this decline. The aluminium content of coated sands decreased by approximately 25% over the first two weeks and then remained relatively constant and well above that of uncoated sand. Similarly, the zeta potential at the pH of the wastewater decreased over the first two weeks form above + 20 to – 70 mV, which was still significantly more electropositive than that of uncoated sand. Zeta potential of coated sand without biogrowth subsequently remained approximately constant, while that of coated sand with biogrowth increased gradually. This result suggests that in the absence of biogrowth, the effective lifetime of the aluminium hydroxide coated sand is approximately 4 months, whereas with biogrowth, the effective lifetime is reduced to approximately 3 months. This information is of importance for assessing the technological potential as well as economic implications of aluminium hydroxide coating of filter media.

Manganese dioxide coated media.

Manganese dioxide in the mineral form pyrolusite, has been used in water treatment for bacterial removal and sorption of iron. Hydrous manganese dioxide is a synthetic material and a well-known ion exchanger. It has been studied extensively as a material for the removal of toxic impurities, such as actinides, mercury and arsenic from wastewater. The removal of pollutants from water by MnO_2 can be carried out by two distinct mechanisms. These are ion exchange and redox chemistry. The latter mechanism is used for the removal of arsenic from water. However, most of the applications of this hydrous oxide rely on ion exchange. Inorganic ion exchangers, such as manganese dioxide, act predominantly as anionic exchangers at low pH and cationic exchangers at higher pH. In acidic conditions the hydrated proton reacts with the MnO_2 surface to give an anionic exchange site.

$$MnO_2 + H^+_{(aq)} \rightarrow MnO_2H^+$$

In alkaline conditions the hydroxyl ion reacts with the MnO_2 to produce a surface for removing cationic species.

$$MnO_2 + OH^-_{(aq)} \rightarrow MnO_2(OH)^-$$

The pH for the change from anionic to cationic behaviour can be obtained from zeta potential measurements. The cationic capacity of the dioxide increases and the anionic capacity decrease with increases in solution pH (White and Asfar-Siddique, 1997).

Knocke and Hamon (1988), Knocke, *et al. (*1991) studied the removal of soluble manganese by both artificial manganese oxide coated sand and the uncoated sand from a filter, which had been used for manganese treatment. Stahl and James, (1991b) used wet oxidation and dry oxidation procedures to coat MnO_2 onto filter sand for the removal of zinc. White and Asfar-Siddique (1997) carried out a study of manganese and iron removal using hydrous manganese dioxide prepared in two ways. In the first method MnO_2 was produced by the reaction of hydrogen peroxide on potassium permanganate as shown below:

$$2MnO_4^-{}_{(aq)} + H_2O_2 \rightarrow 2MnO_2 + 2OH^-_{(aq)} + 2O_2$$

In the second method, $MnO_2$was prepared by reaction of manganese sulphate with potassium permanganate as shown below:

$$3Mn^{2+}_{(aq)} + 2MnO^-{}_{4(aq)} + 2H_2O \rightarrow 5MnO_2 + 4H^+_{(aq)}$$

The manganese dioxide produced by the first method was found to be an excellent material for the removal of iron and manganese from water. Results obtained from this work have demonstrated that the manganese oxide coated media have high adsorption capacity for manganese at pHs above the zero zeta potential pH of 4.4 (White and Asfar-Siddique, 1997).

1.2.6 Magnetic conditioning

In separation technology, magnetic stabilisation has been applied to gas-liquid, solid-liquid and gas-liquid-solid systems (Boehm and Voss, 1999; Clement and Jovanovic, 1997). Magnetically stabilised fluidised bed (MSFB) technology is a promising example of a magnetically assisted process, which permits design of more favourable operating conditions lying outside the normal range. The magnetic properties of the particles provide a new adjustable parameter for managing the process (Moffat, *et al.,* 1994). A number of studies have found that magnetic field intensity, media properties and fluid properties have strong effects on hydrodynamic characteristics of a MSFB (Ganzha and Saxena, 2000; Bohm, *et al.,* 1999). In particular a magnetic field can impart a degree of structural organization in an expanded bed, so that on subsequent packing the media is not randomly packed, but somewhat ordered. This 'conditioning' of the bed is expected to alter its hydraulic conductivity. The use of magnetically stabilised expanded beds for water filtration has not been extensively studied.

1.2.7 Backwash technology

After a period of filtration, the filter bed becomes loaded and clogged since large amounts of suspended particles are retained in the filter medium. When the development of filter headloss is such that the filter can no longer produce water at the desired rate, or the effluent quality deteriorates due to terminal breakthrough, the filter must be cleaned by backwashing. Adequate backwashing is an important stage for all types of filters. Incomplete backwashing will cause a filter to deteriorate quickly, resulting in short filter runs and poor quality effluent. It also causes the formation of mud balls, in which the compacted particles accumulate and grow by adhering to each other and to medium grains at the surface of the bed. The mud balls grow increasingly compact and eventually reach a density great enough to cause them to sink into the sand or to the bottom during the backwashing period. They badly affect filter performance (AWWA, 1971).

Backwashing with water alone at a flow rate great enough to fluidise the media bed is known to be an inherently inefficient cleaning process due to the limited number of collisions between the media grains, therefore, auxiliary wash methods have been employed (Page and Amirtharajah, 1995).

Firstly, surface scour as an auxiliary wash method was developed. There are two kinds of surface scour systems: fixed systems and rotary systems. Usually, they are operated before the up-flow backwashing (AWWA, 1971) in order to prevent the formation of filter mud balls and improve the cleaning of the top-most medium layer. An extra sprinkler is required. Surface wash by jets of water adds from 75 to 275 mm/min of water to the backwash (about 400 mm/min). A expansion of about 10% is induced before the jets are directed into the sand (Fair and Geyer, 1965).

Secondly, air scour as an auxiliary wash method, has been commonly employed in filter backwashing. The use of air scour under a condition known as collapse-pulsing has been proven to be the most effective method of filter cleaning. Air scour provides the agitation necessary to promote intergranular collisions and abrasions lacking in a fluidised water wash. Air scour has been applied in several modes: (1) air scour alone followed by subfluidized water backwash; (2) air scour alone followed by water backwash sufficient to fluidize the media bed; and (3) air scour simultaneously applied with subfluidized water backwash. Several studies have concluded that the air scour simultaneously applied with subfluidized water backwash provides optimum cleaning (Page and Amirtharajah, 1995). Air scour generally proceeds at a rate of 0.75 to 1.25 $m^3/m^2/min$. of filter for several minutes. An extra air supply system is required for the backwashing with air scour.

Thirdly, mechanical raking as an auxiliary wash method also improves backwash performance. The rakes used for mechanical agitation of the media should penetrate the active or expanded media layers. They generally reach to within 50 to 75 mm of the gravel. The raking arms revolve at a rate of 8 to 9 rpm. The teeth are often wedge shaped and are spaced at 150 mm center to centre. Upward flow

is held to between 5 and 7.5 mm/s (Fair and Geyer, 1965). An extra motor and rakes are required.

1.3 Specific research objectives

The central aim of the research reported in this thesis was to determine whether granular filtration media, in natural or modified forms, could be used to allow efficient water filtration with less reliance on the use of chemicals, particularly for flocculation. We believed that this might be achieved by the use filtration media of fine particle size and/or modified surface characteristics. Two indigenous New Zealand materials, SS and TM have characteristics that should be useful for this work. TM exists in much finer grains the majority of water filtration media and its high density and magnetic properties offer potential advantages. For example, the magnetic property of TM offered the possibility of using MSFB technology to achieve greater hydraulic conductivities and improved backwashing. Also TM, because of its magnetite content, was expected to have an IEP higher than conventional silica sand filtration media. SS, because of its vesicular structure posses high surface area and so should enhance the effects of surface modification. Specific research objectives to address the central aim are outlined in Section 1.3.1, 1.3.2, 1.3.3 and 1.3.4 below.

1.3.1 Filtration by a fine magnetic medium: TM

Natural TM concentrate occurs as a fine (75-300 μm diameter) magnetic sand. We wished to determine whether the fine particle size facilitates the removal of fine colloids and whether the magnetic properties allow greater hydraulic conductivity to be achieved during filtration using a MSFB. By analogy with the similar material, magnetite, it was considered likely that TM would also have charge properties that would facilitate the removal of negative colloids. To test this proposition, the isoelectric point of natural TM is required.

Particle size is an important medium property contributing to filtration efficiency. The current work will investigate a range of TM particle sizes in compacted beds

and magnetically conditioned expanded beds to determine the filtration efficiencies and flow rates that can be achieved using this medium.

1.3.2 Modification of TM surface chemistry

Because of the importance of media surface charge characteristics, studies of the IEP of natural TM and its synthetic analogues are necessary. Modification of TM surface chemistry may allow optimisation of performance. The aim of this work will be to develop treatments that will allow control over the surface charge of TM. Coating of the TM particles with films of hydrous oxides of Al, Fe and Mn provide a possible means whereby this could be achieved. Other treatments including thermal modification, oxidation and reduction may also be effective in modifying surface properties.

1.3.3 Modification of pumice media

Pumice, for example the modified pumice material marketed as SS, is finding application in filtration. The porous nature and large surface area of the pumice granules make this material suitable for loading with hydrous oxides and mixed hydrous oxides. In this way it should be possible to prepare media with controllable surface charge. We wished to trial the ability of pumice media, modified to produce high IEP, to remove negative colloids. The porous structure of pumice also allows for the possibility of loading the grains with sufficient magnetite precursor chemicals to incorporate enough magnetite into the particles to provide useful magnetic properties. This may make it possible to use magnetically conditioned beds of fine pumice materials in filtration applications.

1.3.4 Magnetic conditioning during backwashing

A difficulty likely to be encountered when fine media are used are low filtration rates and loss of media during backwashing. Magnetic conditioning offers a means of overcoming both problems. Magnetic stabilisation of the bed in an expanded state should increase hydraulic conductivity during filtration and allow

higher flow velocities during backwashing. Optimum backwashing was expected to be achieved when flow velocity reached the maximum that could be sustained without destabilising the conditioned bed.

1.4 References

Abdullaev, K. M.; Malakhov, I. A.; Nikashina, V. A.; Poletaev, L. N.; Yakobishvili, I. S. 1981. Use of the mineral clinoptilolite for the removal of ammonia from natural waters and industrial wastewaters. *USSR. Energetik.* 1: 30-31.

Ahammed, M. M.; Chaudhuri, M. 1996. Sand-based filtration/adsorption media. *J. Water SRT- Aqua.* 45(2): 67-71.

Alther, G.; Biomin, R. 1999. Organoclay filtration technology for oil removal. *Adv. Filtr. Sep. Technol. 13B (Advancing Filtration and Separation Solutions for the Millenium):* 945-952.

American Water Works Association. 1971. *Water Quality and Treatment-A Handbook of Water Supplies*. America.

Anderson, N. J.; Bolto, B. A.; Dixon, D. R.; Kolarik, L. O.; Priestley, A. J.; Raper, W. G. C. 1982(a). Water treatment with reusable magnetite particles. *Water Filtr., Proceedigs Int. Symp.* (1982): 2.1-2.10. Editor(s): Weiler, R. A.; Janssens, J. G., Publisher: K. Vlaam. Ingenieursver, Antwerp, Belg.

Anderson, N. J.; Bolto, B. A.; Eldridge, R. J.; Kolarik, L. O.; Swinton, E. A. 1980. Color and turbidity removal with reusable magnetic particles. II. Coagulation with magnetic polymer composites. *Water Res.* 14(8): 967-973

Anderson, N. J.; Kolarik, L. O.; Swinton, E. A; Weiss, D.E. 1982(b). Colour and turbidity removal with reusable magnetic particles III. Immobilized metal hydroxide hydroxide gels. *Water. Res.* 16: 1327-1334.

Andrews, R.C. 1993. Water treatment without chemicals for removal of *Giardia. Technical report to WFS.*

Apelian, D.; Eckert, C. E.; Mutharasan, R.; Miller, R. E. 1985. *Refining of Molten Aluminum by Filtration Technology.* Editor(s): Engh, T. A.; Lyng, S.; Oeye, H. A. Proc. Int. Semin. 121-143.

Bailey, R. P.; Bennett, T.; Benjamin, M. M. 1992. Sorption onto and recovery of Cr(VI) using iron-oxide coated sand. *Water. Sci. Technol.* 26(5-6): 1239-1244.

Barnett, E.; Bruce, R.; Wayne, L.; Joe, S. 1990. Plant scale comparison of multi-media and dual media filters. *Adv. Filtr. Sep. Technol.* 2 *(Filtr. Sep. Environ. Control Technol.):* 1-5.

Beckett, R. 1990. *Surface and Colloid Chemistry in Natural Waters and Water Treatment.* Editor: Ronald Beckett. New York: Plenum Press, c 1990.

Benjamin, M. M.; Leckie, J. O. 1981. Multiple-site adsorption of Cd, Cu, Zn and Pb on amorphous iron oxyhydroxide. *J. Colloid Interface sci.* 79: 209-221.

Benjamin, M. M.; Sletten, R. S.; Bailey, R. P.; Bennett, T. 1996. Sorption and filtration of metals using iron-coated sand. *Water Res.* 30(11): 2609-2620.

Beresford, S. W. 1997. *Volcanology and Geochemistry of The Kaingaroa Ignimbrite, Taupo Volcanic Zone, New Zealand.* PhD thesis, University of Canterbury.

Boehm, D.; Voss, H. 1999. Application of magnetic micro-particles in chemical engineering technology. *Chem. Ing. Tech.,* 71(1/2): 43-51.

Bohm, D.; Birgit, V.; Voss, H. 1999. Magnetically stabilized fluidized beds. Hydrodynamic studies. *Chem. Ing. Tech.,* 71(6): 580-583.

Boller, M. 1994. Trends in water filtration technology. *Aqua (London).* 43(2): 65-75.

Bolto, B. A.; Cross, K. W. V.; Eldridge, R. J.; Swinton, E. A.; Weiss, D. E. 1975. Magnetic filter aids. *Chem. Eng. Prog.* 71(12): 47-50.

Bolto, Brian A. 1990. Water treatment technology in Australia. *Surf. Colloid Chem. Nat. Waters Water Treat., Proc. Symp. :* 87-101. Editor: Ronald, B.

Brodsky, A.; Vladislav, Z.; Jiri, V. 1978. *Iron removal from recycled water condensates in boiler operation. Czech.* (1978) 2 pp. Patent Application: CS 74-3415 19740514. CAN 90:192365 AN 1979:192365

Brown, M. P.; Fitzpatrick, C. S. B.; Murrer, J. 1996. Media mixing in multi-media filters. *Proc. World Filtr. Congr., 7th* (1996)1: 218-222. Publisher: Hungarian Chemical Society. Budapest, Hung .

Bryan, G. H.; Filtr. P., B.; Nucl, S. C.; Lynchburg, V. A. 1990. Electromagnetic filtration. *Ultrapure Water* 7(1): 31, 33-34.

Chang, Yujung; Li, Chi-Wang; Benjamin, Mark M. 1997. Iron oxide-coated media for NOM sorption and particulate filtration. *J. AWWA* 89(5): 100-113.

Chen, J.; Truesdail, S.; Lu, F.; Zhan, G.; Belvin, C.; Koopman, B.; Farrah, S. Shah, D. 1998. Long-term evaluation of aluminium hydroxide-coated sand for removal of bacterial from wastewater. *Water. Res.* 32(7): 2171-2179.

Clement, L.; Jovanovic, G. 1997. Magnetically stabilized fluidized bed – new technology for remediation of contaminated soils, sludge and liquid wastes. *WM'97 Proc.* : 893-902.

Colella, C. 1999. Natural zeolites in environmentally friendly processes and applications. *Stud. Surf. Sci. Catal.* 125 : 641-655.

Crossley, C. 1998. Membrane filtration technology in the dye industry. *J. Soc. Dyers Colour.* 114(7/8): 194-196.

De Latour, C. 1975. *Water purification by magnetic filtration. USA.* 2nd (1976): 898-900. Editor(s): Cecil, Lawrence K. Proc. Natl. Conf. Complete WateReuse.

Degner, V. R. 1990. Deep bed filtration technology advancements. *Adv. Filtr. Sep. Technol.* 1 *(Filtr. Sep. Oil Gas Drill. Prod. Oper.):* 243-246.

Dixon, D. R. 1991. The Sirofloc process for water clarification. *Water Supply* 9 *(1, Suppl., IWSA/IAWPRC Jt. Spec. Conf. Coagulation, Flocculation, Filtr., Sediment. Flotation,* 1990): S33-S36.

Draham, I. 1980. Compositional, structural, and magnetic variation in Waipipi titanomagetites. *New Zealand J. of Geo.Geo.* 23: 447-454.

Drakhlin, E. E.; Novikova, N. V.; Petrov, E. G.; Patkovskaya, N. A.; Vilin, A. G. 1983. *Removing iron from underground waters.* Patent CODEN: URXXAF SU 1041523 A1 19830915 Application: SU 82-3406165 19820310. CAN 100:12400 AN 1984:12400 CAPLUS.

Dudeney, A. W. L.; Narayanan, A.; Tarasova, I. I. 1999. Removal of iron from silica sand: integrated effluent treatment by sulfate reduction, photochemical reduction and reverse osmosis. *Process Metall. 9B (Biohydrometallurgy and the Environment Toward the Mining of the 21st Century, Pt. B):* 617-625.

Edwards, M.; Benjamin, M. M. 1989a. Adsorptive filtration using coated sand : A new approach for treatment of metal-bearing wastes. *Journal of WPCF,* 61(9): 1523-1533.

Edwards, M.; Benjamin, M. M. 1989b. Regeneration and reuse of iron hydroxide adsorbents in the treatment of metal-bearing wasters. *J. Water Pollut. Control Fed.* 61: 481-490.

Fair, G. M.; Geyer, J. C. 1965. *Elements of Water Supply and Waste-waster Disposal.* New York, John Wiley & Sons, Inc., America.

Fushimi, H.; Uchimura, T. 1984. Adsorption, desorption, and recovery of heavy metal ions by vermiculite. I. *Nippon Kogyo Kaishi* 100(1155): 417-222.

Ganzha, V. L.; Saxena, S. C. 2000. Hydrodynamic behavior of magnetically stabilized fluidized beds of magnetic particles. *Powder Technol.*, 107(1-2): 31-35.

Gao, N.; Xu, D.; Fan, J.; Yan, X. 1999. Filtration of alumina coated sand. *Zhongguo Jishui Paishui.* 15(3): 8-10.

Gusev, B. A.; Efimov, A. A.; Moskvin, L. N.; Mikhailov, N. N.; Smirnova, M. N.; Cheremnykh, P. A. 1991. Water purification using a high gradient magnetic filter. *At. Energ.* 70(6): 412-413.

Hill, T.; Langdon, A. 1991. Porous ceramic dual media filtration: An improved technology for water filtration. *Water & Wastes in New Zealand.* July: 19-20.

Hill, T.; Langdon, A. 1993. Modified pumice: An indigenous material for water filtration and Aluminium removal. *Water & Wastes in New Zealand.* July: 36-38.

Hunter, K. A. 1980. Microelectrophoretic properties of natural surface active organic matter in coastal seawater. *Limnol. Oceanogr.* 25: 807-822.

Hunter, K. A.; Liss, P. S. 1982. Organic matter and the surface charge of suspended particles in estuarine wates. *Limnol.Oceanogr.* 27: 322-335.

Iwamoto, T.; Haneyama, T.; Ishii, K. 1977. *Removal of heavy metal ions.* (Wako Pure Chemical Industries, Ltd., Japan). Japan. Kokai 3 pp. CODEN: JKXXAF JP 52126685 19771024 Showa. Patent Application: JP 76-43182 19760416. CAN 88:65689 AN 1978: 65689.

Janda, V.; Rudovsky, J. 1994. Removal of ammonia from drinking water by biological nitrification. *Aqua (London).* 43(3): 120-126.

Joshi, A.; Chaudhuri, M. 1996. Removal of arsenic from ground water by ion oxide-coated sand. *Journal of Environmental Engineering.* 122(8):769-772.

Knocke, W. R.; Hamon, J. R. 1988. Soluble manganese removal on oxide-coated filter media. *J. AWWA* 80(12): 65-70.

Knocke, W. R.; Occiano, S. C.; Hungate, R. 1991. Removal of soluble manganese by oxide-coated filter media: sorption rate and removal mechanism issues. *J. AWWA* 83(8): 64-69.

Kolarik, L. O. 1983. Color and turbidity removal with reusable magnetite particles. IV. Alkali activated magnetite - a new solid, reusable coagulant-adsorbent. *Water Res.* 17(2): 141-147.

Kunikane, S., Itoh, M., Magara, Y. 1996. Development of membrane filtration technology for drinking water. *Kankyo Gijutsu.* 25(4): 195-200.

Lai, C. H.; Chen, C. Y.; Shih, P. H.; Hsia, T. H. 2000. Competitive adsorption of copper and lead ions on an iron-coated sand from water. *Water Sci. Technol. 42(3-4, Water Quality Management in Asia):* 149-154.

Lai, C. H.; Lo, S. L.; Lin, C. F. 1994. Evaluating an iron-coated sand for removing copper from water. *Water Sci. Technol.* 30(9): 175-182.

Langdon, A. G.; Hill, T.A.; Smyth, P.R. 1995. Porous ceramic dual media (PCDM) filtration –commercial Benefits. *Water and Wastes in New Zealand. 88*: 26-28.

Leprince, A.; Fiessinger, F.; Bottero, J. Y., 1984. Polymerized iron chloride: an improved inorganic coagulant. *J. AWWA* 76(10): 93-97.

Liu, J. C.; Huang, J. G. 1998. Using iron-coated spent catalyst as an alternative adsorbent to remove Cr(VI) from water. *Water Sci. Technol.* 38(4-5): 155-162.

Lo, S. L.; Chen, T. Y. 1997b. Adsorption of Se(IV) and Se(VI) on an iron-coated sand from water. *Chemosphere.* 35(5): 919-930.

Lo, S. L.; Jeng, H. T.; Lai, C.H. 1997a. Characteristics and adsorption properties of iron-coated sand. *Water Sci. Technol.* 35(7): 63-70.

Loder, T. C.; Liss, P. S. 1985. Control by organic coatings of the surface charge of estuarine suspended particles. *Limnol. Oceanogr.* 30: 418-421.

Mackie, R.; Bai, R. 1993. The role of particle size distribution in the performance and modeling of filtration. *Water Sci. Technol.* 27 (10): 19-34

Manahan, S. E., 1994. *Environmental Chemistry.* Editor(s): Manahan, S. E., Lewis, USA.

Marin, G. R.; Empresa, M. A.; Cordoba, S.A.; Cordoba. 1992. Ripening of silica sand used for filtration. Spain. *Water Res.* 26(5): 683-688.

Maroudas, A. 1965. Particle deposition in granular filter media. *Filtr. Separ.* 2(5): 369-372.

Marshall, K.C. 1976. *Interfaces in Microbial Ecology.* Harvard University press. Cambridge, Massachussets.

Martin, H. L; Norford, S. W.; Diener, G. A. 1993. Metal finishing wastewater pressure filter optimization. *Proc. AESF Annu. Tech. Conf.* 80TH: 559-62.

Martins, J.; Fernandes, R. 1992. Hydrophobic expanded vermiculite as a cleaning agent for contaminated waters. *Water Sci. Technol. 26(9-11, Water Qual. Int. '92, Pt. 5)*: 2297-2299.

Matsumoto, Y.; Matsumoto, Y.; Totsuka, Y. 1984. Evaluation of submerged bilolgical filters. *Shizuoka-ken Kogyo Shikenjo Hokoku* (28): 69-77.

Merkle, P. B.; Knocke, W. R.; Gallagher, D. L. 1994. Filter media mineral coatings: Filtration theory and practice. *Proc. Annu. Conf., AWWA* : 531-557.

Merkle, P. B.; Knocke, W.; Gallagher, D.; Junta-Rosso, J.; Solber, T. 1996. Characterizing filter media mineral coatings. *J. AWWA* 88(12): 62-73.

Michael, T. M., John, M. M.; Jack, P. 1997. *Biology of Microorganisms*. Editor: Paul, F. C., Prentice-Hall, Inc.New Jeresy.

Mintz, D. J. 1960. Water and waste water filtration: concepts and applications. current research. *J. Appl. Chem.* 33: 303-314.

Misaelides, P.; Macasek, F.; Pinnavaia, T. J.; Colella, C. 1999. *Natural Microporous Materials in Environmental Technology.* NATO Science Series. Editor(s): Misaelides, P.; Macasek, F.; Pinnavaia, T. J.; Colella. C. Kluwer Academic Publishers.

Moergeli, B.; Ives, K. J. 1979. New media for effluent filtration. *Water Res.* 13(10): 1001-1007.

Moffat, G.; Williams, R. A.; Webb, C.; Stirling, R. 1994. Selective separations in environmental and industrial processes using magnetic carrier technology. *Miner. Eng.* 7(8): 1039-1056.

Neihof, R. A.; Loeb, G. I. 1972. The surface charge of particlulate matter in seawater. *Limnol. Oceanogr.* 17: 7-16.

Nunge, R. J. 1970. *Flow Through Porous Media.* American chemical society. Publications: Washington D.C.

Onitsuka, T. 1996. Treatment of drinking water by membrane filtration technology. *Kankyo Gijutsu* . 25(4): 209-213.

Ostreicher, E. A. 1977. *Particulate filter medium (AMF Inc., USA). U.S.* Patent 8 pp. CODEN: USXXAM US 4007113 19770208 Application: US 73-358822 19730509. CAN 87:25349 AN 1977: 425349.

Ouki, S. K.; Kavannagh, M. 1999. Treatment of metals-contaminated wastewaters by use of natural zeolites. *Water Sci. Technol.* 39(10-11): 115-122.

Page, G. M.; Amirtharajah, A. 1995. Optimum backwash of dual media filters with air scour: A plant-scale study. *Proc. Annu. Conf., AWWA, Water Research* : 335-357.

Palm, S. K.; Smith, T. R.; Shiuh, J. C.; Roulston, J. S. 1997. *Composite filtration media comprising functional filtration component and matrix component, and preparation and use of these media.* (Advanced Minerals Corporation, USA). Eur. Pat. Appl. Patent 18 pp. CODEN: EPXXDW EP 790070 A1 19970820.

Parks, G. A. 1965. The isoelectric points of solid oxides, solid hydroxides, and aqueous hydroxo complex systems. *Chem. Rev.* 65: 177-198.

Piaskowski, K.; Anielak, A. M. 2000. Natural zeolites and their use in water purification and wastewater treatment. *Pol. Ekol. Tech.* 8(2): 31-41.

Polyakov, V. E.; Tarasevich, Yu. I.; Ovcharenko, F. D. 1977. Study of the sorption of copper ammoniate from aqueous solutions by montmorillonite. *Inst. Kolloidn. Khim. Khim. Vody, Kiev, USSR. Ukr. Khim. Zh. (Russ. Ed.)* 43(8): 823-828.

Rantala, P. 1994. Capillary filtration technology - non-polluting to nature. *Filtr. Sep.* 31(2): 135, 137.

Reyes, O.; Sanchez, E.; Pellon, A.; Borja, R.; Colmenarejo, M. F.; Milan, Z.; Cruz, M. D. 1997. A comparative study of sand and natural zeolite as filtering media in tertiary treatment of wastewaters from tourist areas. *J. Environ. Sci. Health, Part A: Environ. Sci. Eng. Toxic Hazard. Subst. Control.* A32(9 & 10): 2483-2496.

Rosenberg; Kjelleberg, S. 1986. *Hydrophobic Interactions: Role in Bacterial Adhesion.* In " Microbial ecology, vol.9". Editor: Marshall, K. C., Plenum Press, New York.

Rushton, A.; Ward, A. S.; Holdich, R. G. 1996. *Solid-Liquid Filtraion and Separation Technology* . VXH Verlagsgesellschaft mbh, Weinheim (Federal Republic of Germany) & VCH Publishers, Inc., New York, NY (USA).

Sansalone, J. J. 1999. Adsorptive infiltration of metals in urban drainage - media characteristics. *Sci. Total Environ.* 235(1-3): 170-188.

Satpathy, J. K.; Chaudhuri, M. 1995. Treatment of cadmium-plating and chromium-plating wastes by iron oxide-coated sand. *Water Environment Research.* 67(5): 788-790.

Schultz, M. F.; Benhamin, M. M.; Ferguson, J. F. 1987. Adsorption and desorption of metals on ferrihydrite: reversibility of the reaction and sorption properties of the regenerated solid. *Environ. Sci. Technol.* 21: 863-869.

Sethuraman, V. V.; Raymahashay, B. C. 1975. Color removal by clays. Kinetic study of adsorption of cationic and anionic dyes. *Environ. Sci. Technol.* 9(13): 1139-1140.

Sharma, S. K.; Greetham, M. R.; Schippers, J. C. 1999. Adsorption of iron(II) onto filter media. *Aqua.* 48(3): 84-91.

Sikalidis, C. A.; Alexiades, C.; Misaelides, P. 1989. Adsorption of uranium and thorium from aqueous solutions by the clay minerals montmorillonite and vermiculite. *Toxicol. Environ. Chem.* 20-21: 175-180.

Silicon Suppliers (NZ) Ltd. *A process for manufacturing ceramic-like materials and products.* New Zealand Patent No. 212330.

Sims, M. L. 1993. *Novel Technologies for Water Filtration.* MSc (Technology) Thesis, University of Waikato, New Zealand.

Smith, J. E.; Hegg, B. A.; Renner, R. C. 1991. Upgrading existing or designing new drinking water treatment facilities. *Pollution Technology Review* No. 198: 248.

Spevakova, I. 1994. Natural minerals in water treatment. *Kim., Handasa Kim.* 18: 33-36, 39.

Stahl, R. S.; James, B. R. 1991a. Zinc sorption by iron-oxide-coated sand as a function of pH. *Soil Sci. Soc. Am. J.* 55: 1287-1290.

Stahl, R. S.; James, B. R. 1991b. Zinc sorption by manganese-oxide-coated sand as a function of pH. *Soil Sci. Soc. Am. J.* 55: 1291-1294.

Stenkamp, S.; Benjamin, M. 1992. Effect of iron oxide coatings on the filtration properties of sand. *Adv. Filtr. Sep. Technol. 5 (Sep. Probl. Environ.)*: 17-21.

Stumm, W. 1977. Chemical interaction in partical separation. *Enviorn. Sci. Technol.* 11: 1066.

Stumm, W.; Morgan, J. J. 1996. *Aquatic Chemistry. 3rd Edition.* New York: John Wiley & Sons.

Stumm, W.; O'Melia, C. R. 1968. Stoichiometry of coagulation. *J. AWWA 60*: 514-539

Subbotina, E. A.; Tarasevich, Y. I.; Orazmuradov, A. O. 1985. Adsorption of direct dyes on organically substituted montmorillonite. *Izv. Akad. Nauk Turkm. SSR, Ser. Fiz.-Tekh., Khim. Geol. Nauk.* (3): 105-108.

Tenny, A. M.; Derka, J. 1992. hydroxylated ferric sulphate – An aluminium salt alternative. *Water Supply.* 10: 167-174.

Terashima, Y.; Ozaki, H.; Sekine, M. 1986. Removal of dissolved heavy metals by chemical coagulation, magnetic seeding and high gradient magnetic filtration. *Water Res.* 20(5): 537-545.

Tipping, E. 1981. The adsorption of humic substances by iron oxides. *Geochim. Cosmochim. Acta.* 45: 191-199.

Trussell, R. R.; Chang, M. 1999. Review of flow through porous media as applied to head loss in water filters. *J. Environ. Eng.* 125(11): 998-1006.

Ulieru, D. 1998. The filtration technology for ultrapure water recovery from microelectronics fab. *Adv. Filtr. Sep. Technol.* 12: 302-309.

van der Mei, H. C.; de Vries, J.; Busscher, H. J. 1993. Hydrophobic and electrostatic cell surface properties of thermophilic dairy streptococci. *Appl. Environ. Microbiol.* 59(12): 4305-4312.

Vilangines, P.; Savette, B.; Vilangines, R. 1982. Preformed magnesium hydroxide precipitate for second-step concentration of entero-virus from drinking and surface waters. *Canad. J. Microbiol.* 28: 783-787.

Walter, R.; Durkop, J.; Friedman, B.; Dobberkan, H. J. 1985. Interactions between biotic and abiotic factors and viruses in a water system. *Water Sci. Technol.* 17: 139-142.

Watson, A. 1989. Comparison of algal penetration through rapid-gravity filter beds. *J. Inst. Water Environ. Manage.* 3(5): 443-450.

White, D. A.; Asfar-Siddique, A. 1997. Removal of manganese and iron from drinking water using hydrous manganese dioxide. *Solvent Extraction and Ion Exchange.* 15(6): 1133-1145.

Xia, Y. 1989. The application of the dual media concept to upflow filtration. *Water Treat.* 4(2): 125-132.

Yadidia, R.; Abeliovich, A.; Belfort, G. 1977. Algae removal by high gradient magnetic filtration. *Environ. Sci. Technol.* 11(9): 913-916.

Yagi, Y. 1999. Membrane filtration technology for water purification. *Mizu Kankyo Gakkaishi.* 22(4): 248-251.

Yao, K. M. 1971. Water and waste water filtration : concepts and applications. C*urrent research. November* (5): 1105-1112.

Yong, L. 1997. *Aspects of The Performance of A Porous Ceramic Dual Media (PCDM) Filtration System.* MSc. Thesis, University of Waikato.

Zorpas, A. A.; Constantinides, T.; Vlyssides, A. G.; Haralambous, I.; Loizidou, M. 1999. Heavy metal uptake by natural zeolite and metals partitioning in sewage sludge compost. *Bioresour. Technol.* 72(2): 113-119.

Chapter Two: Analytical Methods and Materials

2.1 Introduction

In this study TM and pumice filtration media were investigated. They were characterised by a variety of physical methods including X-ray diffraction (XRD); scanning electron microscopy (SEM) and energy dispersive analysis of X-rays (EDAX); optical microscopy; Brunauer-Emmett-Teller (BET) analysis of surface area and pore size; inductively coupled plasma (ICP) analysis; isoelectric point (IEP) measurement; density measurement; magnetic susceptibility by Gouy method and particle size analysis by laser light scattering. Equipment for TM fabrication included a high energy mechanical mill (SPEX 8000 mill), a stabilized zironia ball mill and a ceramic tube furnace. Details of procedures used are described in the following sections.

2.2 Materials

2.2.1 Titanomagnetite

TM was supplied by BHP New Zealand Steel Limited. It was further purified magnetically, rinsed thoroughly with tap water and oven dried at 100^0C over night. The dried samples were suspended in 0.1 mol/L HCl solution for 20 min, stirred at 500 rpm, after which the supernatant was decanted. This procedure was repeated another three times. The samples were then rinsed thoroughly with distilled water and oven dried at 100^0C for 24 hr. TM prepared in this way is referred to in this study as acid-rinsed titanomagnetite (ARTM).

2.2.2 Pumice

The pumice used was the commercial product, Silicon Sponge (SS), provided by Works Filter Systems, Hamilton, New Zealand. The SS was first rinsed thoroughly with tap water to remove impurities and then suspended in 0.1 mol/L HCl solution over night. The HCl solution was decanted and the pumice rinsed with distilled water and dried in an oven at 100^0C for 24 hr. This material is referred to as acid-rinsed Silicon Sponge (ARSS).

2.2.3 Kaolin suspensions

For filtration studies, suspensions of kaolin were prepared from Clay Ceram Powder (supplied by Waikato Ceramics, Hamilton). The typical chemical and physical properties are summarised by the manufacturer in Table 2.1. Suspensions were prepared by adding the Clay Ceram Powder to tap water.

The following procedure was used:

- Kaolin powder was dispersed in distilled water in a beaker at a concentration of 5 g/L and allowed to stand for 24 hr.
- The supernatant was decanted and discarded, a further 2 L of distilled water was added and the suspension allowed to stand for 15 hr and the sediment discarded.
- The suspension remaining was labelled kaolin stock solution (KSS).
- The suspension used for filtration trials was prepared by adding 84 mL KSS per litre distilled water.

The suspension prepared in this way was stable, had consistency of 35.68 mg/L, an initial turbidity of 42 NTU and a pH of approximately 5.7. The particle size distribution of the suspension was examined by a Laser Diffraction Particle Size Analyser (Malvern Mastersizer-S, Malvern Instruments Ltd. Spring Lane South,

U.K.) and found to lie in the range 0.1- 6.0 μm (volume distribution) and the maximum in volume distribution occurred at a particle size of. 1.07 μm.

In order to investigate the effect of pH on the particle size distribution, the pHs of a series of kaolin suspension were adjusted over the range from 3.42 to 13.02, equilibrated for 24 hr, and examined for particle size distribution. The results show that pH does not effect the particle size distribution. Data are summarised in Appendix 2.1.

Table 2.1 Typical chemical and physical properties of Clay Ceram Powder

Name	Formula	Assay
Silica	SiO_2	52.6%
Alumna	Al_2O_3	32.3%
Magnesia	MgO	0.4%
Ferric Oxide	Fe_2O3	0.7%
Lime	CaO	0.1%
Potash	K_2O	0.5%
Soda	Na_2O	0.2%
Titantum Dioxide	TiO_2	1.0%
Loss on Ignition	1000^0C	12.0%

Property	Units	Value
Specific Gravity		2.66
Surface Area	(m^2/g)	2.87
Oil Absorption	(mL/100g)	43
Bulk Density	(compacted g/cm^3)	0.8
Isoelectric point (IEP)	(pH)	2.70 ± 0.10

2.3 X-ray Diffraction (XRD)

X-ray diffraction is a versatile, non-destructive analytical technique for identification and quantitative determination of various crystalline materials. A basic instrument for such study is the Bragg spectrometer (Figure 2.1).

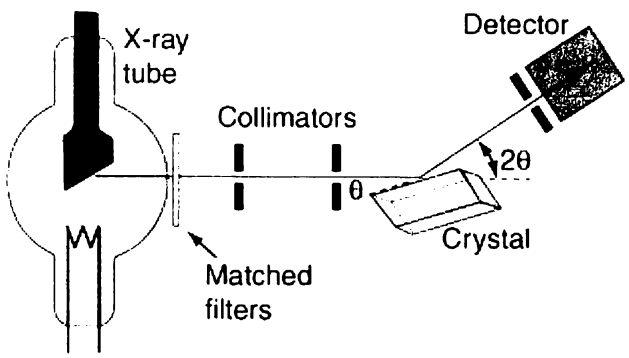

Figure 2.1 Bragg spectrometer

Nearly monochromatic x-rays are produced in an x-ray tube. In order to eliminate as much of the brehmsstrahlung continuum radiation as possible, matched filters are used in the x-ray beam to optimise the fraction of the energy, in the K-α line. Such filters use elements located in the Periodic Table just above and just below the metal in the x-ray target, making use of the strong "absorption edges" just above and below the K- α energy of the target metal.

The x-rays are collimated with apertures of a strong x-ray absorber metal (usually lead) and the narrow resulting x-ray beam is allowed to strike the crystal to be studied. The spectrometer arrangement couples the rotation of the crystal with the rotation of the detector so that the angle of rotation of the detector is twice that of the crystal.

The principle of XRD is based on the Bragg Law (Lipson and Steeple, 1970):

$$n\lambda = 2d\sin\theta \qquad (2\text{-}1)$$

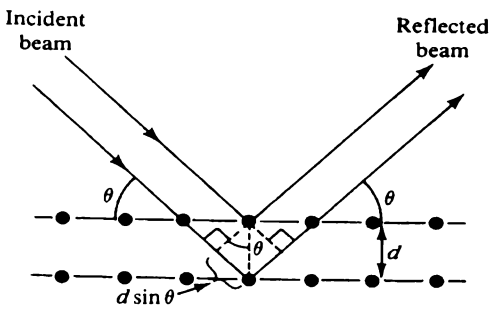

Figure 2.2 Illustration of an X-ray beam reflected by planes

Where θ is the angle of reflection; d is the lattice spacing; λ is the wavelength of the x-rays; and n is the order of the Bragg reflection (Figure 2.2). The Bragg law can be applied experimentally to determine the d-spacing by using X-rays of known wavelength λ, and then measuring θ. Alternatively, to determine the wavelength λ of the radiation, a crystal with planes of known d-spacing is used and θ is measured. X-rays are characterized by a series of line sets, referred to as K, L, M, etc. Only the K lines are useful for x-ray diffraction. There are several lines in the K set, but only the three strongest ($K\alpha_1$, $K\alpha_2$ and $K\beta_1$) are observed in normal diffraction work. The α_1 and α_2 components have wavelengths very close to each other (for example, $K\alpha_1$ = 1.540 Å and $K\alpha_2$ = 1.544 Å for a copper target) so they are not always resolvable as separate lines. The intensity of $K\alpha_1$ is always approximately twice that of $K\alpha_2$ (Cullity, 1978).

Crystal structures consist of unit cells. A unit cell is the smallest architectural unit needed to describe a crystal structure. The axial lengths (a, b, c) of a unit cell and the angles between them (α, β, γ) are the lattice constants or lattice parameters of the unit cell. By giving special values to the axial lengths and angles, various shapes of unit cells can be defined. Only seven different kinds of unit cells are necessary to include all possible crystals. These correspond to the seven crystal systems into which all crystals can be classified, as listed in Appendix 2.2, Bravais (Cullity, 1978) demonstrated that there are exactly fourteen possible point lattices in the seven crystal systems, as shown in Appendix 2.2. The cardinal

principle of crystal structure is that the atoms of a crystal are set in space either on the points of a Bravais lattice or in some fixed relation to those points. Specifically, structures which have points only at the corners are called 'simple' structures, those with points at the corners and an additional one at the centre of the lattice are called 'body-centred' structures, and those with points at the corners and in the middle of all faces are called 'face-centred' structures (Lipson and Steeple, 1970).

The orientation of a plane on a lattice can be represented by Miller Indices (*hkl*), which are defined as the reciprocals of the fractional intercepts, which the plane makes with the crystallographic axes. The interplanar spacing d_{hkl} is a function both of the Miller indices (*hkl*) and the lattice constants (*a, b, c,* α, β, γ). For example, in a cubic system, the interplanar spacing takes on a relatively simple form (Equation 2-2). In tetragonal systems, both *a* and *c* are involved in the interplanar spacing calculation, as shown in Equation (2-3) (Cullity, 1978).

$$d_{hkl} = \frac{a}{\sqrt{h^2 + k^2 + l^2}} \tag{2-2}$$

$$d_{hkl} = \frac{a}{\sqrt{h^2 + k^2 + l^2 (a / c)}} \tag{2-3}$$

In this study the materials were analysed by using a Philips X-Pert system diffractometer, with a generator setting of 45 kV at 40 mA using Cu kα X-ray radiations and a graphite monochromator. The patterns were obtained using a 0.02^0 step size averaging for 5 second per increment. X-ray pattern analysis, α_2 elimination, smoothing and background subtraction were performed using a Philip's software package.

2.4 Scanning electron microscopy (SEM) and energy-dispersive analysis by X-ray (EDAX)

Scanning electron microscopy (SEM), with its high resolution, is widely used for microstructure analysis. With a large depth of focus, it can quickly document the specimen microstructures of particle size and shape, agglomerate shape and roughness of fracture surfaces. With an energy-dispersive spectroscopy attachment, microscale-semiqualitative chemical analysis can be obtained greatly aiding the interpretation of the composition and the purity of the powder.

In this study scanning electron microscopy (SEM) and energy-dispersive spectroscopy (EDAX) were performed using a Hitachi S4000 SEM and a Kevex microanalyser attached to the SEM system. Particle surface condition, particle size, porosity and distribution were observed by the SEM. The elements present in the samples were determined by EDAX. Samples examined by EDAX were coated by a thin film of platinum by vacuum vapour deposition to prevent built up of electrostatic charge.

2.5 Optical microscopy

Optical microscopy examination was carried out using an Olympus BX60 microscope, which was equipped with a Polaroid Digital Camera.

2.6 Isoelectric point (IEP)

In all aqueous colloidal systems, the charges of the solid/liquid interfaces play a decisive role. Surface charge of materials is typically estimated by measuring the electrokinetic potential (zeta potential ξ) at the shear plane of the electrical double layer. There are many ways to determine this parameter. The most widely used methods are micro-electrophoresis, potentiometric titration and streaming potential.

The apparatus used in micro-electrophoresis include such brands as Zeta-Sizer-4 automatic apparatus (Malvern Instruments Ltd.) and Zeta Meter (Zeta-meter, Inc New York). For this method the samples must be fine and light enough to remain suspended for the duration of the experiment. The method is of limited use in measuring zeta potentials of coarse and high density particles. In this study in order to measure IEP of heavy particles of TM, SS, magnetite, iron oxide and aluminium oxide, a MUTEK PCD 03 instrument (Mütek Analytic Inc. Germany) was used.

Practically all solids particles in water carry electric charges. This leads to a concentration of oppositely charged ions, the so-called counter-ions, at the surfaces. If these counter-ions are separated from, or sheared off the particle, a streaming potential can be measured. A streaming potential of zero denotes the point of zero charge, i.e. all existing charges in the sample are neutralized. If the measured potential is unequal to zero, its sign indicates whether the surface charge is positive (cationic) or negative (anionic). The potential itself is a relative parameter that depends on different influential factors, such as electrical conductivity of the sample dispersion; sample viscosity; molecular weight, particle size and temperature. The potential caused by the velocity difference between the particles and the fluid can be measured. The necessary shear flow is induced by periodic movement of a piston in a cylinder filled with the suspension to be investigated. Acceleration and deceleration of the particles causes a measurable potential. Data for variation of potential (mV) with the pH value of the suspension allow the isoelectric point (IEP) of the particles to be determined.

In order to confirm the validity of results obtained by the streaming potential method, IEPs of pure commercial aluminium oxide powder (RC-SP DBM, 0.69 μm, supplied by Malakoff Industries, Inc. Virginia) were studied by both the Zeta-meter and MUTEK PCD 03 instruments. The Zeta-meter IEP value was 5.6 ± 0.1 which compares favourably with the MUTEK PCD 03 value of 5.8 ± 0.1.

2.6.1 Measuring principle of Mutek PCD 03

Streaming current measurements with the Mutek PCD 03 instrument are based on the following principal (Figure 2.3): the central element is a plastic measuring cell (1) with a fitted displacement piston (2). If an aqueous particulate sample is filled into the measuring cell, particles will attach themselves to the plastic surface of the piston and on the cell walls under the action of van der Waals forces. The counter-ions remain comparatively free. A defined narrow gap is provided between cell wall and piston. Driven by a motor (4), the piston (2) oscillates in the measuring cell (1) and creates liquid flow, which entrains the free counter-ions, thus separating them from the adsorbed sample material. At the built-in electrodes (3), the counter-ions induce a current which is converted to a potential, rectified and amplified electronically (5). The streaming c potential is shown on the display (6) with the appropriate sign.

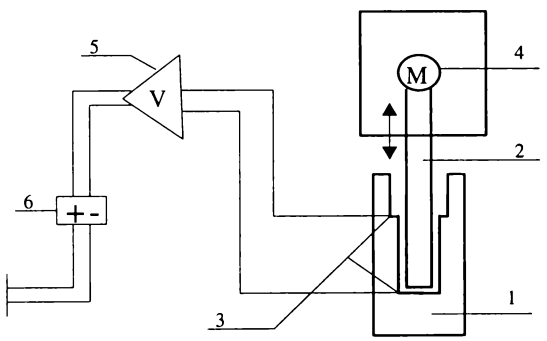

1 plastic measuring cell
2 piston
3 electrodes
4 motor and piston
5 electronics
6 display

Figure 2.3 Schematic of Mutek PCD 03 instrument

2.6.2 IEP measurement with Mutek PCD 03

All samples used in this work were ground to particle size < 250 μm, the amount of sample for each measurement was 0.01 g, de-ionized water was used for the

measuring solution. The measuring procedure was according to the Mutek manual (Mutek Analytic Inc. Germany). The essential steps are set out below.

- 0.01 g samples were dispersed in the volumes of 30 mL de-ionized water.
- The measuring cell was filled with the sample.
- The piston was inserted into the measuring cell.
- The measuring cell was fixed in the instrument with the electrodes facing towards the rear.
- The piston was locked into position. The measuring cell is correctly positioned if the piston can be hooked in the bayonet catch easily.
- The streaming potential was indicated on the display when the motor was turned on.
- The value was recorded after 30 seconds when the potential signal had stabilized.
- Using a measuring pipette, titrant (0.01 mol/L HCl or NaOH) was added drop-wise into the measuring cell and streaming potentials were recorded as a function of pH which was also displayed. The pH at which the streaming potential was zero was obtained by extrapolation. This was the point of zero charge. The pH value at the point of zero charge is the sample IEP under the conditions of the measurement.

2.7 Inductively coupled plasma (ICP)

The amount of coating materials deposited on the media was determined by the Inductively Coupled Plasma (ICP) method. The advantages of ICP analysis are that various metals can be determined simultaneously and different wavelengths can be adopted for sensitive measurement of one element over a large range of concentrations. The instrument used was a GBC Integra Inductively Coupled

Plasma Optical Emission Spectrometer (ICP-OES) (GBC Scientific Equipment Pty Led, 1997), with a wavelength range from 160 to 800 nm, a RF generator 1.5 kW 40 MHz and installed ICP software.

An ICP source consists of a flowing stream of argon gas ionised by an applied radio frequency field typically oscillating at 27.1 MHz. This field is inductively coupled to the ionised gas by a water-cooled coil surrounding a quartz "torch" that supports and confines the plasma.

A sample aerosol is generated in an appropriate nebuliser and spray chamber and is carried into the plasma through an injector tube located within the torch. The sample aerosol is injected directly into the ICP, subjecting the constituent atoms to temperatures of about 6000 K to 8000 K. These result in almost complete dissociation of any molecules present and a significant reduction in chemical interferences can be achieved. The high temperature of the plasma efficiently excites atomic emissions. Ionisation of a high percentage of atoms produces ionic emission spectra. The ICP provides an optically "thin" source that is not subject to self-absorption except at very high concentrations. Thus linear dynamic ranges of four to six orders of magnitude are observed for many elements.

The efficient excitation provided by the ICP results in low detection limits for many elements. This coupled with the extended dynamic range, permits effective multielement determination of metals. The light emitted from the ICP is focused onto the entrance slit of either a monochromator or a polychromator that effects dispersion. A precisely aligned exit slit is used to isolate a portion of the emission spectrum for intensity measurement using a photomultiplier tube. The monochromator uses multiple fixed exit slits and corresponding photomultiplier tubes. It simultaneously monitors all configured wavelengths using a computer controlled readout system. The sequential approach provides greater wavelength selection while the simultaneous approach can provide greater sample throughput (APHA, *et al.,* 1992).

The measurement procedure includes calibration with each batch of samples. Common analytical procedures are summarised below (GBC Scientific Equipment Pty Ltd, 1997):

- Line selection. An individual emission line or lines for each element to be analysed must be selected prior to the analysis. Wavelength scanning is used ensure that the desired concentration range will not cause signal saturation, nor be masked by the background. The wavelengths selected for the measurement of iron and aluminium is 372.0 nm and 396.2 nm.

- Normalisation. In order to compensate for changes in the instrument response, low reference and high reference are nominated when calibration is first set up.

- Set photomultiplier tube (PMT) voltages to adjust sensitivity for optima measurement condition.

- Start the plasma by pressing the yellow plasma ignition switch. Warm up the instrument for 30 min before analysis.

- Run standards and blank. Fit the curves.

- Perform an Auto Run to run the samples with auto-sampler. A full calibration was carried out between each sixty samples to ensure the sensitivity of measurement.

2.8 Brunauer-Emmett-Teller (BET)

In this study the medium surface area and pore size were examined by Quantachrome NOVA – 1000 gas sorption analyser (Quantachrome, Syosset, NY, USA). The medium sample was placed in a cell and out-gassed at 100^0C overnight. The NOVA 1000 can perform rapid and accurate sorption measurements of nitrogen gas on solid surfaces using liquid nitrogen as the coolant. The samples were tested by two different methods: 1) 3 point BET for the measurement of the specific surface area, 2) 25 point Barrett-Joyner-Halenda

(BJH) desorption for the measurement of pore size distribution. The measurement condition is P_0 =775.46 mm Hg; Adsorption tolerance = 0.1000; Desorption tolerance = 0.1000; Adsorption equilibrium time = 60 sec; Desorption equilibrium time =60 sec; Adsorption dwell time 180 sec; Desorption dwell time = 180 sec.

The principle of surface area and porosity measurements are based on Brunauer-Emmett-Teller (BET) method (Brunauer, *et al.,* 1938), which is the most widely used procedure for the determination of the surface area of solid materials. It involves the use of the BET equation (2-4):

$$\frac{1}{W[(P_0 / P) - 1]} = \frac{1}{W_m C} + \frac{C-1}{W_m C}(\frac{P}{P_0}) \qquad (2\text{-}4)$$

where W is the weight of gas adsorbed at a relative pressure P/P_0 and W_m is the weight of adsorbate constituting a monolayer of surface coverage. The term C, is the BET constant and is related to the energy of adsorption in the first adsorbed layer and consequently its value is an indication of the magnitude of the adsorbent/adsorbate interactions.

For the single point BET method with nitrogen, the C value is usually sufficiently large to warrant the assumption that the intercept in the BET equation is zero. Thus, the BET equation (2-4) can be written as (Quantachrome Corporation, 1994):

$$W_m = W(1 - P / P_0) \qquad (2\text{-}5)$$

The standard multipoint BET, experiment requires a minimum of three points in the appropriate relative pressure range. The weight of a monolayer of adsorbate W_m can then be obtained from the slope, s and intercept, i, of the BET plot. The total surface area of the sample can be expressed as:

$$S_t = \frac{W_m N A_{cs}}{M} \qquad (2\text{-}6)$$

where N is Avogadro's number (approximately 6.023×10^{23} molecules/mole), M the molecular weight of the adsorbate and A_{cs} is the cross-sectional area of the adsorbate molecules. The specific surface area S of the solid can be calculated from the total surface area S_t and the sample weight w:

$$S = \frac{S_t}{W} \tag{2-7}$$

The total pore volume is derived from the amount of vapour adsorbed at a relative pressure close to unity, by assuming that the pores are then filled with liquid adsorbate. The volume of nitrogen adsorbed (V_{ads}) can be converted to the volume of liquid nitrogen contained in the pores, by equation (2-7) (Quantachrome Corporation), assuming that macro-pores (≥500 Å) are absent in the sample.

$$V_{liq} = \frac{P_a V_{ads} V_m}{RT} \tag{2-8}$$

where P_a and T are ambient pressure and temperature, respectively, V_m is the molar volume of the liquid absorbate and R the gas constant (8.314 J/K·mol).

The average pore size can be estimated from the pore volume. For example, assuming cylindrical pore geometry, the average pore radius r_p can be determined from equation (2-9):

$$r_p = \frac{2V_{liq}}{S} \tag{2-9}$$

where S is the BET surface area (Quantachrome Corporation, 1994).

2.9 Density

Particle density is one of the more important parameters used to characterise filter media. Density (ρ) is a measurement of the mass (m) per unit volume (V) of a material and is reported in g/cm^3. Porous particles have two densities, the

envelope density and true (also termed the absolute, real, apparent, or skeletal) density. The true density is determined by the absolute volume of the material's solid phase and it is obtained when the volume measured excludes the pores and void spaces between the particles of the bulk sample. The envelope density is determined for porous materials when pore spaces within the material particles are included in the volume measurement. Envelope density will be less than the absolute density for porous materials.

The true density of the sample is measured using Archimedes' principle (Reeds, 1987). The measurement is frequently determined by immersing the sample in a liquid. It is assumed that the liquid fills all the pores. In some cases the material may be subjected to boiling in the test liquid to ensure pore penetration or sometimes the sample is evacuated prior to immersion to assist pore filling.

In this study, the determination of true density of SS used boiling water and evacuation with a venturi aerator for 30 min to exhaust the air from the pores and accelerate water penetration. The method was as follows:

- Weigh the dry SS sample (W_b).
- Boil in water, evacuated for 30 min and allowed to cool to 15°C.
- Weigh a 250 mL volumetric flask (W_c), and then pour the cooled sample and water into the flask making sure all the particles have been transferred.
- Make up to the mark with deaerated water, weigh flask plus suspension weight (W_d).
- Calculate the mass of water (W_w) in the flask:

$$W_w = W_d - W_c - W_b \tag{2-10}$$

Since the density of water is $\rho_{H_2O} = 0.999$ g/cm^3 at 15°C, then the volume of water in the flask is equal to $\frac{W_w}{\rho_{H_2O}}$. The true volume of the material in the flask

(V) = volume of flask – volume of water = 250 - $\frac{W_w}{\rho_{H_2O}}$. Particle density = (mass of dry particles W_b) / (volume of particles V).

To determine envelope density, the traditionally method involves sealing the pores prior to measurement of the volume with a material such as wax. This is difficult and time consuming. In this study, the envelope density of SS was determined by the following method:

- Place a desired amount of SS sample inside a Buchner flask and add enough water to cover the sample. Place the flask on a hotplate and evacuate with a venturi aerator at 0.013 atm for 30 min to exhaust the air in the pores.
- Transfer the sample to a sieve to remove excess water.
- Weight the sample with its pores filled (W_a).
- Dry the samples in oven at 103°C for 24 hr.
- Measure the dry weight of SS sample (W_e).
- Calculate the mass of water (W_f) in the pores:

$$W_f = W_a - W_e \tag{2-11}$$

Since the density of water is $\rho_{H_2O} = 0.999$ g/cm^3 at 15°C, the volume of pores is equal to $\frac{W_f}{\rho_{H_2O}}$. The envelope density = (mass of dry particles W_e) / (true volume of material V + volume of pores $\frac{W_f}{\rho_{H_2O}}$).

2.10 The determination of magnetic properties

Experimentally, the magnetic susceptibility of a compound is determined by measuring the extent to which a sample is attracted or repelled by an applied magnetic field. The effect of the magnetic field is followed by observing the change in the weight of the sample when the field is applied (Gouy Method). The majority of substances are repelled by a magnetic field (diamagnetic substances), and a small decrease in weight, is observed. The effect depends on the total number of electrons in the compound. Other materials are attracted by the field and show a weight gain in a magnetic field (paramagnetic substances). This effect arises from the presence of unpaired electrons.

The experimental procedure was as follows:

- Pack sample carefully up to a calibrated mark in a pre-weighed flat-bottomed Gouy tube.
- Suspend the tube in the balance so that the bottom of the tube is in the centre of the poles (position of maximum field) while the top of the sample is essentially clear of the field.
- Record weight of the sample both with and without the magnetic field switched on.

For pure compounds, the magnetic susceptibility can be calculated using the equation:

$$\chi_M = \frac{\beta \cdot \Delta \cdot M}{m} \times 10^{-3} \qquad (2\text{-}12)$$

Where χ_M is molar magnetic susceptibility; β is tube calibration constant (obtained by a Gouy experiment on a substance of known magnetic susceptibility e.g. Hg $[Co(NCS)_4]$ which has a molar magnetic susceptibility, $\chi_M = 8.085 \times 10^{-3}$ at 293 K; Δ is the weight increase in the magnetic field; M is the relative molecular mass and m is the mass of sample. In the current work, relative

molecular mass M was both unknown and undefined. Thus the magnetic effect was recorded as the weight gain per gram of sample when the magnetic field was applied. These values were compared with the weight gain per gram of magnetite (Fe_3O_4 99%) when exposed to the same field.

2.11 Equipment used in TM fabrication

2.11.1 Milling equipment

Milling has long been used to prepare finely divided materials. For most solid state reactions the formation of products is spatially separate from the reactants, causing reaction kinetics to be dependent on product size and morphology and limited by diffusion rates through the product phases. As a consequence, a high temperature is required to achieve a sufficiently high reaction rate (Schmalzried, 1995). The milling processes may break the product barriers and bring the reactants into constant intimate contact and the reaction could be substantially accelerated. In this study two milling processes were used for the purpose of comparison. One process was grinding starting materials in a low energy ball mill using partially stabilised Zironia balls and 100% acetone. The other one was milling the powders using a high energy mechanical mill (SPEX 8000 mill). The high energy mechanical mill is a powder metallurgy device in which reactant powders are milled under inert atmosphere. The energy transfer to the powder particles in these mills takes place by impacts between fast moving media such as balls, discs or rods between moving media and container wall. Before milling, the powder mixture and the stainless steel balls were placed in a hardened steel vial, which was then put in a glovebox. The glovebox was firstly evacuated and then filled with high purity argon. The vial was sealed under argon atmosphere. The powder was milled for 4 hr. The milling machine was fan cooled during milling.

2.11.2 Heat treatment equipment

Heat treatment of the powders was carried out in a ceramic tube furnace (Ceramic Engineering, Australia), which was fitted with an evacuation and argon refill system. The heat treatment was carried out under flowing argon. The furnace was programmed to operate at a heating and cooling rate of 5^0C/min and can be held at temperatures up to 1200^0C for required duration. The temperatures of the powder were measured using a K type thermocouple and recorded by a data acquisition system using a PC. In this study the temperature was increased to 1015^0C for 15 hr.

The furnace used was Radatherm 1700^0C Horizontal tube furnace (Radatherm Pty Ltd U.K.) with Eurotherm 2400 series programmable control system. The furnace is suitable for work tubes with up to 70 mm in outside diameter and has a 300 mm heated length. It is heated by six Kanthal Super 1800 resistance elements. Maximum temperature was 1700^0C. The chamber is insulated with special high temperature refractory fibreboard. In this study the reaction temperature of up to 1400^0C for 4 hr, under argon atmosphere was used.

2.12 Particle size analysis

Particle size analysis of the kaolin clay used as the model suspension for filtration studies was carried out using a Malvern Mastersizer-S laser diffraction particle size analyser , the (Malvern Instruments Ltd. Spring Lane South, U.K).

The instrument was used according to Mastersizer Manual (Laser Diffraction Particle Size Analysis- The Malvern mastersizer-S). One litre samples were prepared to give an appropriate obscuration (a measure of turbidity) and the scattered light analysed by the instruments software to give either the vulume size distribution or the number size distribution. The volume distribution was used in the present work.

2.13 References

APHA; AWWA; WEF. 1992. *Standard Methods for the Examination of Water and Wastewater.* 18th ed. American Public Health Association, American Water Works Association, Water Environment Federation, the United State of America.

Brunauer, S.; Emmett, P. H.; Teller, E. 1938. Adsorption of gases in multimolecular layers. *J. Am. Chem. Soc.* 60: 309-319.

Cullity, B. D. 1978. *Elements of X-ray Diffraction.* Second edition. California: Addision-Wesley Publishing Company, Inc.

GBC Scientific Equipment Pty Ltd. 1997. *Integra XL Inductively Coupled Plasma Operation Manual.*

Lipson, H.; Steeple, H. 1970. *Interpretation of X-ray Powder Diffraction Patterns.* Macmillan Co. London.

Quantachrome Corporation. 1994. *Operation Manual of Nova-1000 Gas Sorption Analyser.*

Reeds, J. S. 1987. *Introduction to The Principles of Ceramic Processing.* John Wiley & Sons, New York.

Schmalzried, H. 1995. *Solid State Reaction.* Weinheim, Germany.

Chapter Three: Characterisation of Natural and Synthetic Titanomagnetite

3.1 Introduction

Natural TM iron sand has fine particle size, high density and strong magnetic properties. As a filtration medium, it may achieve efficient removal of fine particles. However the filtration rate can be expected to be low and headloss can be expected to be high. In order to improve the hydraulic conductivity of fine TM, magnetic conditioning of the filter bed in an expanded form could be employed. It might be possible to compensate for consequent decreases in filtration efficiency by enhanced electrostatic effects.

Most impurities in natural water have negatively charged surfaces (Hunter and Liss, 1982; van der Mei, *et al.,* 1993). In order to increase the interaction between the particles and the collectors, a filter medium should have opposite surface charge. Natural magnetite has been found to possess positive surface charge in natural water pH range. This is exploited in the SIROFLOC process (Dixon, 1991; Anderson, *et al.,* 1980). Natural TM has some of the characteristics of natural magnetite, e.g. magnetic properties, but surface electrokinetic properties have not been studied. The purpose of the work presented in this chapter was to determine the surface electrokinetic properties and magnetic properties of natural TM.

Theoretically, there are five principal ways in which surface charge may originate (Stumm and Morgan, 1996; Park, 1965).

- Chemical reactions. Many solid surfaces contain ionisable functional group such as -OH. Surface charge is dependent on the degree of ionisation (proton transfer) and consequently on the pH of the suspending medium. For example, the electric charge of a magnetite surface in water can be explained by the acid-base behaviour of the =Fe-OH groups which found on the surface of hydrated magnetite

$$= Fe - OH^{+}{}_2 \xleftarrow{H^+} = Fe - OH \xleftarrow{OH^-} = Fe - O^-$$

Most oxides and hydroxides exhibit such amphoteric behaviour; thus the charge is strongly pH dependent, being positive at low pH values and at high pH a negatively charged surface is formed.

- Lattice imperfections and isomorphous replacements. At the solid phase boundary surface charge may be caused by lattice imperfections and isomorphous replacements within the lattice. For example, if in any array of solid SiO_2 tetrahedra a Si atom is replaced by an Al atom (Al has one electron less than Si), a negatively charged frame-work is established:

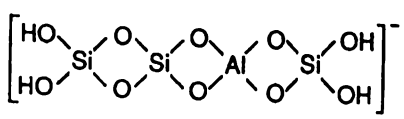

Similarly, isomorphous replacement of the Al atom by Mg atoms in networks of aluminium oxide octahedral also leads to a negatively charged lattice.

- Adsorption of a surfactant ion. A surface charge may also be established by adsorption of a surfactant ion. Preferential adsorption of one type of ion on the surface can arise from London - van der Waals interactions and from hydrogen or hydrophobic bonding.

- Surface corrosion. Physical and chemical surface corrosion may cause some species to be separated from the matrix forming defect surface conditions.

- Surface coating. Coatings of a surface with a cationic material may shift the IEP towards the IEP characteristic of the coating material.

According to Parks (1965), the isoelectric point reflects the chemical composition of the solid and the electrolyte in which it is immersed. Structural or adsorbed anionic impurities shift the IEP to more acid values and cationic impurities shift the IEP to more basic values or toward the IEP characteristic of the impurity

oxide. Oxidation and reduction resulting in nonstoichiometry may be expected to shift the IEP toward that characteristic of the oxidation state produced. Hydration increases the IEP; dehydration and increased structural perfection decrease the IEP.

In the present study the modification of TM was attempted in three ways:

- Chemical cleaning of natural TM with acid and base. The acid and base pre-treatment will facilitate the removal of contamination from the TM surface.
- Coating the TM with films of aluminium and iron hydrous oxides.
- Air oxidation at high temperatures.

3.2 *Properties of natural TM*

Natural TM is derived from the erosion of andesite and rhyolite of volcanic rock and concentration by ocean currents, wave action and wind action. In New Zealand, there are vast areas covered with TM sand such as the Waikato North Head, south of Auckland and Taharoa (Figure 3.1).

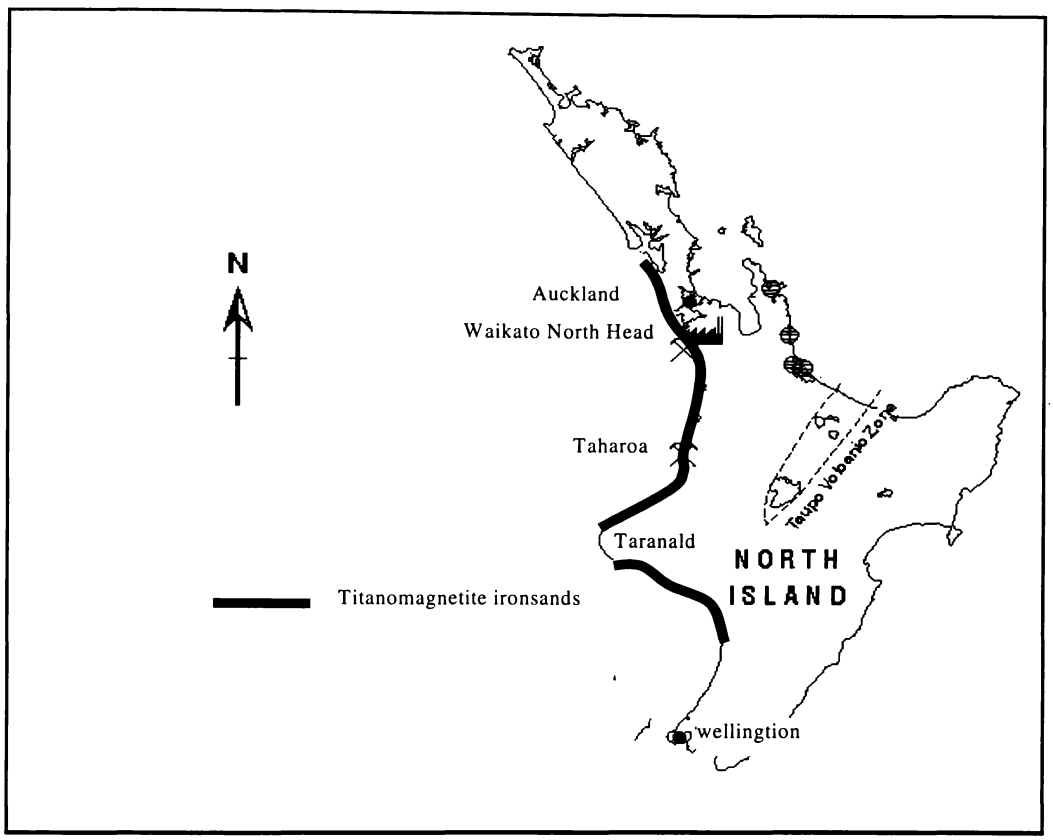

Figure 3.1 Locations of TM iron sand deposits in New Zealand.

3.2.1 *Physical and chemical properties of natural TM*

Naturally occurring TM iron sand has fine particle size, high density and strong magnetic properties. It also has high heat-resistance and high resistance to mechanical wear. The microstructure of natural TM can be regarded as Fe-Ti spinel oxide in which some of the iron has been replaced by other divalent and trivalent cations (Mg, Al, Cr, Mn and Zn) (Keefer and Shive, 1981). According to electronmicroprobe analysis, the most abundant minor cation species are Si and Al at up to 4.92% and 4.09% by weight respectively (see Table 3.1). Other elements such as Ca, P and K are also present. The total concentration of minor

constituents may therefore be appreciable, replacing a significant amount of the iron. The true density of natural TM is 3.81 g/cm^3 (see Section 2.9).

Table 3.1 Chemical composition of TM

Composite	Fe_2O_3+Fe O	TiO_2	SiO_2	AlO_2	MgO	CaO	MnO	P_2O_5	K_2O
Weight %	76.59	8.04	4.92	4.09	3.17	1.75	0.58	0.31	0.11

Composite	Nb	Zr	Y	Sr	Rb	Ga	Cr	Ba	Pb
(ppm)	18	51	15	25	10	47	59	807	8

*Analysis by Geoscience laboratory in Sudbury, Ontario, Canada.
Oxides measured in weight %, Heavy metals measured in ppm.

Elemental analysis by the EDAX method confirmed the main components of natural TM were Fe and Ti (See Figure 3.2).

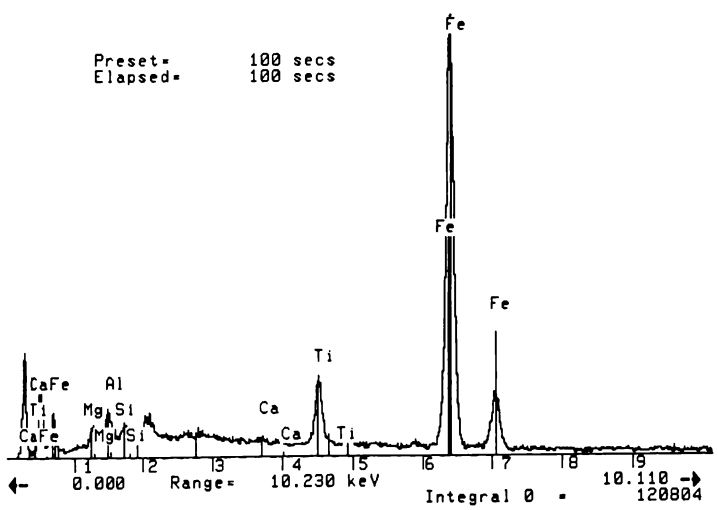

Figure 3.2 EDAX spectrum of natural TM

3.2.2 *XRD, SEM and EDAX of Natural TM*

Characterisation of natural TM was by X-ray diffraction (XRD) and Scanning electron microscopy (SEM) and energy-dispersive analysis by X-ray (EDAX).

The XRD pattern of natural TM is shown in Figure 3.3 and the identification file is given in Appendix 3.1.

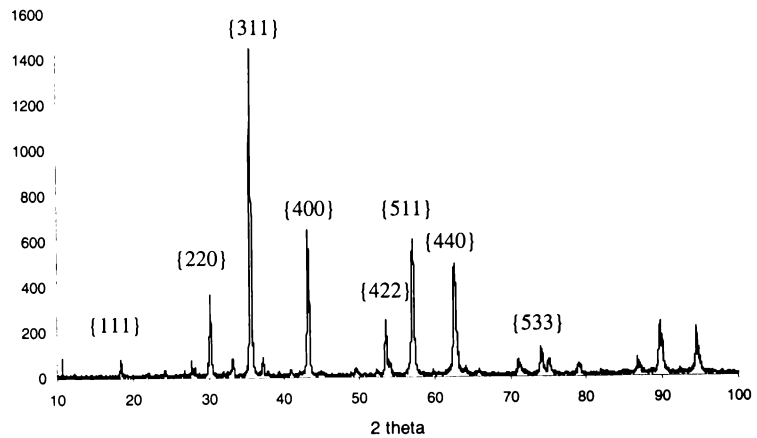

Figure 3.3 XRD pattern of natural TM

The main peaks of natural TM correspond to peaks obtained for magnesium iron aluminium chromium oxide: (Fe, Mg)(Al, Cr, Fe, Ti)$_2O_4$, (JCPDS, 25-1376) see Appendix 3.2.

The morphology of natural TM is shown in Figure 3.4.

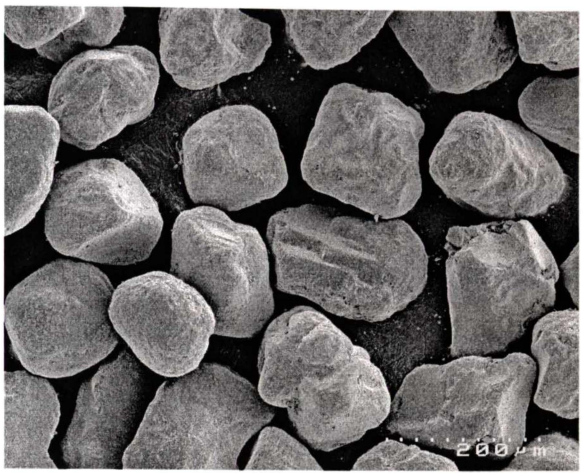

Figure 3.4 SEM micrograph of natural TM

3.2.3 *Isoelectric point of natural TM*

Electrokinetic properties of natural TM were determined by measuring streaming currents with a MUTEK PCD 03 instrument (Mutek Analytic Inc. Germany). The procedure was described in Section 2.5. Data for variation of potential (mV) with the pH of the suspension allowed the isoelectric point (IEP) of the particles to be determined. The streaming potential-pH curves for natural TM are given in Figure 3.5, that show the isoelectric point of water rinsed natural TM is 2.87 ± 0.06 (See Section 3.3.1). The results summarised in Appendix 3.3.

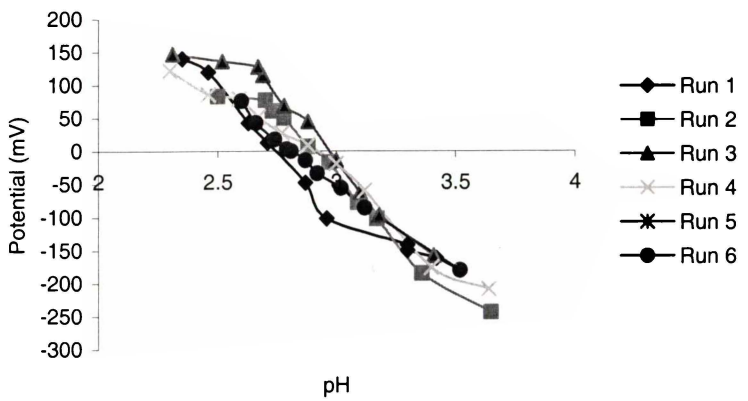

Figure 3.5 Variation streaming potential of TM with pH

3.3 *Effects of acid and alkali pre-treatment on IEP of natural TM*

The effects of water rinsing and acid and alkali treatment on the surface and electric kinetic properties of natural TM were investigated using XRD, SEM, EDAX and isoelectric point (IEP) measurement.

3.3.1 Experimental

Water rinsing

Primary concentrate of TM was further purified by magnetic separation, dispersion in distilled water with vigorous stirring and washing while held with magnetic field. The supernatant was concentrated by centrifugation and dried over night at 100^0C. The rinsing procedure was repeated three times. This material was labelled water rinsed TM (WRTM).

Acid and alkali rinsing

WRTM was equilibrated in de-ionized water at various pHs (pH from 3.51 to 8.20) for 24 hr. Took about 0.01 g of the wet samples for measuring the IEP.

3.3.2 Effect of rinse treatments

The IEP of TM rinsed with distilled water was found to be 2.87 ± 0.09, whereas the IEP of ARTM was found to be 3.64 ± 0.06.

Data for TM treated with the acid and alkali solutions are summarised in Table 3.2. The data indicated that treatment with the acid or alkali solutions raises the IEP. However there is no systematic trend with pH.

Table 3.2 pH effects on IEP of TM (24hr)

pH	3.51	4.27	5.5	6.34	7.04	8.20
IEP	4.01	3.49	3.51	3.63	3.53	3.60

The values reported in Table 3.2 are the means of at least six determinations. The standard deviation of each of determination was approximately 0.06.

3.3.3 Examination of impurities

The impurities separated magnetically during distilled water rinsing had an IEP of 2.80 ± 0.10. SEM and EDAX analysis showed the elemental composition was mainly Si and Al (Figure 3.6). These data are consistent with the impurities being clay particles (Iwasaki, 1962)

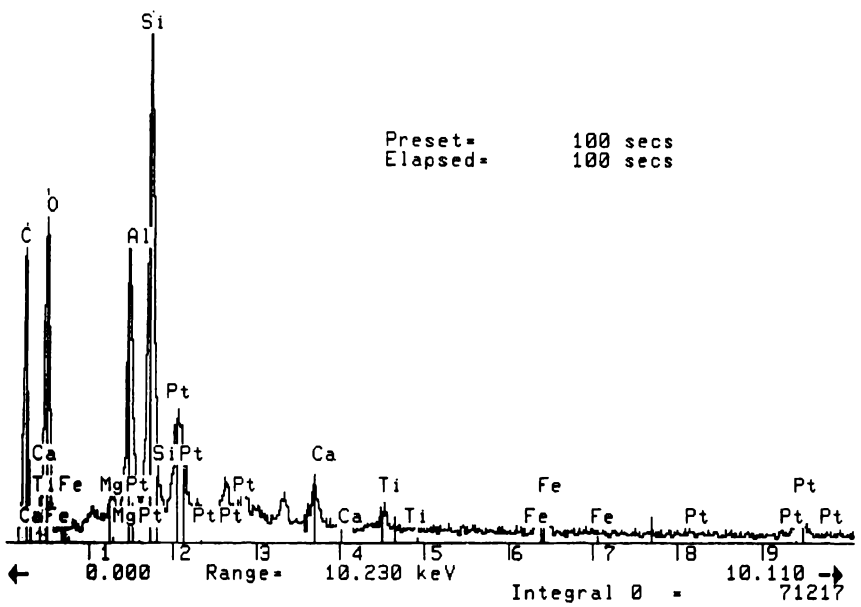

Figure 3.6 SEM and EDAX of silica and aluminium impurity

3.3.4 Effect of equilibration time

TM prepared as described as Section 3.3.1 was equilibrated in HCl and NaOH solutions (1.0, 0.1 and 0.01 mol/L) for times varying from 30 min to 17 day. Results are summarised in Table 3.3 and Table 3.4. Original data are presented in Appendix 3.4 and Appendix 3.5.

The data are quite variable and show no systematic trends. There is some evidence that acid treatment gives rise to higher values and prolonged treatment with both

acid and alkali gives lower values in most cases. However the results are not conclusive. Clearly, with the advantage of hindsight, it would have been useful to include more replicates. Similar variability after acid and alkali treatment of magnetite was observed by Kolarik and Dixon (1980). They attributed the effect to deposition of anionic species onto the surface. Such species may have originated from the sample itself or from the glassware used.

Table 3.3 IEP of natural TM and impurities pre-treatment with HCl

Rinsing solution	Concentration (mol/L)	Time (hr)	IEP	σ
Water	-	-	2.87	0.09
HCl	1.0	0.5	3.79	0.50
		1.5	3.57	
		3.0	3.94	
		4.5	3.76	
		7.5	4.58	
		25	4.02	
		3 (day)	4.39	
		17(day)	2.94	
		Σ/n	3.87	
HCl	0.1	0.5	3.36	0.36
		1.5	3.46	
		3.0	3.47	
		4.5	3.61	
		7.5	3.54	
		25	3.08	
		3 (day)	2.72	
		17(day)	2.85	
		Σ/n	3.32	
HCl	0.01	0.5	3.29	0.25
		1.5	3.54	
		3.0	3.36	
		4.5	3.46	
		7.5	3.40	
		25	3.12	
		3 (day)	3.07	
		17 (day)	3.85	
		Σ/n	3.39	

σ is standard deviation. The values reported in Table 3.3 and Table 3.4 are the means of at least six determinations.

Table 3.4 IEP of natural TM and impurities pre-treatment with NaOH

Rinse solution	Concentration (mol/L)	Time (hr)	IEP	σ
NaOH	1.0	0.5	2.81	0.13
		1.5	2.93	
		3.0	2.95	
		4.5	2.94	
		7.5	3.10	
		25	2.81	
		3 (day)	2.83	
		17(day)	3.14	
		Σ/n	2.94	
NaOH	0.1	0.5	3.18	0.13
		1.5	3.07	
		3.0	3.00	
		4.5	3.10	
		7.5	3.21	
		25	2.98	
		3 (day)	2.87	
		17(day)	2.86	
		Σ/n	3.03	
NaOH	0.01	0.5	3.33	0.15
		1.5	3.29	
		3.0	3.35	
		4.5	3.34	
		7.5	3.19	
		25	3.18	
		3 (day)	3.17	
		17(day)	2.91	
		Σ/n	3.22	

3.4 Studies of synthetic TM

3.4.1 Introduction

The microstructure of a material often depends on how it was synthesised and whether it was prepared in the laboratory or by nature. The formula unit for natural TM is $Fe_{3-x}Ti_xO_4$ ($0<x<1$ and $x\sim0.6$). Normally the minor constituents, M, are included and this compound can be written as $Fe_{3-x-\delta}M_\delta Ti_xO_4$ where δ may be in excess of 0.5. The presence of the minor constituents, especially diamagnetic Mg and Al, has a significant effect on the magnetic properties of the compound (O'Donovan and O'Reilly, 1977).

TM is generally non-stoichiometric with a (Fe + Ti)/O ratio of less than 0.75, i.e. on the oxidised (cation-deficient) side of stoichiometry. If the total number of cations per formula unit adds up to a fraction (R) of the stoichiometric value, 3, the compound may be written as $Fe_{(3-x-\delta)R}M_{\delta R}Ti_{xR}\square_{3(1-R)}O_4$ where $\square$ represents vacant cation lattice sites. At high temperatures ($\geq400^0$C) the composition range in which the cation-deficient spinel structure is stable is strictly limited. $x \sim 0.6$ and $R \sim 0.98$ represent the limit of the monophasic region (Hauptman, 1974). The extent of the region of low-temperature non-stoichiometry ($<400^o$C) appears not to be limited in this way (Readman and O'Reilly, 1970) and oxidation may proceed, maintaining a single spinel phase, until the compound contains virtually no Fe^{2+} ion.

Synthesis of TM has been reported in numerous investigations. Akimoto, *et al.* (1957) reported the first systematic study of the oxidation of TMs for compositions within the Fe_3O_4-Fe_2TiO_4-Fe_2O_3-Fe_2TiO_5 quadrilateral. Wechsler, *et al.* (1984) produced a series of TMs ($Fe_{3-x}Ti_xO_4$), from high purity Fe_2O_3, TiO_2, and Fe sponge at temperatures between 930^0C and 1350^0C. Similar work has been done by Brown and O'Reilly (1996). The purpose of this study was to prepare synthetic analogues of naturally occurring TM, without the impurities formed in natural materials and to study the magnetic and electrokinetic properties of these materials.

The synthetic process normally includes a pelleting and firing procedure. The first step of the process deals with pressing the reaction powders into a desired shape and tries to achieve green body strength to allow further handling. The second step of the process involves a consolidation to develop the desired microstructure and properties. The shaping process transforms the unconsolidated powder into a coherent consolidated body having a particular geometry and microstructure. Normally, the reaction powders are shaped by uniaxial pressing in a rigid die and then isostatic pressing at a pressure of typically 20-200 MPa to achieve strong and dense green bodies.

3.4.2 Materials and methods

Starting materials

The chemicals used are listed in Table 3.5. Stoichiometric amounts of high purity commercial grade Fe_2O_3, TiO_2 and Fe powders were weighed to ± 0.0001 g.

Table 3.5 Materials for synthesis TM

Chemicals	Purity	Appearance	Manufacturer
Fe	99.9%	Gray	Johnson Matthey
Fe_2O_3	99.99%	Reddish brown	Johnson Matthey
TiO_2	99%	White powder	APS Ajax Cinechem

Stoichiometric calculation

For phase composition investigations, stoichiometric calculation of the chemicals required is needed. Table 3.6 lists the atomic weights of elements Fe, Ti, O. The molar mass of the reaction compounds is assumed to be as Equation 3-1

Table 3.6 Atomic weights of the elements Ti, Fe, O, and their oxides

Formula	Ti	Fe	O	TiO_2	Fe_2O_3	$Fe_{2.4}Ti_{0.6}O_4$
Molar mass (M)	47.900	55.847	15.999	79.898	159.691	226.769

$$14\ Fe_2O_3 + 9\ TiO_2 + 8\ Fe \Rightarrow 15\ Fe_{2.4}Ti_{0.6}O_4 \qquad (3\text{-}1)$$

14 9 8 15

According to this equation,

$\frac{W_A}{M_A} = 14$, $\frac{W_B}{M_B} = 9$, $\frac{W_C}{M_C} = 8$ and $\frac{W_D}{M_D} = 15$, where: $M_{A, B, C, D}$ = molar mass (or formula weight) of Fe_2O_3; TiO_2; Fe; $Fe_{2.4}Ti_{0.6}O_4$; respectively and $W_{A,B,C,D}$ = weight of Fe_2O_3; TiO_2; Fe; $Fe_{2.4}Ti_{0.6}O_4$ required respectively.

Therefore, the weights of the starting powders required for a given amount of mixture (W_D) can be worked out using Equations (3-2) to (3-4).

$$W_A = \frac{14}{15}\frac{M_A}{M_D} W_D = 0.65725\ W_D \qquad (3\text{-}2)$$

$$W_B = \frac{9}{15}\frac{M_B}{M_D} W_D = 0.21139\ W_D \qquad (3\text{-}3)$$

$$W_C = \frac{8}{15}\frac{M_C}{M_D} W_D = 0.13135\ W_D \qquad (3\text{-}4)$$

Specifically, if W_D = 20.0000 g, then, W_A = 13.1450 g Fe_2O_3, W_B = 4.2279 g TiO_2 and W_C = 2.6269 g Fe.

The synthetic process

The methods selected for synthesising TM ($Fe_{2.4}Ti_{0.6}O_4$) were similar to the method of Brown and O'Reilly (1996). The two synthetic procedures are illustrated in Figure 3.7. In addition, a high temperature synthetic condition was used in this study. The two synthetic methods involved a number of steps to ensure that the powders were mixed as well as possible before being reacted. In order to avoid the mixture forming a cake and to achieve full mixing, the first method involved grinding the starting materials in a low energy ball mill using partially stabilised zirconia (PSZ) balls and acetone. The acetone was subsequently evaporated at 60^0C.

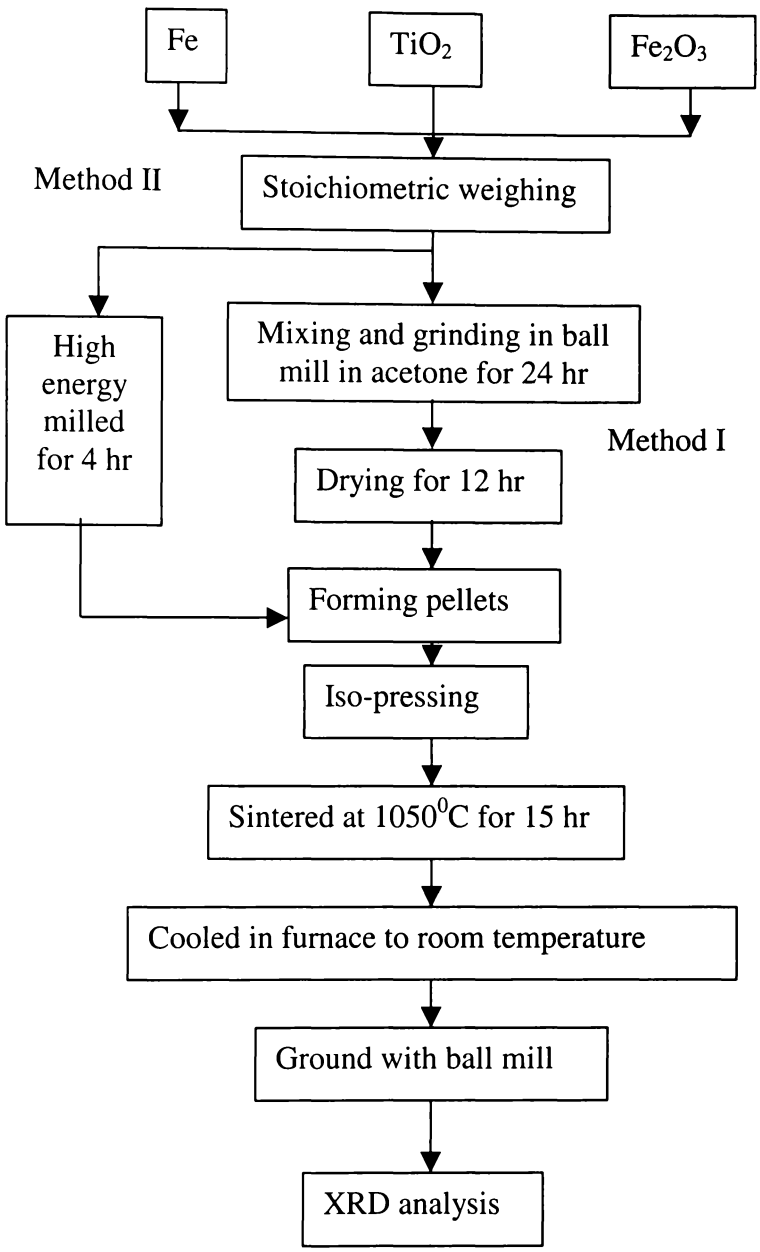

Figure 3.7 Flow diagram for the synthesis of TM

The second method involved milling the powder in a high energy ball mill. In both methods I and II, pellets were produced and then sintered at 1050^0C for 15 hr. In a third method, the powders produced using low and high-energy ball milling were directly sintered at 1400^0C for 4 hr. The high temperature (1400°C) synthetic processes were carried out under an argon atmosphere.

The following is the detailed description of methods I and II.

Method I:

- Stoichiometric quantities of iron (III) oxide, iron metal and titanium oxide powders were weighed and mixed together in acetone in a low energy ball mill. The milling duration was 24 hr.
- The mixed powders were pressed into a disc of 8 mm diameter and 20 mm height at a pressure of 30 MPa using a uniaxial hydraulic press. The disc was then pressed again at 200 MPa using a cold isostatic press.
- The powders were sealed in a quartz tube under vacuum of 10^{-2} torr and sintered at 1050^0C for 15 hr.
- The sintered pellets were allowed cool to room temperature.
- The disc samples were milled for 4 hr in a low energy ball mill to yield a very fine powder with average particle size of approximately 5 μm.

Method II:

- The powders were accurately weighed according to the stoichiometric calculation.
- The weighed (20g) materials were milled in a high-energy mechanical mill (SPEX 8000) at speed of 1500 rpm for 4 hr.

- The milled powder was pressed into a disc of 8 mm diameter and 20 mm height at a pressure of 30 MPa by using a uniaxial hydraulic press. The disc was then pressed again at 200 MPa using a cold isostatic press.
- The powder was sealed in a quartz tube under a vacuum of 10^{-2} torr and sintered at 1050^0C for 15 hr.
- The sintered disc was cooled to room temperature.
- The disc sample was milled for 4 hr using a low energy ball mill to yield a powder with a fine particle size of approximately 5 μm.

3.4.3 Results

X-ray diffraction analysis

The XRD patterns of the powders produced after milling the mixtures of Fe_2O_3, TiO_2 and Fe powders for 24 hr using the low energy roller mill and for 4 hr using the high energy ball mill are shown in Figure 3.8.

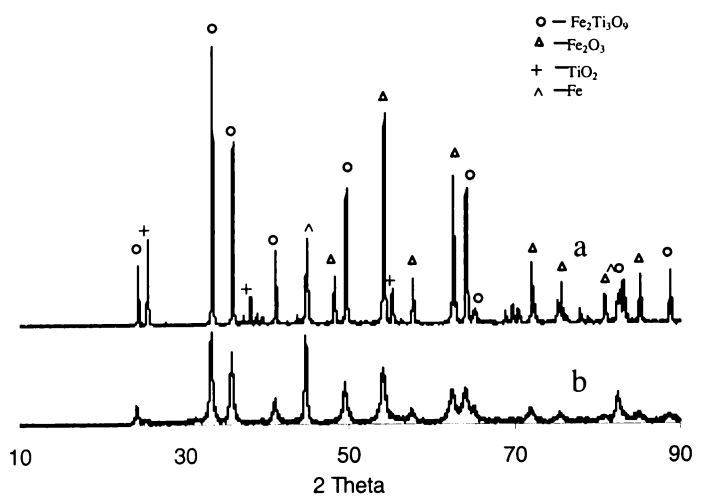

Figure 3.8 XRD patterns of (a) the powder produced using low energy ball milling; (b) the powder produced using high energy ball milling.

The XRD patterns show the powder produced by using two milling processes produce different products. The powder produced by using low energy ball mill

(Figure 3.8 a) had a mixture of crystal phases: $Fe_2Ti_3O_9$ (JCPDS 29-1494), Fe_2O_3 (JCPDS 13-0534), TiO_2 (JCPDS 02-0387) and Fe (JCPDS 03-1050). It is clear that some residual Fe and TiO_2 remain. On the other hand, the powder produced by high energy ball mill (Figure 3.8 b) consisted mainly of $Fe_2Ti_3O_9$, Fe_2O_3 and Fe. This shows that in both milling processes, Fe_2O_3 and TiO_2 reacted during milling.

Figure 3.9 shows the XRD patterns of the powders produced by heating the milled powders to 1050°C. The main peaks of the synthetic product of the high energy ball milled powder (Figure 3.9 a) correspond to peaks obtained for synthetic iron titanium oxide ($Fe_{2-x}Fe_{2x}Ti_{1-x}O_4$) (JCPDS 24-0536). The synthetic products of the low energy ball milled powder were a mixture of $Fe_2Ti_3O_9$ (JCPDS 40-0850) and $FeFe_2O_4$ (JCPDS 19-0629).

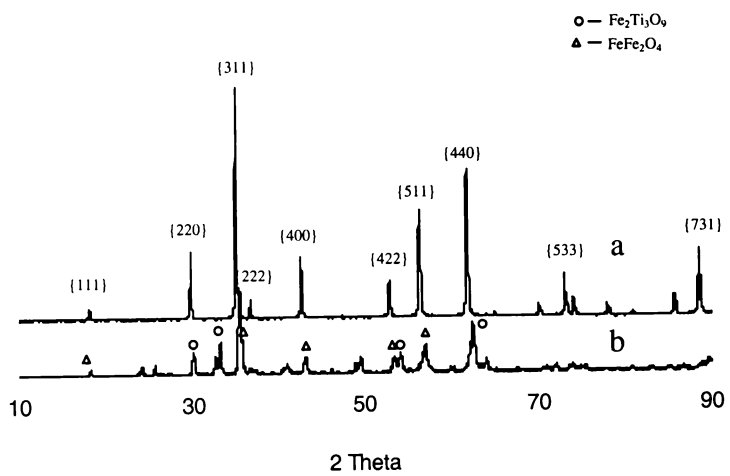

Figure 3.9 XRD pattern of synthetic TM heated to 1050°C (a) high energy ball mill powder; (b) low energy ball mill powder.

The XRD patterns of the powders produced by heating the ball milled powders to 1400°C are shown in Figure 3.10. Both of the products were $Fe_{2-x}Fe_{2x}Ti_{1-x}O_4$. However, the high energy ball milled product gave sharper peaks of higher intensity indicating a higher degree of crystallinity.

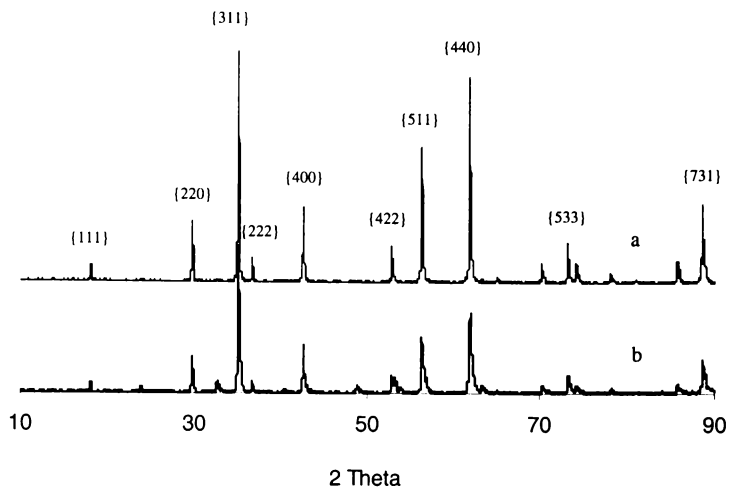

Figure 3.10 XRD patterns of TM heated to 1400°C (a) high energy ball mill powder; (b) low energy ball mill powder.

Electrokinetic properties

Electrokinetic properties of the powders produced using low and high energy ball milled and heating at 1050°C and 1400°C were determined by recording streaming currents described in Section 2.6. Data are summarised in Table 3.7. The IEP of acid and alkali rinsed TM (natural TM) is included for comparison. It is clear that the behaviour of the synthetic product is similar to that of the natural product.

Table 3.7 IEP of natural and synthetic TM

Materials	Natural TM	High energy ball mill powder	Low energy ball mill powder	High energy ball mill powder synthesis at 1050°C	Low energy ball mill powder synthesis at 1050°C	High energy ball mill powder synthesis at 1400°C	Low energy ball mill powder synthesis at 1400°C
IEP	3.64	3.74	3.59	3.81	3.61	3.90	3.72

The values reported in Table 3.7 are the means of at least six determinations. The standard deviation of each of determination was approximately 0.06.

Magnetic properties

The magnetic properties of natural and synthetic TM were examined by measuring the weight change in an applied magnetic field (Gouy Method). The measuring procedure was described in Section 2.10. Pure magnetite (Fe_3O_4, 99.99 %, Alfa Aesar) data are presented for comparison. Results are shown in Table 3.8.

Table 3.8 Magnetic properties of natural and synthetic TM

Materials	Mass (m) ± 0.001 (g)	Weight increase (Δ) ±0.001 (g)	Δ/m ±0.002	$(\Delta/m)/(\Delta/m)_{Fe3O4}$ (%)±0.3%
Fe_3O_4(99.99%)*	0.541	10.610	19.612	100
Natural TM	1.121	17.720	15.790	80.5
High energy ball mill powder	0.856	5.248	6.131	31.3
Low energy ball mill powder	0.536	2.748	5.127	26.1
High energy ball mill powder synthetic at 1050^{0}C	1.064	8.626	8.107	41.3
Low energy ball mill powder synthetic at 1050^{0}C	0.818	5.976	7.306	37.3
High energy ball mill powder synthetic at 1400^{0}C	0.738	10.593	14.354	73.2
Low energy ball mill powder synthetic at 1400^{0}C	1.119	13.110	11.716	59.7

*Pure magnetite (Fe_3O_4, 99.99%, Alfa Aesar)

* Errors estimated according to Morris, 1997 (Morris, 1997).

3.4.4 Discussion

The high energy ball milling process brings the reactants into intimate contact and energy transferred to the powder facilitates the reaction. Figure 3.8 shows the XRD patterns of the products formed by two milling processes. Both of the unheated products have $Fe_2Ti_3O_9$ and Fe_2O_3 phases, but TiO_2 phase could not be detected in the high energy ball milled powder. It is apparent that the TiO_2 fraction reacted with other materials and produced new phases under the conditions of high energy ball milling.

The present study shows that the synthetic TM ($Fe_{2-x}Fe_{2x}Ti_{1-x}O_4$, x = 0.4) can be prepared by heating the milled stoichiometric starting materials (Fe_2O_3, TiO_2 and Fe) at high temperature. For the high energy ball milled powder, the TM can be formed at 1050°C. For the low energy ball milled powder a temperature of 1400°C was required.

At the temperature of 1050°C, the products obtained from the high energy ball milled powder presented a single phase ($Fe_{2-x}Fe_{2x}Ti_{1-x}O_4$, x = 0.4); while the products obtained from low energy ball milled powder produced $Fe_2Ti_3O_9$ and $FeFe_2O_4$. Heating both powders to 1400°C, produced a single phase TM ($Fe_{2-x}Fe_{2x}Ti_{1-x}O_4$, x = 0.4) (Figure 3.10). The product formed from the low energy ball milled powder showed relatively weak peaks in the XRD patterns.

The IEP of the various products formed were all quite similar, varying from 3.59 to 3.90. On the other hand, the products presented variable magnetic properties. Table 3.8 lists the magnetic properties of each product. The high energy ball milled powder heated to 1400°C exhibited the strongest magnetic properties, followed by the product of low energy ball milling heated to the same temperature.

3.5 Oxidation of TM at high temperature

3.5.1 Materials and methods

Synthetic TM prepared at 1050°C using high energy ball milled and low energy ball milled powders were selected for this study. The samples were placed in a high temperature furnace (Radatherm Horizontal tube furnace) in air at 1400°C for 4 hr and then cooled in the furnace to room temperature.

3.5.2 Results

X-ray diffraction analysis

The XRD patterns of the oxidation products are shown in Figure 3.11. The same product was obtained from both synthetic TM samples and contained a mixture of the phases: Fe_2TiO_5 (JCPDS 09-0182) and Fe_2O_3 (JCPDS 24-0072).

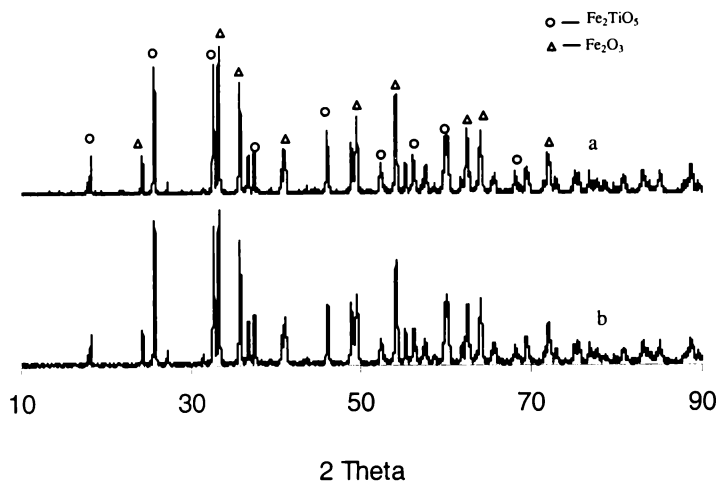

Figure 3.11 XRD pattern of oxidised synthetic TM (a) high energy ball milled powder; (b) low energy ball milled powder.

Electrokinetic properties

Electrokinetic properties of the two oxidized products were determined as described in Section 2.6. The results are summarised in Table 3.9.

Table 3.9 IEP of oxidized synthetic TM

Materials	Oxidized synthetic TM produced from high energy ball milled powder	Oxidized synthetic TM produced from low energy ball milled powder
IEP	3.81	3.83

The values reported in Table 3.9 are the means of at least six determinations. The standard deviation of each of determination was approximately 0.06.

Magnetic properties

The magnetic properties of oxidized synthetic TM were determined using the method described in Section 2.10. The results are summarised in Table 3.10.

3.5.3 Discussion

The products of oxidized synthetic TM are a mixture of Fe_2TiO_5 and Fe_2O_3. The oxidation processes had pronounced effect on the magnetic properties of the materials. The Fe^{2+} cation oxidized to Fe^{3+} and the magnetic properties were lost (Table 3.10). On the other hand, the IEP of the products remained at about 3.8. Apparently, oxidation of Fe(II) to Fe(III) has little effect on IEP. This is consistent with the IEP of TM being dominated by the Fe(III) component

Table 3.10 Magnetic properties of oxidized synthetic TM

Materials	Mass (m) ± 0.001 (g)	Weight increase (Δ) ± 0.001 (g)	Δ/m ± 0.002	$(\Delta/m)/(\Delta/m)_{Fe3O4}$ (%)± 0.3%
Fe_3O_4	0.541	10.610	19.612	100
Natural TM	1.121	17.720	15.790	80.5
Oxidized synthetic TM from high energy ball mill powder	0.984	0.017	0.020	0.1
Oxidized synthetic TM from low energy ball mill powder	0.906	0.032	0.003	0.1

3.6 Chemical treatments of TM

3.6.1 Coating trials: TM and aluminium

The IEP of natural and synthetic TM is lower than is desirable for applications involving filtration of water containing negative colloids. The work in this section reports attempts that were made to increase the IEP by chemical treatments.

Polymerised aluminium precursor solutions

It is known that by adding NaOH to an $AlCl_3$, $Al(NO_3)_3$, or $Al(ClO_4)_3$ solution, $Al(OH)_3$ is formed at a NaOH/Al mole ratio of 3.0 to 3.3, but the initial reaction products are clear solutions at a NaOH/Al mole ratio ≤ 2.5. Clear solutions can be obtained even at a NaOH/Al mole ratio of 2.7 if NaOH is added very slowly. It has been recognised that the hydrolysed species in these partially neutralised solutions are positively charged OH-Al polymers (Hsu and Bates, 1964; Tsai and Hsu, 1985). The OH-Al polymers resemble fragments of crystalline $Al(OH)_3$. Crystalline $Al(OH)_3$ exists in three polymorphs: gibbsite, bayerite and nordstrandite. They are composed of the same fundamental units: two planes of

close-packed OH^- with Al^{3+} sandwiched between them. The Al^{3+} reside in two-thirds of the octahedral holes and are distributed in hexagonal rings. In the interior, each Al^{3+} shares six OH^- with three other Al^{3+} and each OH^- is bridged between two Al^{3+} (Figure 3.12). At the edge, however, each Al^{3+} shares only four OH^- with two other Al^{3+} and the other two co-ordination sites are occupied by one OH^- and one H_2O molecule; neither is bridged between Al^{3+}. Kinniburgh (1975) suggested the following configuration:

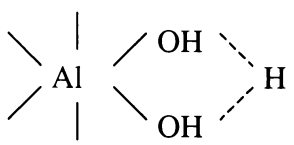

A necessary requirement for a stable structure is that the repulsion between Al^{3+} be approximately balanced by the attraction of Al-OH-Al linkages. This principle

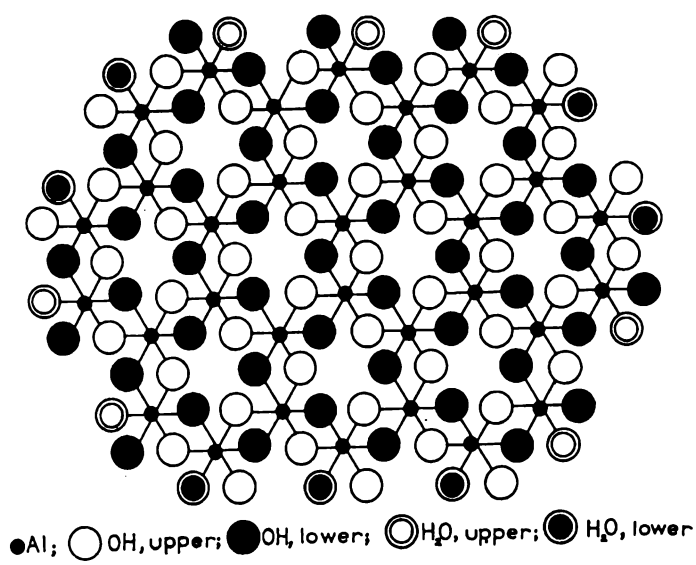

Figure 3.12 Schematic representation of the unit layer of $Al(OH)_3$. Edge, unshared OH may protonate as a function of pH to form H_2O

also should hold for the OH-Al polymers in solution. That is, if the OH-Al polymers are of stable structure, the arrangement of Al^{3+} and OH^- in the product should follow a pattern similar to $Al(OH)_3$ solids. In the $Al(OH)_3$ structure,

however, each OH^- at the edge is linked to only one Al^{3+} and therefore is in rapid equilibrium with the H^+ or OH^- in solution. The isoelectric point of $Al(OH)_3$ is in the range from pH 8.0 to 9.2 (Parks, 1965). Therefore, $Al(OH)_3$ particles, large or small, are always positively charged in an acid medium (Stol, *et al.,* 1976; Smith and Hem, 1972; Schoen and Roberson, 1970). The schematic illustration of a series of positively charged OH-Al polymers is shown in (Figure 3.13). The polymers are named according to the number of aluminium atoms contained, for example the polymer containing 13 aluminium atoms is known as Al_{13}. The amount of Al_{13} polymer is related to Al concentration, the OH/Al ratio and the rate of base addition to Al solutions.

Some studies have revealed that such partially neutralized solutions are metastable and eventually turn turbid, with crystalline $Al(OH)_3$ developing after prolonged ageing, accompanied by a decrease in solution pH (Tsai and Hsu, 1985; Hsu, 1988).

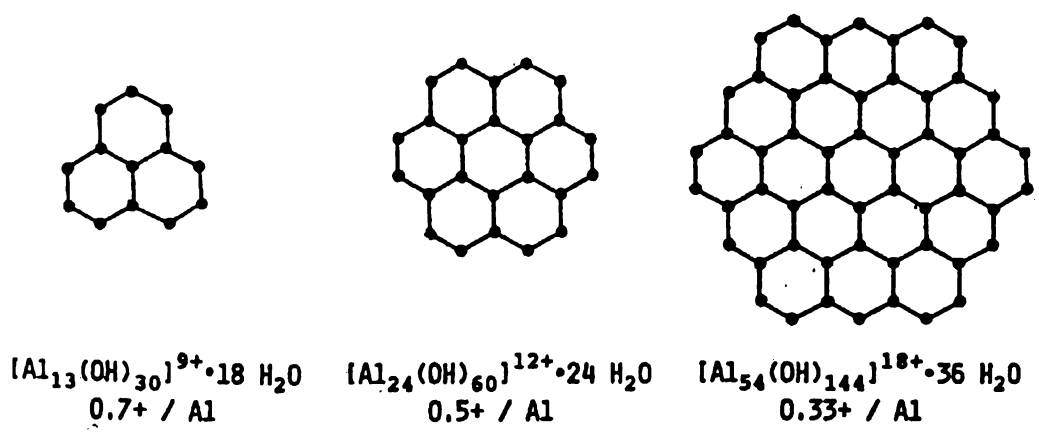

Figure 3.13 Schematic representation of a series of positively charged OH-Al polymers of structures resembling fragments of gibbsite (modified from Hsu & Bates, 1964). Two OH^- are shared between two adjacent Al^{3+} (black dots). Each edge Al^{3+} is co-ordinated by 4 OH^- and 2 H_2O. OH^- and H_2O are not shown in the sketch for the sake of clarity.

Johansson (Johansson, 1960; 1963) prepared well-crystallised basic Al sulphates or selenates by adding Na_2SO_4 or Na_2SeO_4 to a partially neutralised Al solution of a NaOH/Al mole ratio of 2.5. The x-ray structural analysis suggested that these crystals were composed of a fundamental unit of composition

$[Al_{13}O_4(OH)_{24}(H_2O)_{12}]^{7+}$. This structure consists of one Al^{3+} at the centre, tetrahedral co-ordinated to 4 O^{2-} and surrounded by 12 Al^{3+}, each co-ordinated to 6 OH^-,H_2O, or the O^{2-} shared with the Al^{3+} at the centre (Figure 3.14). Johansson suggested that the OH-Al poly-nuclear complex in solution was of the same configuration. The existence of this species in solution also was suggested by Aveston (1965) using ultra-centrifugation and potentiometric titration and by Rausch and Bale (1964) and Bottero, *et al.* (1982) using small-angle X-ray diffraction analysis.

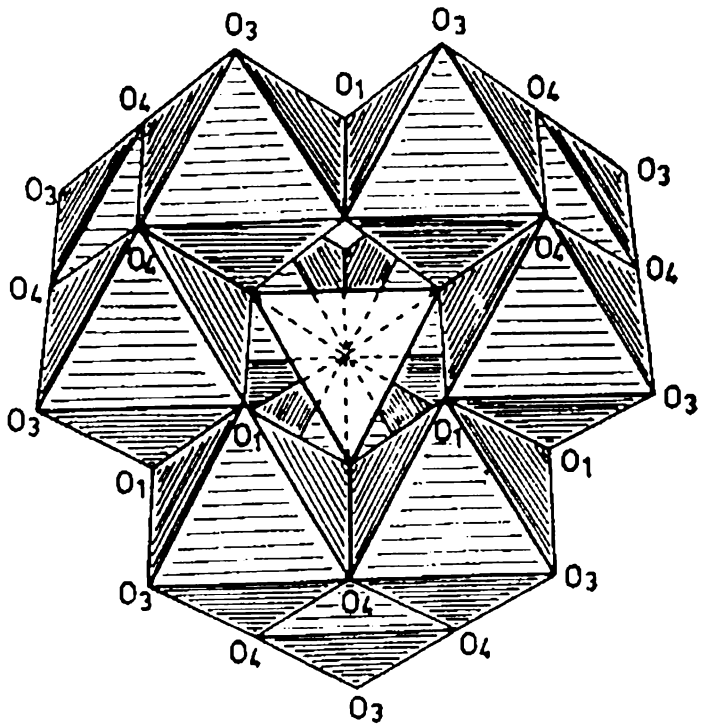

Figure 3.14 Truncated tetrahedral structure of $[Al_{13}O_4(OH)_{24}(H_2O)_{12}]^{7+}$ polymers showing the tetrahedral AlO_4 at the centre, surrounded by 12 Al^{3+} ions in octahedral configuration. The 12 octahedrally co-ordinated Al^{3+} ions may be viewed as being composed of four trioctahedral $Al_3(OH,H_2O)_{12}$ units (modified from Johannson, 1960)

For the preparation of surface films of hydrolysed aluminium species it was envisaged that the use of the aluminium polymers would be more likely to form coherent films with minimum consumption of aluminium. The adsorption of a monolayer of aluminium polymer followed by further polymerisation was envisaged.

In this study the aluminium polymer precursor solution used to treat TM was prepared by adding NaOH very slowly to an $AlCl_3$ solution with vigorous stirring until a Na/Al mole ratio of 2:1 was obtained. The partially neutralised clear solution was believed to contain aluminium polycations consisting of 13 Al atoms. Appendix 3.6 (a) shows the crystal morphology of Al_{13}. It is similar to that described by Turner (1976a). According to Turner, with increased ageing of the parent OH-Al solution, the population of the tetrahedral crystals gradually decreased, whereas an X-ray amorphous spherical precipitate gradually developed. This in turn, was replaced by irregularly shaped crystals with a distinctly different XRD pattern and greater resistance to acid dissolution. With very old OH-Al solutions, only the irregularly shaped crystals were observed upon the addition of Na_2SO_4. With a NaOH/Al mole ratio of 1, the precipitate was dominated by X-ray amorphous spherical particles, with only trace amounts of tetrahedral crystals even from freshly prepared OH-Al solutions (Turner, 1976a; 1976b).

Surface treatment method

TM used in this study was ARTM (see Section 2.21). The coatings were carried out under various pH conditions. The following procedure was used.

- The desired amount of ARTM was placed in a Buchner flask and evacuated with a venturi aerator until all air had been excluded. The Al_{13} polymer solution was then sucked into the flask and the system stirred.

- NH_3 solution (25%) was added to the mixture up to achieve desired pH value.

- The liquid was decanted and the solid mixture was oven dried at 100^0C for 24 hr.
- The dried samples were rinsed thoroughly with various pH de-ionized water until rinsings were clear.
- The samples were oven dried at 100^0C for a further 24 hr.
- The above steps were repeated for various pH conditions.
- The samples obtained were named: '$ARTM_{Al\text{-}n}$' (n=1-5).

A flow diagram for the coating procedure is illustrated in Figure 3.15 below.

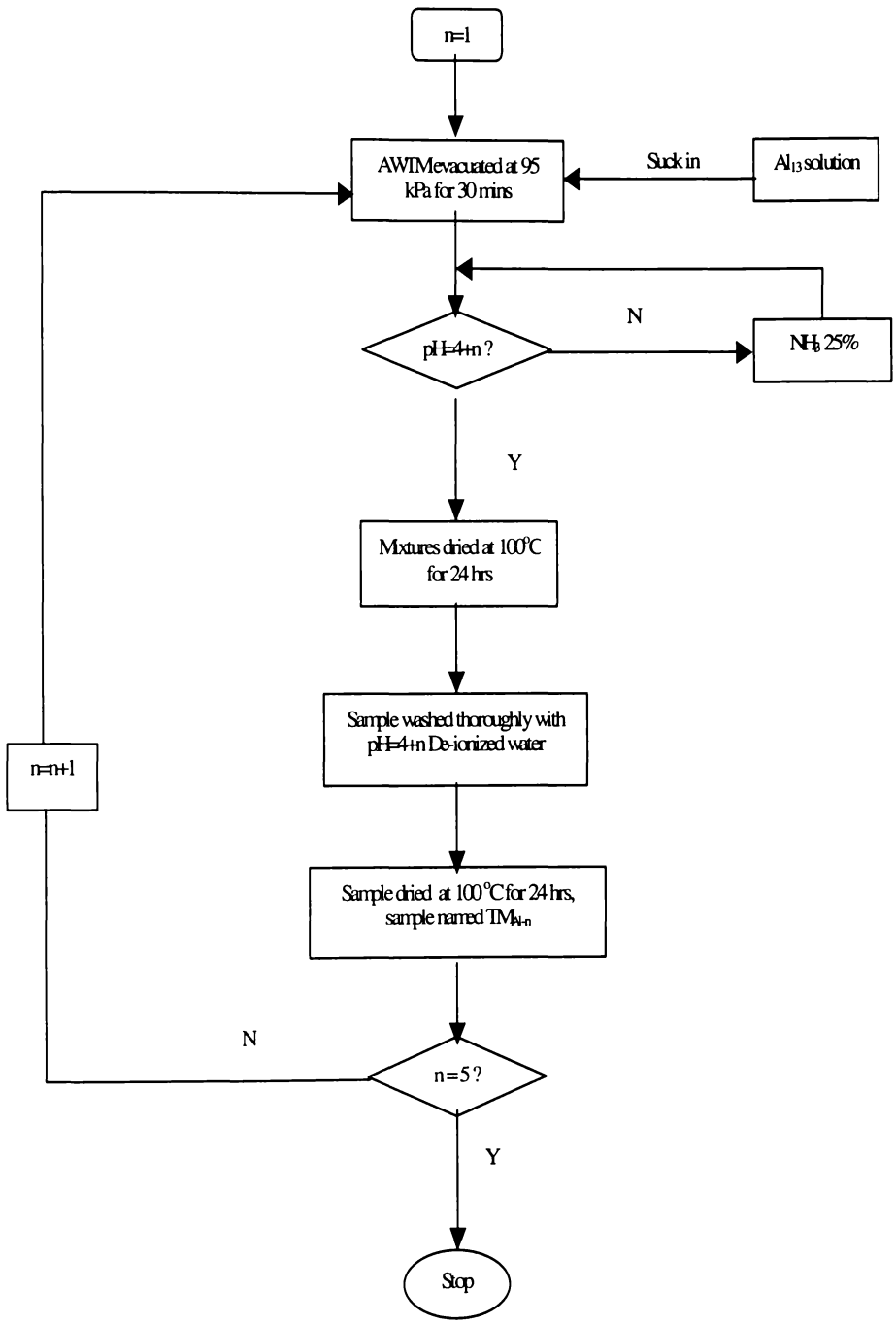

Figure 3.15 Flow diagram for treatment of TM with Al polycations at various pH values.

3.6.2 *Results and discussion*

The amount of aluminium deposited in the surface films was determined by extracting the treated ARTM sample with 4 mol/L HNO_3 and analysing the extract using ICP Emission Analysis. The measurement procedure was described in Section 2.7. Table 3.11 gives the ICP analysis data and IEP data for untreated ARTM and ARTM samples treated with aluminium at various pH values.

The results indicate that the IEP of the aluminium treated ARTM was not affected by the various pH coating conditions. Further, the Al extracted from the aluminium treated ARTM was little higher than the Al extracted from untreated ARTM (iron data for the untreated ARTM and aluminium treated ARTM are also included) It appears that any film of $Al(OH)_3$ formed on ARTM is unstable and is lost from the surface during rinsing.

Table 3.11 Properties of Al coating films on ARTM at various pHs.

Materials	ARTM	$ARTM_{Al\text{-}1}$	$ARTM_{Al\text{-}2}$	$ARTM_{Al\text{-}3}$	$ARTM_{Al\text{-}4}$	$ARTM_{Al\text{-}5}$
pH ± 0.01		5.68	6.83	7.58	8.30	9.13
IEP ± 0.06	3.64	3.74	3.72	3.71	3.45	4.18
Al x 10^3 ± 0.001(mole /g)	1.257	1.599	1.602	1.788	1.685	1.737
Fe x 10^3 ± 0.001(mole /g)	0.889	0.879	0.868	0.875	0.854	0.873

The IEP of ARTM is 3.64 (see Section 3.3.2). At the pH of the Al_{13} precursor solution (pH = 4.16), the ARTM will be negatively charged. Adsorption of the polymers should have been favoured by electrostatic forces. It had been expected the $Al(OH)_3$ formed when NH_3 solution was added to the Al_{13} would be positive providing the pH remained below the IEP of $Al(OH)_3$ (pH = 8.90). This was so except for the experiment in which the final experiment pH was 9.13. The charge

of the ARTM and $Al(OH)_3$ should have been favourable for the formation of a coating film. It appears that if such films were formed, they did not survive the rinsing and drying steps that followed the Al treatment. It could be that the smooth, non-porous nature of ARTM surface is unfavourable for the retention of coating films.

3.6.3 Coating trials: TM and iron

Polymerised iron precursor solutions

Addition of base to $Fe(NO_3)_3$, $Fe_2(SO_4)_3$, $Fe(ClO_4)_3$ or $FeCl_3$ solutions in amounts insufficient to precipitate hydrous oxide results in the rapid formation of a red hydrolytic polymer (Murphy, *et al.,* 1976; Dousma and de Bruyn, 1979). The formation consists of several steps: 1) formation of low-molecular-weight species; 2) formation of a red cationic polymer; 3) ageing of the polymer, with eventual conversion to oxide phases; and 4) precipitation of oxide phases directly from low-molecular-weight precursors. Hsu and Ragone (1972) analysed the precipitates obtained by adding sodium sulphate solution to hydrolysed 0.01 mol $Fe(ClO_4)_3$ solutions and obtained results that indicate that the polymer is cationic.

Hydrolysed Fe(III) solutions containing the red polymer are not at equilibrium. The changes observed on ageing solutions containing the polymer include changes in chemical composition (Hsu and Ragone, 1972; Murphy, *et al.,* 1975), decrease in pH (Hsu and Ragone, 1972; Murphy, *et al.,* 1975), increase in light absorption (Dousma and de Bruyn, 1978), increase in turbidity or light scattering (Hsu and Ragone, 1972; Dousma and de Bruyn, 1978), increase in sedimentation coefficients and increase in particle size (Murphy, *et al.,* 1975; Dousma and de Bruyn, 1978), decrease in the rate of degradation of the polymer by acid (Sommer, *et al.,* 1973).

Brady, *et al.* (1968), Coda, *et al.* (1975) and Christoph, *et al.* (1979) studied the structural data and found that the iron atoms in the polymer have co-ordination number 6. The presumed $Fe(O,OH,H_2O)_6$ octahedron in the polymer is most likely connected by sharing vertices or edges. Brady, *et al.* (1968) suggested they

may form long chains or ribbons, which are coiled and to some extent cross linked.

In this study, the iron polymer precursor solution used to coat the TM was prepared by adding NaOH to $FeCl_3$ solution in a mole ratio of 2:1. Appendix 3.6 (b) shows the crystal morphology of the Fe polymer. Before ageing, the solution was evacuated until no more air was released in order to saturate the TM surface. NH_3 solution was added to complete the hydrolysis process.

Surface treatment method

TM was treated according to the procedure outlined in Section 2.2.1. The coating procedure was as described in Section 3.6.1.

The samples obtained were named: '$ARTM_{Fe\text{-}n}$' (n=1-5).

3.6.4 Results and discussion

The ICP analysis data and IEP data for untreated ARTM and ARTM samples treated with iron at various pH values are shown in Table 3.12.

Table 3.12 Properties of Fe coating films on ARTM at various pHs

Materials	ARTM	$ARTM_{Fe\text{-}1}$	$ARTM_{Fe\text{-}2}$	$ARTM_{Fe\text{-}3}$	$ARTM_{Fe\text{-}4}$	$ARTM_{Fe\text{-}5}$
pH ± 0.01		5.28	6.71	7.42	8.08	9.40
IEP ± 0.06	3.64	3.52	3.51	3.38	3.71	3.54
Al x 10^3 ± 0.001(mole /g)	1.257	1.021	0.997	1.097	1.205	1.174
Fe x 10^3 ± 0.001(mole /g)	0.889	0.731	0.925	0.857	0.866	0.849

The results indicated that the IEPs of the iron treated ARTM were not significantly different from the untreated ARTM. Also the iron data after

treatment are very little different from the data for the untreated systems. It appears that coating films were not formed.

As was case for the aluminium treated systems, it had been envisaged that the formation of hydrolysis product films on the surface of TM would have been favoured by electrostatic interactions. The IEP results indicate that neither the favourable nor unfavourable conditions led to formation of a stable coating film. These results are similar to those obtained for the Al systems. If films were formed, they did not survive the rinsing and drying steps that followed the treatment.

3.7 Summary

The principal findings of the work described in this chapter are summarised below:

- Natural TM contains significant quantities of particulate clay, which can readily be removed by water, acid and alkali rinsing. The IEP of the clean surface of natural TM equilibrated for 24 hr at pHs from 3.51 to 8.20 was found in the range from 3.49 ± 0.06 to 4.01 ± 0.06. When measured immediately after rinsing, the value was 2.87 ± 0.09

- The data are quite variable and show no systematic trends. There was some evidence that acid treatment gave rise to higher values and prolonged treatment with both acid and alkali gave lower values in most cases. However the results were not conclusive.

- The IEP of the natural TM was lower than had been anticipated. Synthetic TM ($Fe_{2-x}Fe_{2x}Ti_{1-x}O_4$, x = 0.4) and oxidized synthetic TM were found to have IEPs in the range from 3.59 ± 0.06 to 3.90 ± 0.06, which is similar to that of the cleaned and equilibrated natural TM.

- Surface treatment with polymerised aluminium and iron solutions had no significant effect on IEP.

- The synthetic TM prepared at 1400°C possessed magnetic properties similar to those of natural TM. Oxidized synthetic TM lost magnetic properties.

- From the studies reported in this chapter it appears that in order to ensure the media is positively charged, it will be necessary to perform filtration at pHs less than 3.6.

3.8 References

Akimoto, S.; Katsura, T.; Yoshida, M. 1957. Magnetic properties of $TiFe_2O_4$-Fe_3O_4 system and their change with oxidation. *J. Geomagn. Geoelectr.* 9: 165-178.

Anderson, N. J.; Bolto, B. A.; Eldridge, R. J.; Kolarik, L. O.; Swinton, E. A. 1980. Colour and turbidity removal with reusable magnetic particles. II. Coagulation with magnetic polymer composites. *Water Res.* 14(8): 967-973

Aveston, J. 1965. Hydrolysis of the aluminium ion: Ultra-centrifugation and acidity measurements. *J. Chem. Sco.* 8: 4438-4443.

Bottero, J. Y.; Tchauber, D.; Cases, J. M.; Fiessinger, F. 1982. Investigation of the hydrolysis of aqueous solutions of Al chloride. 2. Nature and structure by small-angle x-ray scattering. *J. Phys. Chem.* 86: 3667-3673.

Brady, G. W.; Kurkjian, C. R.; Lyden, E. F. X.; Robin, M. B.; Saltman, P.; Spiro, T.; Terzsis, A. 1968. The structure of an iron core analog of ferritin. *Biochemistry* 7: 2185 - 2192.

Brown, A. P.; O'Reilly, W. 1996. The magnetic hysteresis properties of ball-milled monodomain titanomagnetite, $Fe_{2.4}Ti_{0.6}O_4$. *Geophysical Research letters.* 23(20): 2863-2866.

Christoph, G. G.; Corbato, C. E.; Hofmann, D. A.; Testtenhors, R. T. 1979. The crystal structure of boehmite. *Clays Clay Miner.* 27(2): 81-86.

Coda, A.; Kamenar, B.; Prout, K.; Carrothers, J. R.; Rollett, J. S. 1975. Crystal structure of μ-oxo-bis[tetraethylenepentaamineiron(III)] iodide. *Acta Crystallogr. , Sect. B* 31: 1438-1442.

Dixon, D. R. 1991. The Sirofloc process for water clarification. *Water Supply* 9 *(1, Suppl., IWSA/IAWPRC Jt. Spec. Conf. Coagulation, Flocculation, Filtr., Sediment. Flotation,* 1990): S33-S36.

Dousma, J.; de Bruyn, P. L. 1978. Hydrolysis-precipitation studies of iron solutions. II. Aging studies and the model for precipitation from iron(III) nitrate solutions. *J. Colloid Interface Sci.* 64: 154-20.

Dousma, J.; de Bruyn, P. L. 1979. Hydrolysis-precipitation studies of iron solutions. III. Application of growth models to the formation of colloidal iron(III) oxyhydroxide from acid solutions. *J. Colloid Interface Sci.* 72: 314-20.

Hsu, P. H. 1988. Mechanisms of gibbsite crystallization from partially neutralized aluminum chloride solutions. *Clays Clay Miner.* 36: 25-30.

Hsu, P. H.; Bates, T. F. 1964. Formation of X-ray amorphous and crystalline aluminium hydroxides. *Mineral. Mag.* 33: 749-768.

Hsu, P. H.; Ragone, S. E. 1972. Aging of hydrolyzed iron(III) solutions. *J. Soil Sci.* 23(1): 17-31.

Hunter, K. A.; Liss, P. S. 1982. Organic matter and the surface charge of suspended particles in estuarine wates. *Limnol.Oceanogr.*, 27: 322-335.

Iwasaki, I. 1962. Iron wash ore slimes – some mineralogical and flotation characteristics. *Trans. AIME*, 223: 97.

Johansson, G. 1960. On the crystal structures of some basic aluminum salts. *Acta Chem. Scand.* 14: 771-773.

Johansson, G. 1963. On the crystal structures of some basic aluminum sulfate. $13Al_2O_3.6SO_3.XH_2O$. *Ark. Kemi* 20: 321-342.

Keefer; C. M.; Shive, P. N. 1981. Curie temperature and lattice constant reference contours. *Journal of Geophysical Research.* 86(B2): 987-998.

Kinniburgh, D. G.; Syers, J. K.; Jackson, M. L. 1975. Specific adsorption of trace amounts of calcium and strontium by hydrous oxides of iron and aluminium. *Soil Sci. Soc. Am. J.* 39: 464-470.

Kolarik, K. O.; Dixon, D. R. 1980. Effects of pretreatments on the surface characteristics of a natural magnetite. *Proc. Int. Symp. Fine particles processing.* 1: 652-665.

Morris, A. S. 1997. *Measurement and Calibration Requirements for Quality Assurance to ISO 9000.* Editor: O'Connor P. D. T., John Wiley & Sons.

Murphy, P. J.; Posner, A. M.; Quirk, J. P. 1975. Gel filtration chromatography of partially neutralized ferric solutions. *J. Colloid Interface Sci.* 52: 229-238.

Murphy, P. J.; Posner, A. M.; Quirk, J. P. 1976. Characterization of partially neutralized ferric nitrate solutions. *J. Colloid Interface Sci.* 56: 270-283.

O'Donovan, J. B.; O'Reilly, W. 1977. Range of non-stoichiometry and characteristic properties of the products of laboratory maghemitization. *Earth and planetary science letters.* 34: 291-299.

Parks, G. 1965. The isoelectric points of solid oxides, solid hydroxides, and aqueous hydroxo complex systems. *Chem. Rev.* 65: 177-198.

Rausch, W. V.; Bale, H. D. 1964. Small angle x-ray scattering from hydrolyzed aluminum nitrate solutions. *J. Chem. Phys.* 40: 3391-3394.

Readman, P. W.; O'Reilly, W. 1970. The synthesis and inversion of non-Stoichiometric titanomagnetites. *Phys. Earth Planet. Inter.* 4: 121-128.

Schoen, R.; Roberson, C. E. 1970. Structures of aluminum hydroxide and geochemical implication. *Am. Mineral.* 55: 43-77.

Smith, R. W.; Hem, J. D. 1972. Effect of aging on aluminum hydroxide complexes in dilute aqueous solutions. *U. S. Geol. Surv. Water Supply Paper* 1827-D.

Sommer, B. A.; Margerum, D. W.; Renner, J.; Saltmen, P.; Spiro, T. G. 1973. Reactivity and aging in hydroxyiron(III) polymers, analogs of ferritin cores. *Bioinorg. Chem.* 2(4): 295-309.

Stol, R. J.; Van Helden, A. K.; de Bruyn, P. L. 1976. Hydrolysis precipitation studies of aluminum (III) solutions. 2. A kinetic study and model. *J. Colloid Interface Sci.* 57: 115-131.

Stumm, W.; Morgan, J. J. 1996. *Aquatic Chemistry , 3rd Edition.* New York: John Wiley & Sons.

Tsai, P. P.; Hsu, P. H. 1985. Studies of aged OH-Al solutions using kinetics of Al-ferron reactions and sulfate precipitation. *Soil Sci. Soc. Am. J.* 48: 59-65.

Turner, R. C. 1976a. Effect of aging on properties of polynuclear hydroxyaluminum cations. *Can. J. Chem.* 54: 1528-1534.

Turner, R. C. 1976b. A second species of polynuclear hydroxyaluminum cations, its fomation and some of its properties. *Can. J. Chem.* 54: 1910-1915.

van der Mei, H. C.; de Vries, J.; Busscher, H. J. 1993. Hydrophobic and electrostatic cell surface properties of thermophilic dairy streptococci. *Appl. Environ. Microbiol.* 59(12): 4305-4312.

Wechsler, B. A.; Lindsley, D. H.; Prewitt, C. T. 1984. Crystal structure and cation distrivution in titanomagnetites ($Fe_{3-x}Ti_xO_4$). *American Mineralogist* 69: 754-770.

Chapter Four: The Effect of Particle Size, Magnetic Conditioning and pH on Filtration by Titanomagnetite

4.1 Introduction

Effective grain size, uniformity coefficient (UC) and surface charge are the principal characteristics of the media that affect filtration efficiency. While good quality water can be achieved using fine media, pressure drops are generally too high to obtain adequate flow velocities. In order to increase hydraulic conductivity, we wished to investigate magnetically conditioned expanded beds of TM (125-250 micron particle size). It was anticipated that expansion of the filtration beds might be accompanied by lower filtration efficiency. The extent to which this could be compensated for by pH adjustment to maximise electrostatic interactions was of interest.

Backwashing is a very important stage in filter operation. Effective backwash will be obtained at the minimum bed expansion that allows maximum interstitial flow velocity. Excessive backwash flow lead to fluidisation of the bed, reduction of interstitial flow velocity and eventually, loss of media. Magnetic conditioning has the potential to allow greater backwash flow velocities without increased bed expansion and hence greater interstitial flow velocities and cleaning efficiency.

4.1.1 Hydraulic conductivity of filtration media

Hydraulic conductivity is an important parameter in water filtration technology. It reflects the water permeability of the medium and controls the flow velocity achievable in the filter. When water flows through a gravity filter bed, the medium provides a resistance to the water flow and pressure gradient forms. For a constant head (pressure difference) and a given filter section area, the water flux depends

on properties of the medium and the water temperature. The relationship between the head loss and the flow velocity was first described by Darcy (Darcy, 1856):

$$Q = KA(h_1 - h_2) / L \tag{4.1}$$

where Q is flux of water (m^3/s), A is bed section area (m^2), K is hydraulic conductivity (m/s), h_1, h_2 are the heads of water at bed depth *1* and *2* (m) and L is depth of medium (m). Figure 4.1 shows the experimental set-up he employed. Darcy's Law is valid only under streamline conditions and low flow velocities.

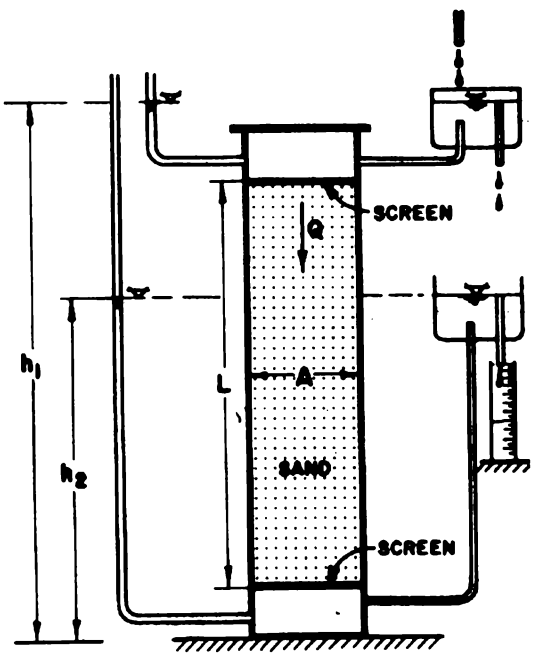

Figure 4.1 Darcy's experiment

The hydraulic conductivity of a filter medium depends on both matrix and fluid properties. The relevant fluid properties are density and viscosity, or in the combined form, the kinematic viscosity, ν. The relevant solid matrix properties are pore size distribution, shape of pores, tortuosity, specific surface area and porosity. Various formulae have been devised to relate hydraulic conductivity to the properties of the solid matrix. Nutting (1930) expressed the hydraulic conductivity K as:

$$K = k\gamma / \mu = kg / \nu \tag{4.2}$$

where k, the permeability of the porous matrix, depends solely on properties of the solid matrix, μ is viscosity coefficient and v is kinematic viscosity, γ is specific weight and g is gravity acceleration.

One of the derivations of permeability and its relationship to porous medium properties was proposed by Kozeny (1927). He treated the porous medium (uniform spheres) as a bundle of capillary tubes of equal length and obtained the equations for motion and permeability in the forms:

$$\begin{aligned} q &= -(c_o n^3 / \mu . M^2) grad . p \\ k &= c_o n^3 / M^2 \end{aligned} \tag{4.3}$$

where c_o is Kozeny's constant; n is porosity defined as: $n = U_v/U_b$ (where U_v is the volume of the void space and U_b is the bulk volume of a porous medium), M is bulk specific surface defined as the total interstitial surface area of the pores (A_s) per unit bulk volume (U_b) of the porous medium). Sometimes the term mass specific volume, M_s,, is used where M_s, is A_s per unit mass of the porous medium:

$$M = A_s / U_b = A_s(1-n) / U_s = (1-n) M_s \tag{4.4}$$

where U_s is the volume of the solid spheres. For spheres of uniform radius r:

$$M_s = 4\pi r^2 / \tfrac{4}{3}\pi r^3 = 3 / r \tag{4.5}$$

The expression for k in (4.3) is called Kozeny's equation. Combining equations (4.4) and (4.5) and substituting in (4.3) gives:

$$k = c_o[n^3 / (1-n)^2] / M_s^2 = c_o[n^3 / (1-n)^2] . r^2 / 9 \tag{4.6}$$

When tortuosity (T) is considered, we obtain the following modified Kozeny's equation:

$$\begin{aligned} k &= c_o T . n^3 / M^2 \\ k &= c_o T . [n^3 / (1-n)^2] / M_s^2 \end{aligned} \tag{4.7}$$

or

$$k = c_o T . [n^3 / (1-n)^2] r^2 / 9 \tag{4.8}$$

where $T = (L / L_e)^2 < 1$, is tortuosity. L is the straight line of the pass length, L_e is the tortuous line of the pass length.

4.1.2 *Effect of medium size and bed depth on filtration efficiency*

The effect of medium size

A filtration medium is generally defined by the following factors:

- Effective grain size.
- Uniformity coefficient.
- Grain sharpness (e.g. angular, crushed material, or round river and sea sand).
- Porosity.
- Density.
- Friability.

In the classification of granular media, the terms "effective size" and "uniformity coefficient" are often used. The mean effective size is the mesh size allowing passage of 10% of the medium. The mean uniformity coefficient is the ratio of the mesh size allowing passage of 60% of the medium to that of the mesh size allowing passage of 10%. The uniformity coefficient for a desirable medium is 2.0 or less (Degremont, 1991). Friability is a measure of the quantity of usable material remaining after crushing.

In the selection of a filtration medium size for rapid filters, it is necessary to consider two factors: the passage of water downward through the medium and the passage of water upward through the medium. From the standpoint of filtration, it is desirable to have a medium that will prevent floc from passing through the filter, hold the floc as loosely as possible to permit easy backwashing, prevent the formation of mud deposits and hold as large a volume of floc as possible without clogging. From the standpoint of backwashing, it is desirable to have a medium of such particle size that it will cleanse itself and be free from adhering floc at the

end of a backwash and permit the passage of water at sufficient velocity to remove all the sediment without losing media.

The effect of filter medium particle size, shape and porosity on filter behaviour has been widely studied. Coarser and more angular materials yield longer filter run times but have a detrimental effect on filtered water quality (Cheremisinoff, 1995).

Several methods are available for the measurement of the size of the granular media and include microscopic inspection, sieving, elutriation and sedimentation. Generally, the particle size determined depends on the length of the dimension measured (or determined indirectly) and on the method of measurement. The two main methods for determining particle size and particle-size distribution are sieve analysis and hydrometer analysis. In sieve analysis, the tested granular material is shaken on a sieve with square openings of specified size, so that the 'size' of a particle is based on the side dimension of a square hole in a screen. However, as particles are seldom spherical or of any regular shape that would permit one to determine whether or not they would slip through a sieve hole, this arbitrary definition of size actually means only that we have measured some dimension of a particle that will permit it to slip through a square hole. In hydrometer analysis, the size of a particle is the diameter of a sphere that settles in water at the same velocity as the particle. Other methods include direct measurement by light microscopy, electron microscopy and electrical counting of particles passing through an aperture of known diameter.

The effect of bed depth

The depth of filter medium is another important characteristic of a filter. In order to prevent suspended particles from passing throughout the filter (breakthrough), a layer of sufficient thickness is necessary. The depth of the layer should be determined by experiment.

A number of theoretical and empirical formulae are available for estimating the depth of filter sand for pilot plant tests. Kawamure (1999) studied optimal bed

depth for rapid sand filters and found L/d, the ratio of bed depth (L) to grain size (d) for optimum performance was 1000.

4.1.3 Effect of surface charge of filter medium on filtration efficiency

When particles pass through a filter medium, retention forces will be present. For fine particles, surface forces such as van der Waals forces and electrical forces play an important role. As outlined in Section 1.2.3 a key to improving filtration efficiency is to control the filter medium surface charge so that the particles and filter medium have a charge of opposite sign.

4.1.4 Magnetic conditioning of filtration beds

Applications of magnetically stabilised fluidised beds (MSFB) in separation technology were outlined in Section1.2.6. The use of magnetically conditioned expanded beds for water filtration has not been extensively studied. The purpose of the studies reported in this chapter was to determine whether the magnetic conditioning of an expanded bed of fine medium offered any advantages over the unconditioned bed. In particular we wished to test whether such a system could filter suspensions of fine particles at realistic flow velocities without prior flocculation.

4.1.5 Backwashing

The earliest method of backwashing was to use an upward filtered water flow to cause an expansion of the filter bed and carry the particles detached from medium grains out of the filter. Many investigations have been focused on the optimisation of backwashing. In order to improve the backwashing efficiency, numerous auxiliary wash methods have been tested and employed. These include surface-wash agitation and water and air scour washing. Surface-wash agitation as an auxiliary wash method effectively prevents the formation of mud balls. Air scour as an auxiliary wash method provides the most effective cleaning of a filter. But complex operation and extra equipment are required for both auxiliary wash methods.

Backwashing with water alone uses an up-flow of clean water at a flow velocity great enough to fluidise the media bed. Therefore, the backwash water flow velocity is the most important factor in determining backwashing performance. The principal mechanism for removal of particles from medium grains in a fluidised wash is hydrodynamic shear. A greater backwashing velocity causes a bigger expansion of medium bed and larger void between medium grains. If the backwashing velocity is too low, adequate expansion of medium bed will not occur. The interstitial flow velocity is also lower due to the lower wash velocity. The optimum backwashing velocity causes the minimum fluidisation of bottom medium grains. The interstitial flow velocity and the hydrodynamic shear between medium grains increases with an increasing wash velocity of the un-fluidised bed. When medium bed just fluidises and the flow velocity reaches the minimum fluidisation velocity, the interstitial flow velocity and the hydrodynamic shear between medium grains are highest. After this point, the increase of wash velocity results in deceased interstitial velocity and hydrodynamic shear between medium grains. Loss of medium may occur. Magnetically controlling the bed volume may allow minimum fluidisation of bottom medium grains and higher interstitial flow velocity.

4.2 TM filter beds

4.2.1 Size distribution of natural TM

The effective size and uniformity coefficient of natural TM particles were obtained by sieving. Primary concentrate TM iron sand (300 g) was thoroughly washed with tap water and dried in an oven at 100^0C for 24 hr. The dried sand (298.27 g) was separated by a series of sieves: 75, 90, 125, 250 and 425 μm. The sand retained by each sieve was weighed and its percentage of the total sample weight was calculated. Results are recorded in Table 4.1.

Table 4.1 Size distribution data for natural TM

Mesh size (μm)	Weight passed by the sieve		Weight retained by the sieve	
	Weight ± 0.01(g)	%	Weight ± 0.01(g)	%
425	298.01	99.91	0.26	0.09
250	292.28	97.99	5.74	1.92
125	52.01	17.44	240.26	80.55
90	3.07	1.03	48.94	16.41
75	1.73	0.58	1.34	0.45
<75	-	-	1.73	0.58
Sum			298.27	100%

According to the data in Table 4.1, a size distribution curve for natural TM can be drawn as shown in Figure 4.2. The effective diameter (d_{10}) of TM was determined from the curve (following the procedure described by Degremont (1991) to be as d_{10} = 120 μm. This is the mesh size of the sieve that allows passage of 10% of the particles. The sieve size which allows of passage of 60% of the TM grains to pass (d_{60}) was determined to be d_{60} = 180 μm. Thus, the value of uniformity coefficient, $K_{60} = d_{60} / d_{10}$ = 180/120= 1.5. The uniformity coefficient of TM medium is less than 2.0 and indicates TM is a satisfactory filtration medium.

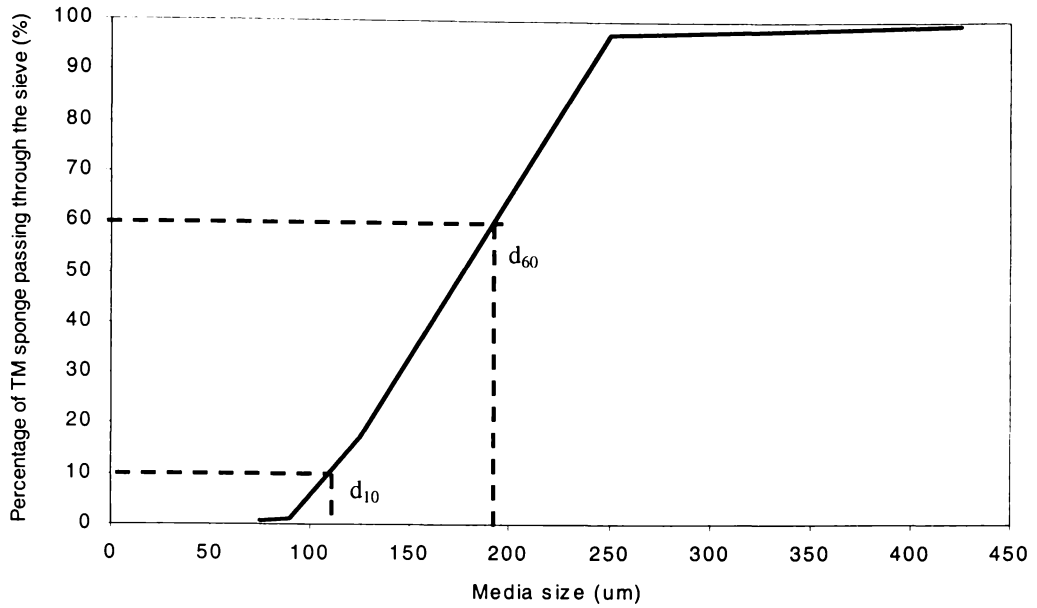

Figure 4.2 Size distribution curve for TM

4.2.2 Effect of bed depth on filtration efficiency and flow rate

The effect of bed depth was determined. The size fraction between 125-150 μm of the ARTM described in Section 2.2.1 was obtained by sieving.

The experimental set up shown in Figure 4.3, consisted of a raw water container (25 L plastic container), a gear pump (Model No. 75225-05 190-260 VAC, 50/60 HZ 1.4 AMP, Cole-Parmer Instrument Co. USA) and a series of glass columns of 24 mm internal diameter. Head pressure was kept at 2.0 m.

The bed was filled with dry medium and backwashed to give approximately a 100% increase in bed volume. It was then allowed to settle by stopping the flow. A constant head pressure of 2.0 m was maintained by pumping water to keep the header tank full.

Figure 4.4 shows the flow velocity versus bed depth. Generally, the flow velocity decreased as the bed depth increased and the data show a non linear trend line, corresponding to Darcy's law.

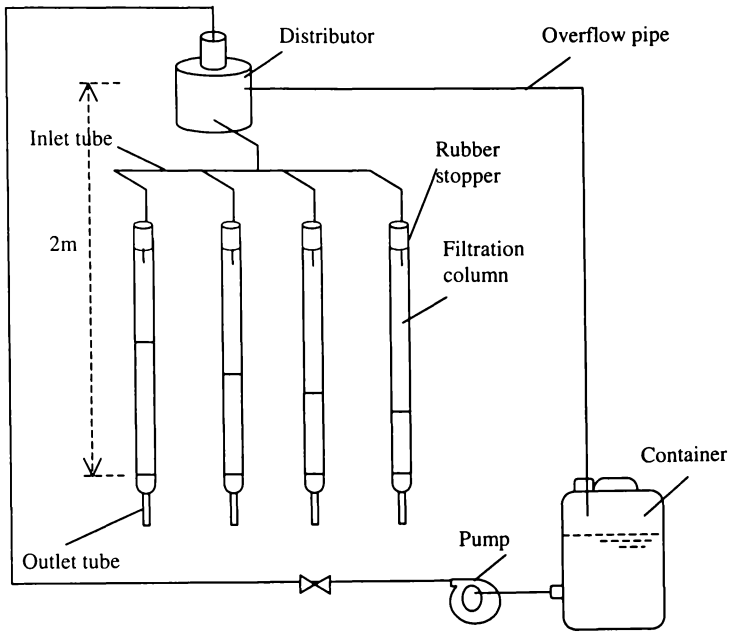

Figure 4.3 Schematic diagram of apparatus used to study filtration performance

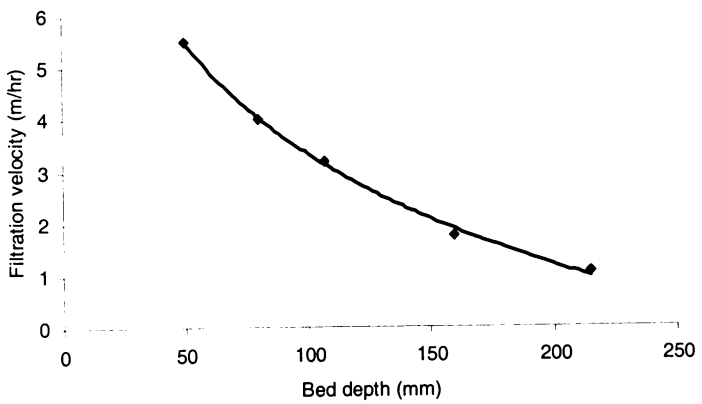

Figure 4.4 Effect of bed depth on filtration velocity at a constant head pressure of 2 m. (125-150 μm TM)

In filtration experiments, turbidity removal for various bed depths (30 mm; 55mm and 80mm) was studied. Dilute suspension kaolin was prepared according to the method of outlined in Section 2.2.3 (maximum volume distribution at a particle size of: 1.07 μm; IEP of 2.70 ± 0.10). It had an initial turbidity of 42 NTU and a concentration of 35.68 mg/L. The pH of the suspension was 5.7.

The results for turbidity removal for various bed depths (30 mm, 55 mm and 80 mm) are shown in Figure 4.5. There was a marked improvement in filtration efficiency in going from a bed depth of 30 mm to a bed depth of 55 mm. A further small improvement was observed when the bed depth was increased to 80 mm (The flow rate was less than 4 m/hr). According to Kawamure (1999) a bed depth of 125 to 150 mm would be necessary for optimum filtration. However at this bed depth, the flow rate would be 2 to 3 m/hr, which is too low to be useful for conventional filtration.

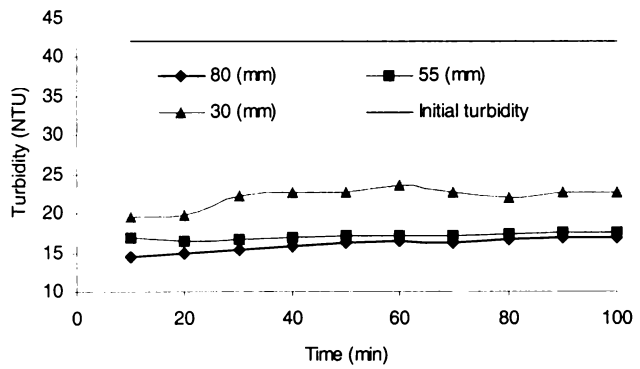

Figure 4.5 Effect of bed depth on filtration efficiency (pH=5.7). (Data obtained after 10 min)

The variation of filter flow velocities for various bed depths is shown in Figure 4.6. The 30 mm bed gave higher initial filtration velocities but these decreased more rapidly, presumably due to the higher rate of cake formation. The deeper beds (55 mm and 80 mm) showed less flow reduction with time.

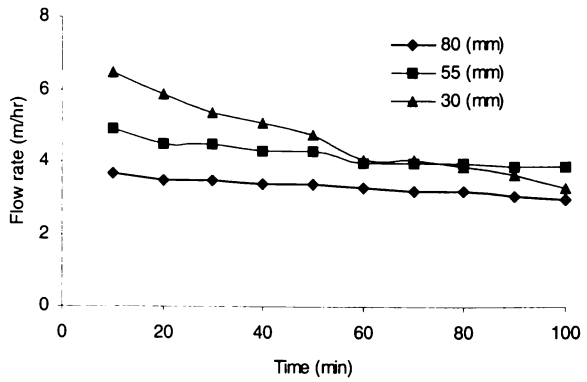

Figure 4.6 Variation of flow velocity with time

4.2.3 Effect of TM particle size on filtration efficiency

The effect of particle size on filtration performance was studied using the two size ranges: 32-45 μm (medium obtained by milling) and 150-180 μm. Filter bed depth was 55 mm. A kaolin suspension was prepared as previously described (Section 2.2.3). The results of turbidity removal and flow velocity are shown in Figure 4.7.

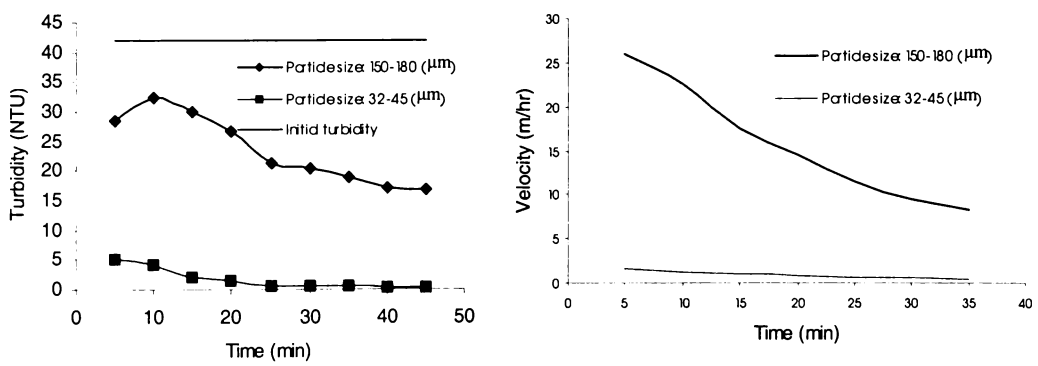

Figure 4.7 Effect of medium particle size on kaolin removal (pH=5.7)

It is clear from the data that very much improved filtration efficiency is obtained for the medium of small particle size but the flow velocity is about 1-2 m/hr. This would normally be regarded as being too slow for conventional filtration. Comparison of the flow velocities after 5 minutes for the TM of the two particle

sizes indicates a 25 fold decrease in flow velocity for the fine particles size as predicted by the Kozeny equation (see Section 4.1.1).

4.2.4 Effect of pH on TM filtration efficiency

The effect of medium surface charge on filtration efficiency was studied by lowering the pH of the experimental system to 3.5. At this pH, the ARTM has positive surface charge (IEP of ARTM was 3.64 ± 0.06); and kaolin particles will have a negative surface charge (IEP of kaolin was 2.70 ± 0.10). Filtration experiments were performed for various bed depths (26 mm for 150-180 μm TM, 55 mm for 150-180 μm and 32-45 μm TM). Kaolin suspensions were prepared according the general procedure of Sections 2.2.3. The results of turbidity removal as a function of time for two bed depths and two particle sizes are shown in Figure 4.8.

Both fine (32-45 μm) and coarse (150-180 μm) media with 55 mm bed depths achieved 99% turbidity reduction, but the velocity is different. For the coarse medium at shallower bed depths (i.e. 26 mm) filtration efficiency even at pH 3.5 was unsatisfactory. At pH 5.7 (see Figure 4.5) the turbidity reduction for the 55 mm bed of 150-180 μm mediums was only 64%. These results demonstrate the importance of electrical forces in filtration.

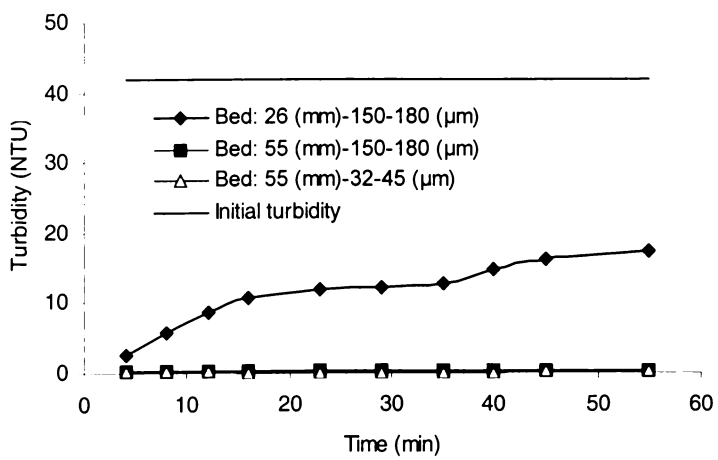

Figure 4.8 Filtration of kaolin suspension by TM at pH = 3.5

4.3 Filtration by magnetically conditioned beds

4.3.1 Magnetic conditioning of TM filtration beds

Magnetic conditioning of filtration beds was achieved using the field generated by a pair of 300-turn Helmholtz coils. According to Biot-Savart's Law (Matthew, 1995), a uniform magnetic field is produced with Helmholtz pairs if the coil separation is equal to the average radius of each coil (see Figure 4.9).

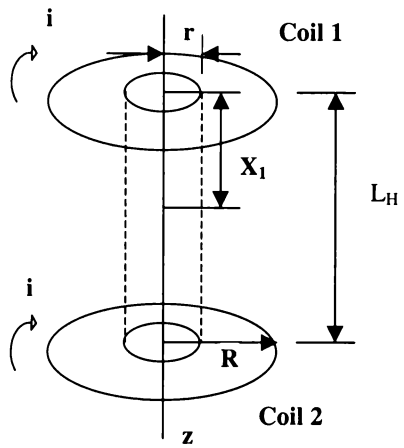

Figure 4.9 Important dimensions of a Helmholtz pair.

Equation (4.9) was used to calculate the magnetic field intensity, Γ.

$$\Gamma = \left[\frac{\mu_0 \cdot N \cdot i \cdot R^2 \cdot a_z}{2 \cdot (R^2 + x_1^2)^{\frac{3}{2}}}\right]_{coil1} + \left[\frac{\mu_0 \cdot N \cdot i \cdot R^2 \cdot a_z}{2 \cdot (R^2 + (L_H - x_1)^2)^{\frac{3}{2}}}\right]_{coil2} \qquad (4.9)$$

where Γ is total magnetic field intensity (T); μ_0 ($\mu_0 = 4\pi \times 10^{-7} (Wb / A \cdot m)$) is permeability of free space; i is direct current *(A)*; R is radius of coil (m); a is a unit vector along the z axis; L_H is distance between the two coils (m) and N is the number of turns of each coil.

When $R = L_H$, a uniform magnetic field is created which is bounded within a cylinder of radius r, centred about the central axis (z) of the coils and bounded by

the ends of the coils. At the centre point between the two coils of a Helmholtz pair (i.e. $X_1 = L_H/2$), the total field is given by:

$$\Gamma = \frac{8 \cdot \mu_0 \cdot N \cdot i}{R \cdot (5)^{3/2}} \tag{4.10}$$

Figure 4.10 summarises experimental data for field intensity as a function of axial location for a pair of Helmholtz coils with N = 300 turns, a maximum current of i = 5 A (5 A 30 V, DC power supply) and R = 0.089 m.

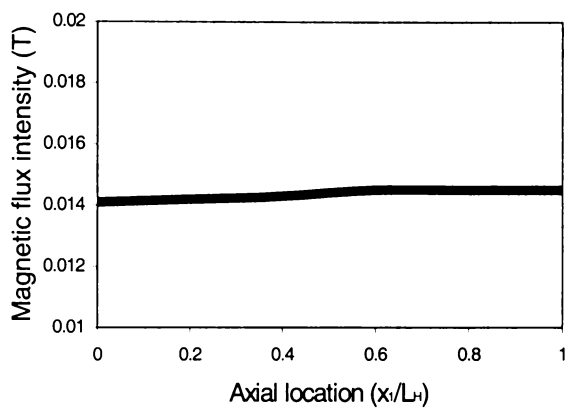

Figure 4.10 Plot of magnetic field intensity versus axial location for a Helmholtz pair

Thus a uniform magnetic field of about 0.015 T would act on the medium in a column placed between the coils.

4.3.2 The effect of magnetic field strength on magnetic conditioning

The effect of various magnetic fields was investigated in an experiment using a 24 mm diameter column of TM (bed depth of 45 mm). The bed was backwashed to give approximately a 150% increase in bed volume. A field was applied and the bed was allowed to settle by ceasing backwash flow. Data for settled bed volumes for various field strengths are summarised in Table 4.2.

The results show that horizontal fields at a maximum field strength, of 0.018 T had an 18% effect on the settled volume. In contrast the vertical field stabilised bed expansions ranging from 13% to 93% for the field strength range.

Table 4.2 Settled bed volumes for the various field conditions.

Field strength		Vertical Field		Horizontal Field	
i (A)	Γ (T)	Bed depth (mm)	% bed expansion	Bed depth (mm)	% bed expansion
6	0.018	87	93	53	18
5	0.015	82	82	51	13
4	0.012	77	71	49	9
3	0.009	69	53	47	4
2	0.006	60	33	46	2
1	0.003	51	13	45	0

For a vertically conditioned bed, the bed volume decreased with increasing down-flow velocity. Under constant 2 m head pressure (see Figure 4.3), down-flow velocity was controlled by an outlet valve. The bed depth decreased from 80 mm to 68 mm under the influence of increasing down-flow velocity (field strength 0.018 T). Data for bed depth and % bed expansion as a function of down flow velocity are summarised in Table 4.3.

Table 4.3 Down-flow velocity versus bed expansion (%) under magnetic field of 0.018 (T)

Down-flow velocity (m/s)	8.5	5.1	4.5	4.1	3.1	1.9
Bed depth (mm) *	68	70	71	73	78	80
Bed expansion (%)	51	56	58	62	73	78

* Initial bed depth: 45 (mm).

4.3.3 Hydraulic conductivity of magnetically conditioned beds

Hydraulic conductivity was measured using the apparatus shown in Figure 4.11. The internal diameter of the glass columns was 24 mm and the medium bed depth was 45 mm. Three magnetic field configurations were used: no field, vertical field and horizontal field.

Measurements were performed under constant total head and head loss across the bed under various flows and bed configurations.

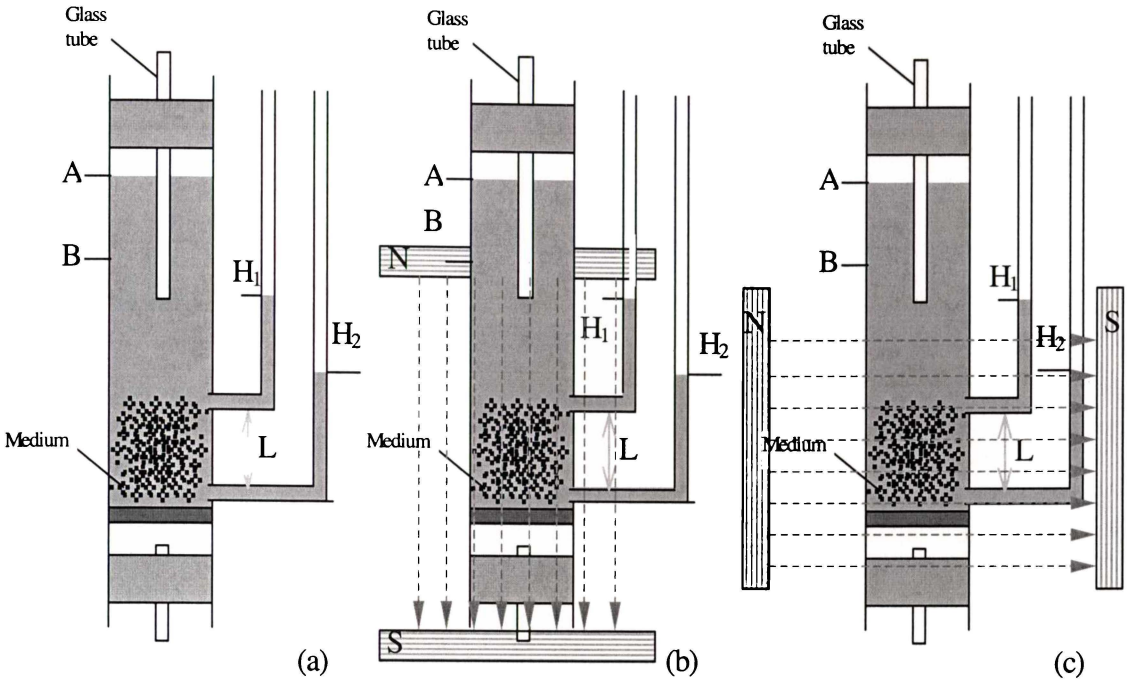

Figure 4.11 Apparatus for measurement of TM hydraulic conductivity. (a) Without magnetic field. (b) Under vertical magnetic field. (c) Under horizontal magnetic field. ----➤ Indicates direction of the magnetic field.

The TM bed was expanded by controlled backwash flows, the field was applied, the backwash flow was stopped and the bed was allowed to settle to its magnetically conditioned volume.

Data for hydraulic conductivity of naturally packed TM are summarised in Table 4.4. The mean hydraulic conductivity is $(3.2 \pm 0.1) \times 10^{-4}$ m/s.

Hydraulic conductivity data for the magnetically conditioned beds stabilised at various bed depths by fields ranging from 0 to 0.018 T are summarised in Figure 4.12. It is clear that for a vertically applied field, conditioning to give relatively minor expansions of the bed had a pronounced effect on hydraulic conductivity. The hydraulic conductivity was increased nearly two-fold, when the volume of the bed expanded by 15%. In contrast a horizontal field had no appreciable effect on hydraulic conductivity even when the bed was significantly (18%) expanded.

Table 4.4 Hydraulic conductivity of naturally packed TM

Run	$\Delta H \times 10^3$ (m)	$Q \times 10^7$ (m^3/s)	$K \times 10^4$ (m/s)
1	135	2.9	3.1
2	135	3.0	3.2
3	135	3.0	3.2
4	135	2.9	3.2
5	157	3.6	3.3
6	157	3.1	3.3
			3.2 ± 0.1

Also shown on Figure 4.12 is the behaviour predicted by the Kozeny equation (see Section 4.1.1.). The fit is good for vertical fields and bed expansions of up to about 17%. At greater bed expansions for vertical fields and for horiazontal fields, experimental hydraulic conductivities are less than the predicted values indicating that non linear tortuosity effects may be involved.

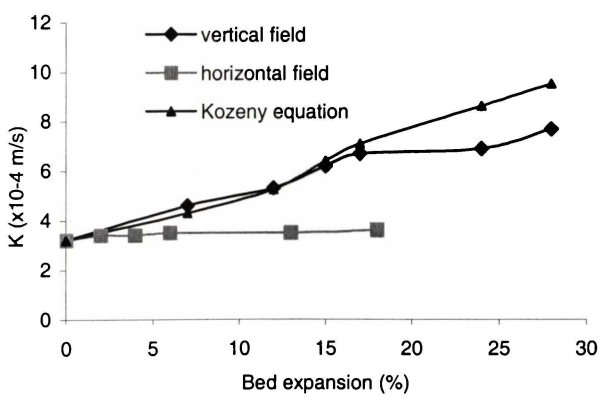

Figure 4.12 Hydraulic conductivity of TM beds as a function of the bed expansion achieved by vertical and horizontal fields ranging up to 0.018 T. predictions based upon the Kozeny equation (see Appendix 4.1) are also shown.

Figure 4.13 illustrates the observed medium packing under vertical, horizontal and magnetic field free conditions. Under a vertical magnetic field, the individual magnetic particles were observed to connect to each other along the magnetic

field direction parallel to the flow direction. The bed settled when backwashing was terminated but the orientation of the grains remained. When a horizontal magnetic field was applied, the particles aligned perpendicular to the flow direction and when the backwash flow ceased the bed compacted to a greater extent than for the vertical field. Hydraulic conductivity of the expanded horizontally conditioned beds was unchanged from the value obtained for the unconditioned bed

An explanation for these effects appears to be found in the alignment of the majority of the filter grains. For the vertical field the alignment is vertical (see Figure 4.13a). This allows a degree of channelling through the bed. In contrast, the alignment of particles with a horizontal field is shown in Figure 4.13b where it is the possible that a more tortuous pathway is produced which may inhibit the increased flow that would otherwise be expected due to increases in porosity factor resulting from bed expansion.

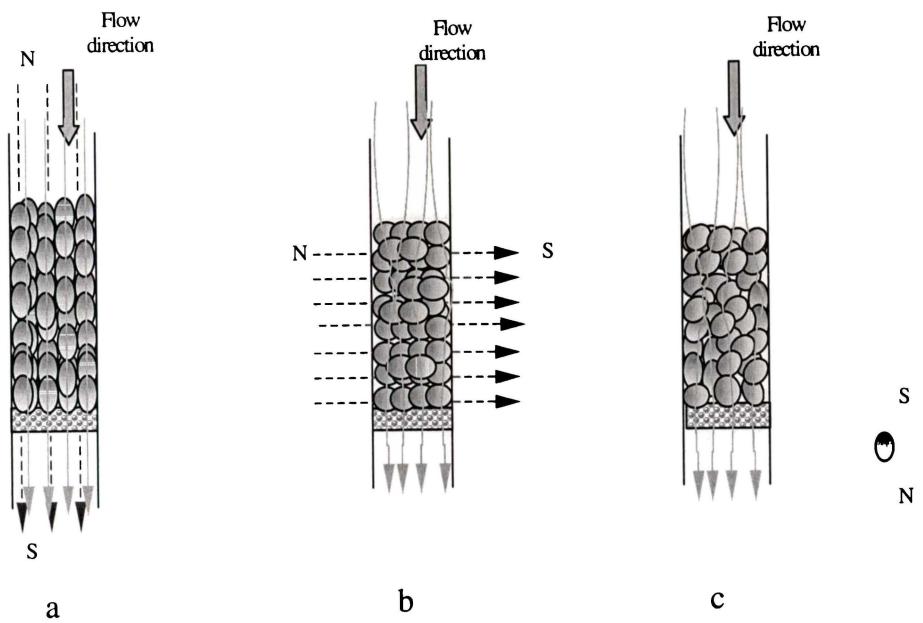

Figure 4.13 Media in column under (a) a vertical magnetic field (b) a horizontal magnetic field (c) no field.

4.3.4 Filtration study

Figure 4.14 shows the effect of filtration of kaolin suspensions at pH 8.1 and 2.9 by magnetically conditioned and unconditioned beds. Filtration efficiency was improved as pH was lowered. The turbidity reduction achieved by the magnetically conditioned (28% expanded) bed was approximately 17% while the unconditioned bed achieved turbidity reduction of 29%. The reduced efficiency was presumably due to the higher flow rates associated with the expanded beds.

The effect of pH was dramatic. At the pH 2.9 the filtration efficiency was markedly improved and turbidity reduction for both conditioned and un-conditioned bed was over 90%. Apparently electrostatic interactions more than compensate for the reduced efficiency observed at the higher flow velocities using the expanded beds. This result suggests that fine ARTM filtration media with a high specific surface area could be used at low pH to enhance electrostatic removal of suspended particles, while maximising hydraulic conductivity by magnetic conditioning in an expanded configuration. Comparison of the unconditioned bed data of Figure 4.14 with those of Figure 4.8 indicates that the filtration at the higher pH of 3.5 was more efficient than at pH 2.9. It is possible that at the lower pH, which is quite close to the IEP of kaolin, the surface charge on the kaolin is much reduced giving rise to a much reduced attractive interaction.

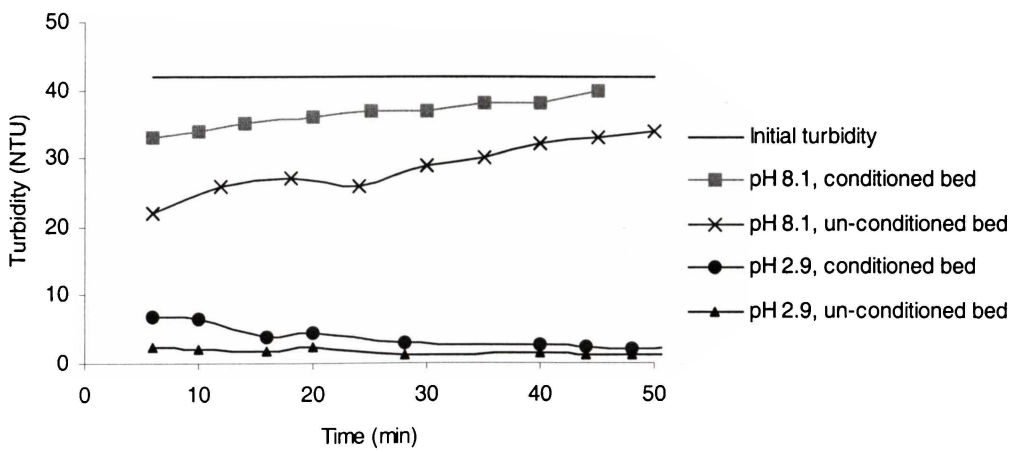

Figure 4.14 Turbidity reduction by ARTM (150-180 μm) in conditioned and unconditioned beds at two pH values.

4.4 Backwashing

4.4.1 Experimental method for backwashing

Two filter beds were prepared for a backwashing study using the following method:

- A suspension of kaolin was prepared in tap water to give an initial turbidity of 441 NTU (pH 5.7).
- Compacted ARTM (size range: 125-250 μm) filter beds (630 mm) were prepared in two glass columns of 24 mm internal diameter, backwashed and allowed to settle.
- Colloid suspension was filtered through the ARTM beds for 30 min. Outlet turbidity decreased from 441 NTU to 201 NTU.

The two columns were then backwashed. One bed was backwashed under normal conditions. The other was magnetically conditioned during backwashing. For both experiments the backwash bed expansion e_o was maintained at:

$$e_o = \frac{l_1 - l_o}{l_o} = \frac{1500 - 630}{630} = 1.38$$

where l_1 and l_o are expanded bed depth and initial bed depth. Higher backwash flow velocities were possible for the bed that was magnetically conditioned.

Data for the volume of backwash water (V) versus outlet turbidity are shown in Figure 4.15.

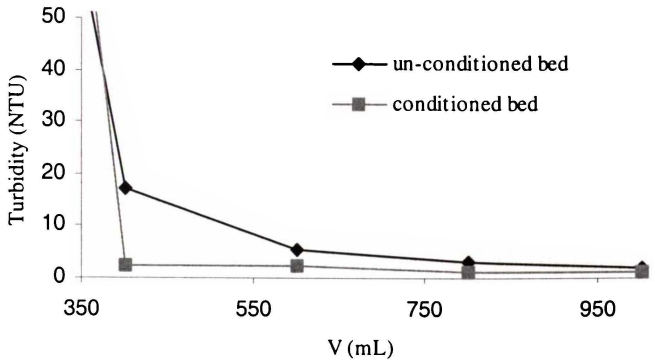

Figure 4.15 The effect of vertical magnetic conditioning on backwash efficiency

4.4.2 Results and discussion

The outlet turbidity decreased much more sharply for the magnetically conditioned bed. For the ordinary bed, the outlet turbidity decreased to 17.3 NTU after passing 400 mL backwash water, whereas for the magnetically conditioned bed, outlet turbidity decreased to 2.42 NTU after the same volume had passed. A backwash volume of about 1000 mL was required to reduce the turbidity of the backwash water from unconditioned bed to a similar value.

The backwashing volumetric flow rate for the magnetically conditioned bed was 10.6 ($L/s.m^2$) and for the unconditioned bed was 7.36 ($L/s.m^2$). As anticipated, the magnetically conditioned bed allowed higher interstitial flow velocity and hydrodynamic shear between medium with the same bed expansion.

4.5 Summary

Principal findings of the work described in this chapter are summarised below:

- The hydraulic conductivity of TM (150-180 μm) was found to be (3.2 ± 0.1)x10^{-4} m/s. The effect of particle size was as predicted by the Kozeny equation. Flow velocity through a TM bed of 55 mm was about 4 m/hr and produced a turbidity reduction in a kaolin suspension is about 64% at pH 5.7 and 99% at pH 3.5.

- A TM medium (bed depth 55 mm) of reduced particle size (32-45μm) gave a turbidity reduction of 96% at a flow rate of about 1.5 m/hr at pH 5.7. While the turbidity reduction is promising, the flow rate (for a 2 m head) is too slow to be useful in conventional filtration applications

- Surface electrical forces can be controlled by solution pH and play an important role in the filtration process. When the pH was adjusted so that filter medium and suspended particles could be expected to have opposite surface charge, filtration efficiency was improved.

- A vertically aligned uniform magnetic field applied to an expanded bed formed during backwashing can condition the bed of ARTM in an expanded state. The hydraulic conductivity of the expanded bed increased approximately linearly with bed volume. By increasing the volume of the bed by 28%, the hydraulic conductivity was more than doubled. Some initial reduction of the conditioned bed volume occurred under conditions of down flow.

- With a horizontally aligned magnetic field, the volumes of the conditioned beds were less than those obtained for vertically conditioned beds and hydraulic conductivity was not affected.

- Filtration studies showed that the filtration efficiency of the vertically conditioned beds was less than for the unconditioned beds. This was more

than compensated for by the electrostatic effects produced by a choice of pH that ensured medium and suspended particles were of opposite charge.

- Backwashing performance can be improved by magnetic conditioning of the bed. Higher interstitial flow velocities at a given bed expansion are possible.

4.6 References

Cheremisinoff, P. N. 1995. *Handbook of Water and Wastewater Treatment Technology.* Marcel Dekker, Inc. New York.

Darcy, H. 1856. *Les Fontaines Publiques de La Ville de Dijon.* Dalmont, Paris.

Degremont. 1991. *Water Treatment Handbook.* Sixth edition, publ. Lavoisier. 1: 378-379.

Kawamure, S. 1999. Design and operation of high rate filters. J. *AWWA* 91(12): 77-90.

Kozeny, J. 1927. Űber kapillare Leitung des Wassers im Boden, *Sitzungsber. Akad. Wiss. Wien.* 136: 271-306.

Matthew, N. O. 1995. *Elements of Electromagnet Ices.* New York, Oxford; University press. C1995: 299.

Nutting, P. G. 1930. Physical analysis of oil sand. *Bull. Amer. Ass Petr. Geol.* 14: 1337-1349.

Chapter Five: Modification of Silicon Sponge with Aluminium and Iron Surface Coatings

5.1 Introduction

Natural pumice possesses a porous structure, which contributes to its large specific surface area. It has proven to be a useful medium in filtration applications. In this study a commercial pumice product, Silicon Sponge (SS) was used. SS is a graded and thermally modified pumice marketed by Works Filter Systems, Ltd. of Hamilton. SS has good resistance to abrasion and is finding application as an alternative to anthracite in dual media filters (Hill and Langdon, 1993). The large proportion of free silica sites at the grain surface react with water to form hydroxyl groups, resulting in a negatively charged surface. We wished to extend the usefulness of SS by modifying its surface charge to facilitate removal of negative particles. Treatment with solutions containing polycations of iron and aluminium was envisaged. While attempts to coat TM by treatment with polycations were largely unsuccessful, it was considered that the porous nature of SS might assist in the anchoring of hydrous oxide films onto SS.

In addition it may be possible to form magnetic coatings by using an appropriate mixture of Fe(II) and Fe(III) in the treatment solution. An overall aim of this work was to produce small SS particles having high IEPs and magnetic properties.

5.2 Properties of SS

5.2.1 Physical and chemical properties of SS

SS is a chemically inert, non-magnetic, non-inflammable and non-explosive grey or off-white material (Bolen, 1990). The chemical composition of SS used in this study was determined by the Geosicence laboratory in Sudbury, Ontario, Canada. Results are summarised in Table 5.1.

Table 5.1 Chemical composition of SS

Composite	SiO_2	AlO_2	Na_2O	Fe_2O_3	K_2O	CaO	MgO	TiO_2	MnO
Weight (%)	71.02	12.83	4.02	2.88	2.67	1.56	0.32	0.27	0.11

Composite	Nb	Zr	Y	Sr	Rb	Ga	Cr	As	Ba	Pb	Th
(ppm)	7	183	29	137	106	15	10	21	682	17	13

*Oxides measured in weight %, Heavy metals measured in ppm.

The morphology of SS used in this study is illustrated by the SEM shown in Figure 5.1; the true density of SS (size range: 125-250 μm) was 2.02 g/cm^3 and envelope density was 0.56 g/cm^3. The macro-pore volume was 1.24 mL/g(SS) (Section: 2.8). The specific surface area was determined by the BET method. Results for SS (particles size range: 125-250 μm) are summarised in Table 5.2.

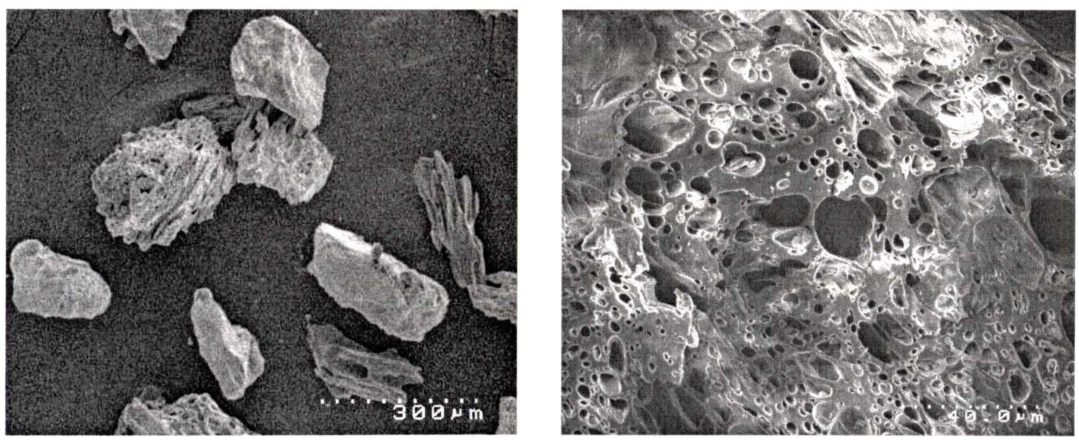

Figure 5.1 SEM micrograph of SS

Table 5.2 BET analysis results for SS

Materials	Specific surface area* (m^2/g)	Pore area* (m^2/g)	Pore volume* (cc/g)
SS	3.93 ± 0.01	1.10 ± 0.01	(6.95 ± 0.01) x10^{-4}

* Quantachrome Corporation. 1994.

5.2.2 Size distribution of SS

The effective size and uniformity coefficient of the SS fraction containing particles less than 1.2 mm was obtained by sieving. 150 g acid rinsed SS (ARSS) (Section 2.2.2) was separated by a series of sieves: 35, 75, 90, 125, 150, 250, 425, 600, 710 and 1180 μm. The ARSS retained by each sieve was weighed and its percentage weight of the total sample was calculated. Results are recorded in Table 5.3.

Table 5.3 Size distribution data for ARSS

Mesh size (μm)	Weight passed by the sieve		Weight retained by the sieve	
	Weight ± 0.01(g)	%	Weight ± 0.01(g)	%
1180	149.16	99.44	0.84	0.56
710	125.05	83.37	24.11	16.07
600	86.98	57.99	38.07	25.38
425	29.72	19.81	57.26	38.17
250	7.09	4.73	22.63	15.09
125	2.01	1.34	5.08	3.39
90	1.45	0.97	1.54	1.03
75	0.89	0.59	0.56	0.37
35	0.38	0.25	0.47	0.31
<35	-	-	0.38	0.25
Sum			150	100%

According to the data in Table 5.3, a size distribution curve for ARSS can be drawn as shown in Figure 5.2. The effective diameter (d_{10}) of ARSS was determined from the curve to be as d_{10} = 300 μm. This is the mesh size of the sieve that allows passage of 10% of the particles. The sieve size which allows passage of 60% of the ARSS grains (d_{60}) was determined to be as d_{60} = 600 μm. Thus, the value of uniformity coefficient, $K_{60} = d_{60} / d_{10}$ = 600/300 = 2. A uniformity coefficient 2 indicates SS is a satisfactory filtration medium.

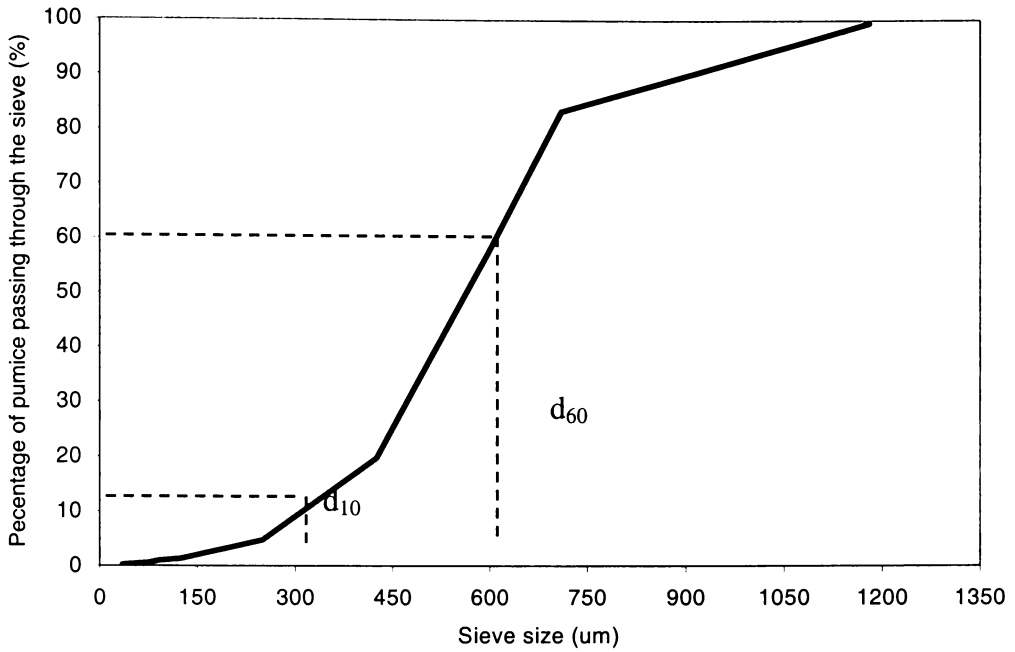

Figure 5.2 Size distribution curve for ARSS

5.3 *Modification ARSS by aluminium surface coatings*

5.3.1 Materials and method

In this study the aluminium polymer precursor solution used to coat the ARSS was prepared as described in Section 3.6.1. The ARSS was prepared as described in Section 2.2.2. The size fraction between 125 to 250 μm was obtained by sieving.

The procedure for coating involved repeated treatment cycles:

- The desired amount of ARSS was placed in a Buchner flask and evacuated with a venturi aerator until all air had been excluded for the SS pores. The Al_{13} polymer solution was then sucked into the flask and stirred.
- Ammonium hydroxide NH_3 (specific gravity 0.91, 25%) solution was added to the mixture to adjust the pH to pH 9.

- The liquid was drained off and remaining material oven dried at 100^0C for 24 hr.

- The dried samples were rinsed thoroughly with de-ionized water until rinse water was clear.

- The samples were oven dried at 100^0C for a further 24 hr.

- The sample obtained in this way was named: 'S_{al-n}' (n=1-9), where n indicates the number of coating cycles.

- The above steps were repeated for 3, 5, 7 and 9 cycles. A flow diagram for the coating procedure is illustrated in Figures 5.3.

Treatment at various pHs

The coating procedure described above was repeated for pHs ranging from 5.37 to 9.11. Only single treatment cycles were used for each pH. The dried samples were rinsed thoroughly with de-ionized water adjusted to the pH of the experiment until rinsing was clear. The samples obtained in this way were named: '$S_{al-pH-n}$' (n= 5.37 to 9.11), where n indicates the pH at the NH_3 treatment step.

A flow diagram for the coating procedure is illustrated in Figures 5.4.

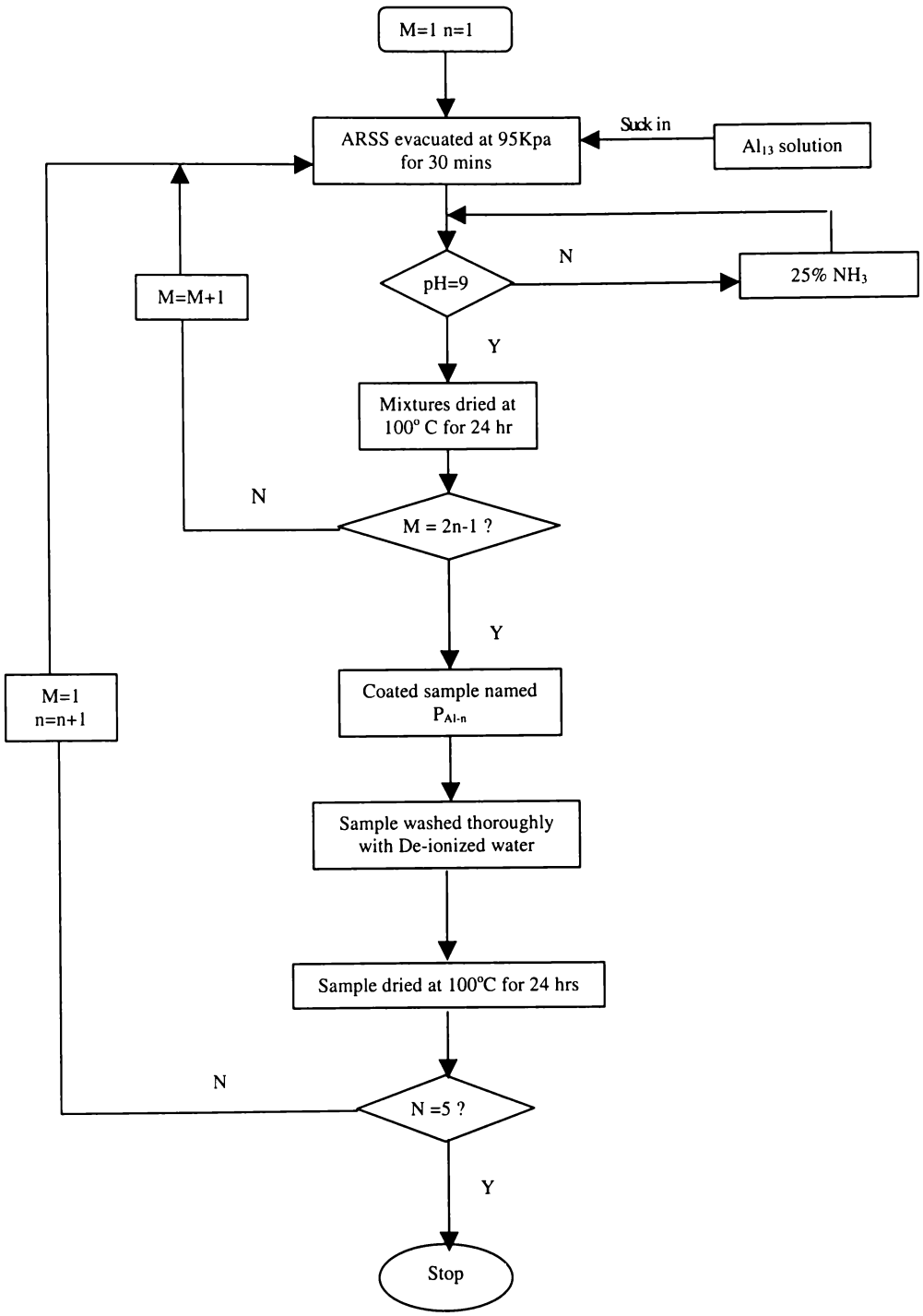

Figure 5.3 Flow diagram for multiple treatment with Al

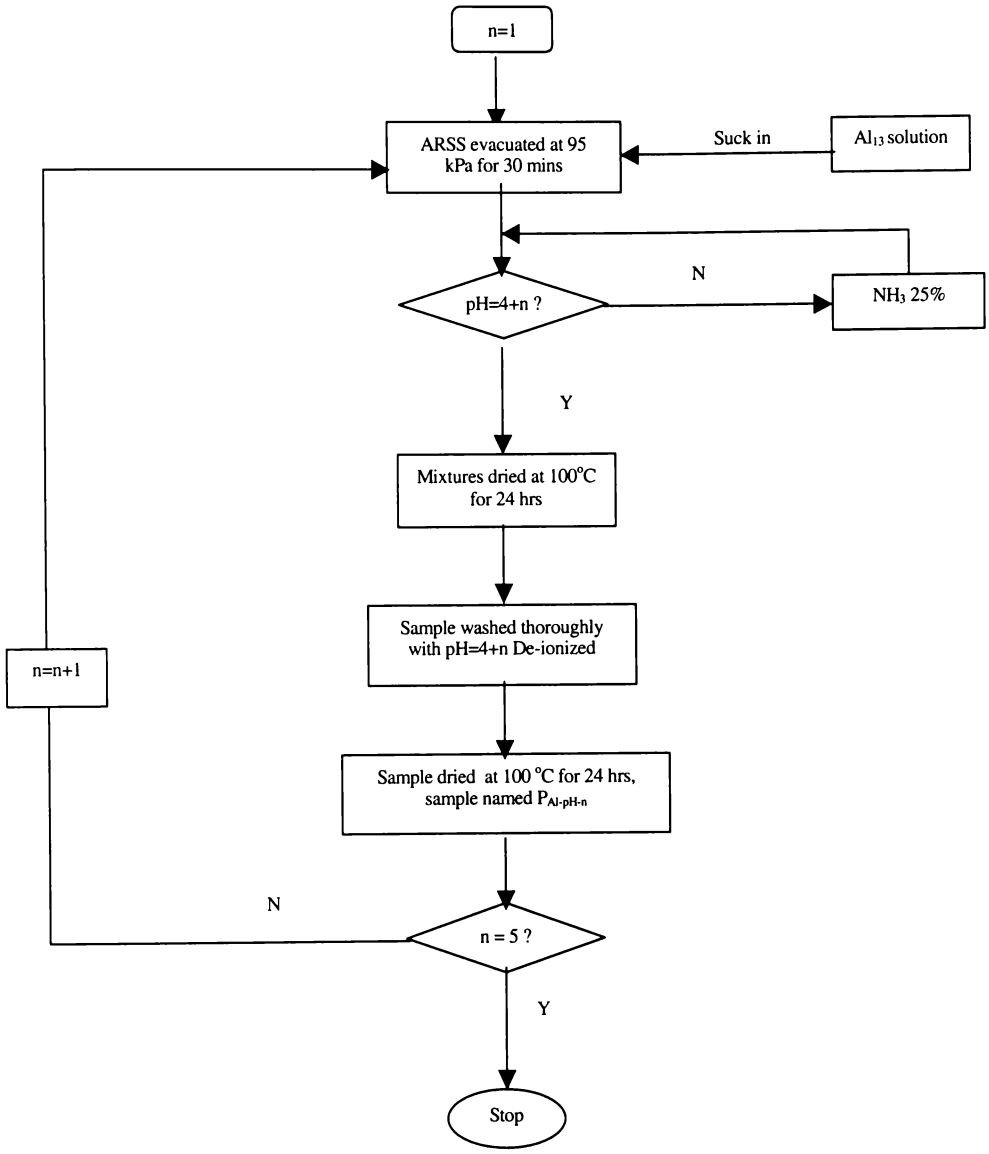

Figure 5.4 Flow diagram for treatment with Al at different pH values.

5.3.2 Results and discussion

Characterisation of coating films

Table 5.4 gives the Inductively Coupled Plasma (ICP) analysis data and IEP data for untreated ARSS and ARSS samples treated by an increasing number of exposure cycles and at various pH values. Untreated ARSS gave 0.006 x 10^{-3} mole/g aluminium while the treated samples gave values generally in the range from 0.379 to 0.833 x 10^{-3} mole/g. The amount of aluminium extracted increased with treatment cycle number until the third cycle after which further exposures had little effect on aluminium content. The experiments revealed that the pH of the experiment was an important parameter. Little aluminium was retained when the pH was lower than 6.3.

Electrokinetic properties of the coated ARSS samples were determined using the procedure described in Section 2.6. The present results show that the number of coating cycles and amount of aluminium deposited on the medium surface were not critical factors affecting the IEP. The pH of coating was an important parameter and when the value was over 6.3, an IEP in the range 7.54 ± 0.06 to 8.52 ± 0.06 was observed for the coated ARSS.

X-ray studies

The XRD patterns of the ARSS and Al_{13} polymer coated ARSS are shown in Figure 5.5. The six main peaks in the Figure 5.5 (a) correspond to peaks obtained for the SiO_2 (α-Cristobalite) (see Table 5.5). The X-ray pattern of ARSS does not show strong crystalline structure because the highly vesiculated material is the product of an explosive eruption and poorly crystallized magmas; vitric ashes and tuffs are dominated by largely uncrystallised glassy fragments. Gas escapes non-violently, as the volcanic magma cools and small crystals (microlites) have time to grow. This process results in the formation of small crystals of α-cristobalite, which are apparent in the traces (Cas and Wright, 1987).

Table 5.4 Properties of ARSS coated with aluminium

Materials	PH ± 0.01	Al x 10^3 ±0.001 (mole/g)	IEP ± 0.06
ARSS	-	0.006	4.10
S_{al-1}	9.00	0.379	7.25
S_{al-3}	9.00	0.745	8.43
S_{al-5}	9.00	0.702	8.52
S_{al-7}	9.00	0.679	7.76
S_{al-9}	9.00	0.610	7.87
$S_{Al-pH-5.37}$	5.37	0.023	5.73
$S_{Al-pH-6.33}$	6.33	0.626	7.54
$S_{Al-pH-7.44}$	7.44	0.833	7.25
$S_{Al-pH-8.13}$	8.13	0.666	7.72
$S_{Al-pH-9.11}$	9.11	0.806	7.18
$Al(OH)_3$			8.90

The XRD pattern of the aluminium polycation treated ARSS, Figure 5.5(b), has some of the features of ARSS including very weak α-cristobalite peaks as well as some features that appear to be due to the coating film of $Al(OH)_3$. Four of the peaks in Figure 5.5 (b) correspond to peaks obtained for β-$Al(OH)_3$ (Bayerite) (see Table 5.6).

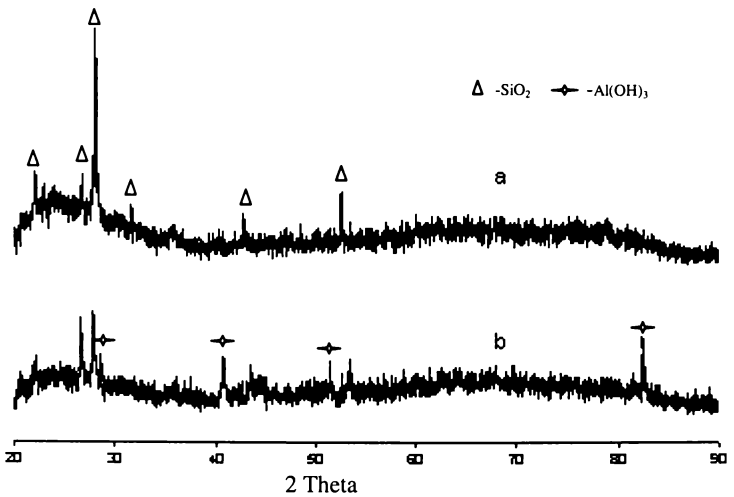

Figure 5.5 XRD pattern of (a) original ARSS; (b) Al coated ARSS ($S_{Al\text{-}pH\text{-}7.44}$)

The JCPDS X-ray data (International centre for diffraction data) of α-cristobalite and Al(OH)3 are summarised in Appendix 5.1.

Table 5.5 Comparison of d-spacings of α-cristobalite and ARSS

Crystal plane {hkl}	111	101	102	211	220	212
SIO_2* (α-Cristobalite)	3.1359	4.0397	2.8411	2.1179	1.7590	1.8714
ARSS	3.1800	4.0300	2.8400	2.1200	1.7500	1.8800

*JCPDS- International center for diffraction data (39-1425)

Table 5.6 Comparison of d-spacings of β-$Al(OH)_3$ and aluminium coated ARSS

Crystal plane {hkl}	100	101	111	201	112	300
β-$Al(OH)_3$* Bayerite	4.3600	3.1900	2.2100	1.8300	1.7100	1.4500
$Al(OH)_3$	4.3300	3.1900	2.2100	1.8300	1.7100	1.4300
Coated ARSS	-	3.2000	2.2100	-	1.7200	1.4500

* JCPDS - (12-0457)

Morphology of coated ARSS

The appearance of untreated ARSS is shown in Figure 5.1. The vesicular structure is obvious. The surface of untreated ARSS is characterised by its pore structure and large surface area. After coating, the pore structure is no longer visible (see Figure 5.6) and polished cross-sections show that the pores are partially filled with coating product (see Figures 5.7). Elemental analysis by EDAX indicated that locations A, C and D, contain a large fraction of aluminium (Figure 5.8) and thus these points must be features associated with the coating treatment. The point B, which is low in aluminium (Figure 5.9), presumably represents a portion of the capillary that has not been filled.

Figure 5.6 SEM micrograph of Al treated ARSS.

Figure 5.7 SEM micrograph of a polished cross section of Al treated ARSS.

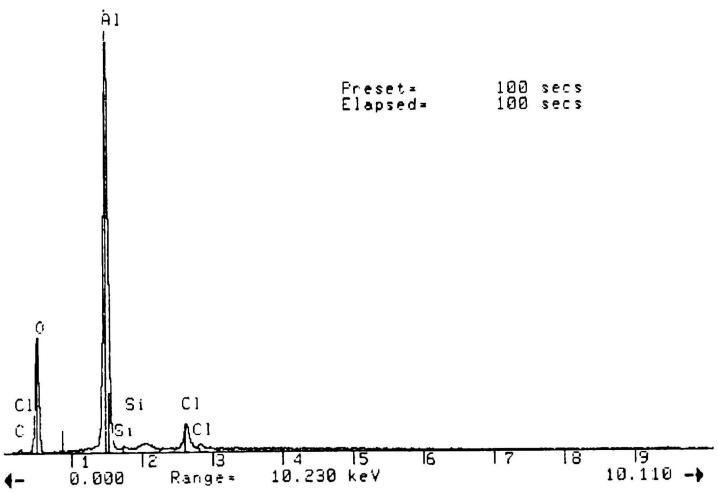

Figure 5.8 EDAX spectrum of Al treated ARSS at point A, C and D (see Figure 5.7).

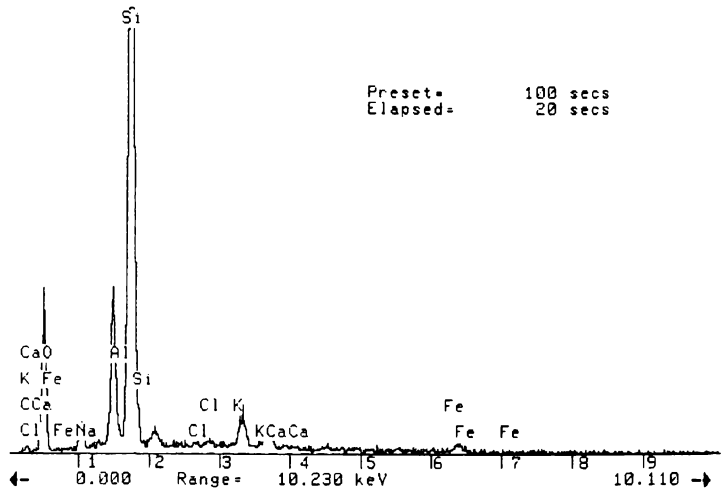

Figure 5.9 EDAX spectrum of Al treated ARSS at point B (see Figure 5.7).

Surface area of coated ARSS

The specific surface area, micro-pore area and micro-pore volume of coated-coated ARSS ($S_{al\text{-}n}$ and $S_{Al\text{-}pH\text{-}n}$) were obtained by BET, as listed in Table 5.7. 3 point BET of ARSS for coated with aluminium are summarised in Appendix 5.3.

Table 5.7 BET results of ARSS for coated with aluminium

Materials	Specific surface area* ± 0.01 (m^2/g)	Pore area* ± 0.01 (m^2/g)	Pore volume* ± 0.01 (cc/g)
ARSS	3.93	1.10 E+00	6.95 E-04
$S_{al\text{-}1}$	2.72	7.48 E-01	4.69 E-04
$S_{al\text{-}3}$	2.87	8.48 E-01	5.32 E-04
$S_{al\text{-}5}$	2.89	8.27 E-01	5.12 E-04
$S_{al\text{-}7}$	3.41	9.85 E-01	6.15 E-04
$S_{al\text{-}9}$	6.04	1.63 E+00	1.00 E-03
$S_{Al\text{-}pH\text{-}5.37}$	1.55	4.83 E-01	2.97 E-04
$S_{Al\text{-}pH\text{-}6.33}$	2.14	6.95 E-01	4.38 E-04
$S_{Al\text{-}pH\text{-}7.44}$	2.25	7.27 E-01	4.59 E-04
$S_{Al\text{-}pH\text{-}8.13}$	3.37	1.02 E+00	6.48 E-04
$S_{Al\text{-}pH\text{-}9.11}$	2.46	7.02 E-01	4.42E-04

* Quantachrome Corporation. 1994.

With the exception of $S_{al\text{-}9}$, the specific surface area of coated ARSS was less than the untreated SS. This may be due to the coating materials filling the macro-pores ARSS. The SEM micrograph of Al treated ARSS (Figure 5.5) supported this hypothesis.

5.4 Modification ARSS by iron surface coatings

5.4.1 Materials and method

The formation and structure of species formed in hydrolysed iron solutions is outlined in Section 3.6.3. The ARSS was prepared as described in Section 2.2.2. The coating procedure used was similar to that used to coat ARSS with aluminium.

- The desired amount of ARSS was placed in a Buchner flask and evacuated with a venturi aerator until all air had been excluded. The iron polymer solution was then sucked into the flask and stirred.
- Ammonium hydroxide NH_3 (specific gravity 0.91, 25%) solution was added to the mixture up to pH = 6.0.
- The liquid was drained off and remaining material was oven dried at 100^0C for 24 hr.
- The dried sample was rinsed thoroughly with various pH de-ionized water until rinse water was clear.
- The sample was oven dried at 100^0C for a further 24 hr.
- The sample obtained in this way was named: 'S_{Fe}'.

5.4.2 Results and discussion

Characterisation of coating films

Table 5.8 gives the ICP analysis data and IEP data for ARSS and ARSS treated with iron polymer. ARSS gave 0.005 x 10^{-3} mole/g iron while the treated samples gave a value of 0.875 x 10^{-3} mole/g.

The isoelectric point of iron treated ARSS gave the value of 5.27 ± 0.06 and the bulk precipitate iron hydroxide have IEP of 5.82 ± 0.06.

Table 5.8 Properties of ARSS coated with iron

Materials	Fe x 10^3 ± 0.001 (mole/g)	IEP ± 0.06
ARSS	0.005	4.10
S_{Fe}	0.875	5.27
Bulk Precipitate	-	5.82

X-ray studies

The XRD patterns of iron oxide hydroxide and iron coated ARSS are shown in Figure 5.10. The six main peaks correspond to peaks obtained for FeO(OH) (see Table 5.9). The coated ARSS has some features that appear to be due to a coating film of FeO(OH). The JCPDS X-ray data of FeO(OH) are summarised in Appendix 5.2.

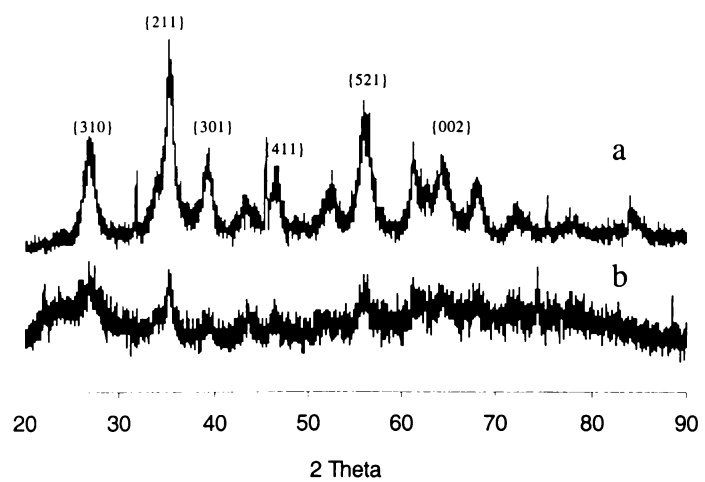

Figure 5.10 XRD pattern of (a) iron oxide hydroxide (b) iron coated ARSS

Table 5.9 Comparison of d-spacings of FeO(OH) and iron coated ARSS

Crystal plane {hkl}	310	211	301	411	521	002
FeO(OH)* (Akaganeite-M)	3.3330	2.5502	2.2952	1.9540	1.6434	1.5155
FeO(OH)	3.3308	2.5475	2.2972	1.9479	1.6433	1.5116
Coated ARSS	3.3163	2.5531	2.2796	1.9479	1.6367	1.4524

* JCPDS - (34-1266)

5.5 Modification of ARSS by synthetic magnetite coatings

5.5.1 Coating materials

Synthetic magnetite can be prepared by neutralising aqueous Fe(II) and Fe(III) ions in the appropriate stoichiometric mixture of one mole Fe(II) to two mole Fe(III) (Jolivet and Tronc, 1988). The synthetic colloids consist of small particles of approximately 120 Å, which were confirmed by XRD to be magnetite. The particles were black in colour and were strongly magnetic.

5.5.2 Method for coating ARSS with synthetic magnetite

Preparation of magnetite colloid

The magnetite precursor solution (MPS) was prepared by mixing 20 mL $FeCl_2.4H_2O$ and 40 mL $FeCl_3$ at the various concentrations of: 0.5; 1.0; 1.5 and 2.0 mol/L, respectively. All solutions were thoroughly deaerated with nitrogen, which was continuously bubbled during the preparation. The formation of magnetite colloid was initiated by addition of ammonium hydroxide solution (specific gravity 0.91, 25%) (see Table 5.10) with vigorous stirring. Care was taken to exclude oxygen during all stages. The reaction solution was sealed with an airtight plastic film for 30 min and the supernatant was eliminated under N_2 pressure using a pipette. The solid was rinsed in the reaction flask with degassed distilled water introduced under N_2 pressure. This process was repeated twice. The colloid was then oven dried at 100^0C for 24 hr.

Table 5.10 The amount of NH_3 reactioned with various Fe concentrations

$(Fe^{2+}+Fe^{3+})$ concentration (mol/L)	0.5	1.0	2.0
NH_3 (25%) (mL)	20	40	80

Coating of ARSS with magnetite

- The desired amount of ARSS was placed in a Buchner flask (the flask was placed in an ultrasonic bath) and evacuated with a venturi aerator until all air had been excluded. The MPS was then sucked into and the flask and vigorously agitated for 30 min.
- Ammonium hydroxide NH_3 (specific gravity 0.91, 25%) solution was added to the mixture to precipitate magnetite.
- The liquid was drained off and the remaining material was oven dried at 100^0C for 24 hr.
- The dried samples were rinsed thoroughly with de-ionized water until rinse water was clear.
- The samples were oven dried at 100^0C for a further 24 hr.
- The sample obtained in this way was named: '$S_{mag\text{-}n}$', where *n* indicates the concentration.

5.5.3 Results and discussion

Characterisation of coating films

Table 5.11 gives the ICP analysis data and IEP data for ARSS treated with MPS at various concentrations. The weight of Fe_3O_4 (W_{Fe3O4}) deposited in the film was estimated using the following calculation:

$$W_{Fe3O4} = W_{Fe} \times \frac{M_{Fe3O4}}{3 \times M_{Fe}} = 1.38 \times W_{Fe}(mg/g)$$

where M_{Fe3O4} and M_{Fe} indicates the relative molar masses of Fe_3O_4 and Fe.

Table 5.11 Properties of synthetic magnetite and ARSS coated with magnetite

Materials	Fe ± 0.001 (mg/g)	Fe x10^3 ± 0.001 (mole/g)	Fe_3O_4 ±0.01(mg/g)	IEP ± 0.06
ARSS	0.289	0.005	-	4.10
Fe_3O_4 (99.99%)*	-		-	4.90
Synthetic magnetite				4.90
$S_{mag-0.5}$	31.324	0.561	43.29	4.37
S_{mag-1}	48.635	0.871	67.22	4.52
S_{mag-2}	47.563	0.852	65.73	4.50

* Pure magnetite (Fe_3O_4, 99.99%, Alfa Aesar)

The isoelectric point of the synthetic magnetite was found to be 4.9. This value is considerably lower than the value of 6.5 reported for natural magnetite using micro-electrophoresis (Iwasaki, *et al.*, 1962). More recent work using streaming potentials has yielded values in the range 4.0 to 5.7 (Morimoto and Kittaka, 1973; Kittaka, 1974) consistent with the present work.

The results show that the IEP of the coated samples had values slightly higher than ARSS but less than that of the pure synthetic magnetite. The amount of magnetite deposited did not change with concentration of the MPS.

The magnetic properties of the coated ARSS were examined by measuring weight changes in an applied magnetic field (Gouy Method). For pure precipitates of Fe_3O_4, the magnetic susceptibility χ_M was calculated using the equation (2.12):

$$\chi_M = \frac{\beta \cdot \Delta \cdot M}{m} \times 10^{-3}$$

For coated ARSS, the relative molecular mass M of the coating film was both unknown and undefined. Thus the magnetic effect was recorded as the weight gain per gram of sample (Δ/m) when the magnetic field was applied. This value was compared against the weight gain per gram of commercial magnetite (Fe_3O_4 99%, Alfa Aesar) when exposed to the same field. Results are shown in Table 5.12.

Table 5.12 Magnetic properties of magnetite and magnetite coated ARSS

Materials	Mass (m) ±0.001 (g)	Weight increase (Δ) ±0.001 (g)	Δ/m ±0.002	$(\Delta/m)/(\Delta/m)_{Fe3O4}$ (%) ±0.3%
Fe_3O_4 (99.99%)*	0.541	10.610	19.612	100
Natural TM	1.122	17.720	15.790	80.5
ARSS	0.213	-0.005	-0.023	-
Synthetic magnetite	0.376	5.350	14.244	72.6
$S_{mag-0.5}$	0.242	0.125	0.515	2.6
S_{mag-1}	0.242	0.330	1.370	7.0
S_{mag-2}	0.244	0.325	1.329	6.8

*Commercial magnetite, Fe_3O_4 99%, Alfa Aesar

The macro-pore volume of ARSS is 1.24 mL/g (Section 5.2.1). If the pores were filled with a solution of concentration 1.0 mol/L of MPS, there will be 1.24 x 10^{-3} mol Fe/g SS (W_{Fe} = 69.25 x 10^{-3} g/g) in the pores assuming the amount of surface material is negligible. After reaction with NH_3 solution, the expected weight of Fe_3O_4 (W_{Fe3O4}) deposited in the pores can be estimated as 95.6 x 10^{-3} g/g i.e. about 10% of the product would be magnetite. If the magnetic effect of the treated ARSS is a function of amount of Fe deposited as magnetite in the pores, a magnetic effect of approximately 10% of that of pure magnetite can be expected. S_{mag-1} gave a magnetic effect that was 7% of that of pure magnetite, which is in

reasonable agreement with the value expected. However the data for masses of magnetite deposited at other concentrations do not support this interpretation.

X-ray studies

XRD studies confirmed that the synthetic product was magnetite. According to the literature (David and Welch, 1956; Berry and Thompson, 1962) magnetite possess spinel-type structure. The d-spacings of the samples in this study were examined and are presented together with published magnetite data in Table 5.13. The XRD spectrum of the synthetic magnetite is shown in Figure 5.11. The six peaks in the figure correspond to Miller indices {*hkl*} of {220}, {311}, {400}, {422}, {511}, {333} and {440}, respectively. The JCPDS X-ray data file for Fe_3O_4 is summarised in Appendix 5.2. It was not possible to detect any crystalline phase in the magnetite coated ARSS.

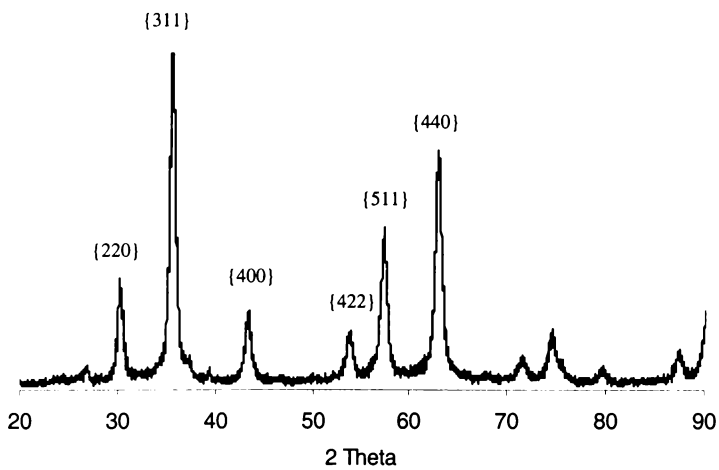

Figure 5.11 XRD pattern of synthetic magnetite

Table 5.13 Comparison of d-spacings of Fe_3O_4 and synthetic magnetite

Crystal plane {hkl}	220	311	400	422	511	440
Fe_3O_4 * (Magnetite)	2.9660	2.5300	2.0960	1.7120	1.6140	1.4830
Synthetic materials	2.9623	2.5257	2.0868	1.7048	1.6119	1.4776

*JCPDS - (11-0614)

5.6 Summary

The principal findings of the research described in this chapter are summarised below:

- Treatment of ARSS with hydrolysed Al and Fe solutions is an effective way of raising the IEP of ARSS. A single exposure to the Al(III) coating solution raised the IEP of ARSS from 4.10 ± 0.06 to 7.25 ± 0.06. A further 3 to 5 coating cycles raised the IEP by up to one pH unit but the effect was not constant and coating cycles beyond 5 had no effect.

- When the pH of the coating experiment was varied there was little change in IEP for pHs above 5.37. In general the IEP data for the coated ARSS were similar to the values for pure $Al(OH)_3$ precipitate.

- Treatment with hydrolysed iron solutions raised the IEP of ARSS to 5.27 ± 0.06, somewhat less than the IEP of pure precipitate (5.82 ± 0.06).

- Loading of ARSS with synthetic magnetite colloid raised the IEP to 4.52 ± 0.06 and produced a magnetic effect that was about 7.0% of the magnetic effect obtained for pure magnetite.

5.7 References

Berry, L. G.; Thompson, R. M. 1962. *X-Ray Powder Data for Ore Minerals: The Peacock Atlas.* Editor(s): Berry, L. G.; Thompson, R. M. The Geological Society of America Memoir 85, New York.

Bolen, W. P. 1990. *Pumice and Pumicite Supply Demand Relationships. Encyclopedia of Chemical Processing and Design.* Editor: Mc Ketta, J. J., Marcel Dekker Inc. New York.

Cas, R. A. F.; Wright, J. V. 1987. *Volcanic Successions: Modern and Ancient: A Geological Approach to Processes.* Allen and Unwin. London.

David, I.; Welch, A. J. E. 1956. Oxidation of magnetite and related spinels. Constitution of γ-ferric oxide. *J. Chem. Soc. Faraday Trans.* 52: 1642-1650.

Hill, T., Langdon, A. 1993. Modified pumice: An indigenous material for water filtration and aluminium removal. *Water & Wastes in New Zealand.* July: 36-38.

Iwasaki, I.; Cooke, S. R. B.; Kim, Y. S. 1962. Iron wash ore slimes. Some mineralogical and flotation characteristics. *Trans. AIMM.* 223: 97-108.

Jolivet, J. P.; Tronc, E. 1988. Interfacial electton transfer in colloidal spinel iron oxide. Conversion of Fe_3O_4-γFe_2O_3 in aqueous medium. *J. Colloid Interface Sci.* 125: 688-701.

Kittaka, S. 1974. Isoelectric point of aluminum oxide, chromium(III) oxide, and iron(III) oxide. I. Effect of heat treatment. *J. Colloid Interface Sci.* 48: 327-333.

Morimoto, T.; Kittaka, S. 1973. Electrification of iron oxide in water. *Bull. Chem. Soc. Japan.* 46(10): 3040-3043.

Quantachrome Corporation. 1994. Operation Manual of Nova-1000 Gas Sorption Analyser.

Chapter Six: Modification of Silicon Sponge by Surface Coatings of Al(III)/Fe(III) and Al(III)/Fe(III)/Fe(II) Mixed Hydrous Oxides

6.1 Introduction

Aluminium and iron polycations can be prepared by partial neutralisation of the acidic Al(III) and Fe(III) solutions, e.g. $AlCl_3$ and $FeCl_3$. The nature of the polymeric species formed depends on various factors such as the strength of Al(III) or Fe(III), the basic ratio defined as the ratio of the moles of base added and/or bound to the moles of Al(III)/Fe(III) ions, [OH/Al(III) or Fe(III)], the time of Al(III)/Fe(III) hydrolysis (aging time), the anions in solution, the mixing mode of base with the Al(III)/Fe(III) solution and the nature and the strength of the base (Schneider, 1984; van der Woude, *et al.*, 1983). The most important parameters that govern the nature of the species are the basic ratio, the aging temperature and time.

Al(III)/Fe(III) polycations were prepared following the procedure described by Leprince *et al.* (1984). Acidic $AlCl_3$ and $FeCl_3$ (98%, BDH Laboratory. Supplies, Poole, England). 100 mL (1 mol/L) solutions with the Al/Fe mole ratios of 1:9; 3:7; 5:5; 7:3 and 9:1, respectively were neutralised by drop-wise addition of 100 mL (3 mol/L) sodium hydroxide (Scharlau Chemie S.A) solution. The crystal morphology of the Al(III)/Fe(III) = 1:9 product formed is shown in Appendix 6.1 (a).

Titration curves

Typical titration curves for various Al(III)/Fe(III) mole ratios are shown in Figure 6.1.

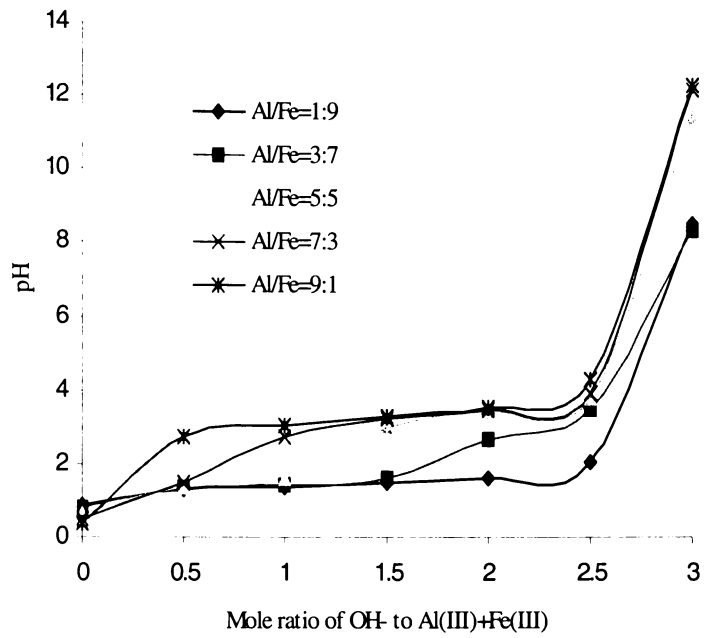

Figure 6.1 Curves for the titration of Al(III)/Fe(III) mixed solutions with NaOH solution

The results indicate that for the iron rich systems, the neutralisation reactions occur between pH 1 and 2. For Al(III)/Fe(III) mole ratios of 3:7, 5:5 and 7:3, two distinct neutralisation processes for pHs 1-2 and 3-4 can be recognized. The extent of the buffer region at the high pH increases as the mole ratio of Al increases. These data are consistent with initial neutralisation of predominantly Fe(III) species at low pHs followed by neutralisation of Al(III) species at higher pHs. After the neutralisation of all the Al(III) the pH rose steeply and a precipitate was formed.

Isoelectric points

IEP data for the precipitates formed for the various mixtures are summarised in Table 6.1.

Table 6.1 IEP of precipitates of Al(III)/Fe(III) in various mole ratios

Al(III)/Fe(III) mole ratio	$Fe(OH)_3$	1:9	3:7	5:5	7:3	9:1	$Al(OH)_3$
IEP ± 0.06	5.81	5.90	6.43	6.52	6.61	7.35	8.90

It is clear that IEP increases with Al(III) content giving IEP values in a range between the IEP of pure iron and pure aluminum systems. The trend of the IEP versus Al(III) fraction is shown in Figure 6.2. The IEP trending of the precipitates shows a polynomial regression and remains approximately constant in the range of Al(III) to Al(III) + Fe(III) mole ratios of 3:7 to 7:3.

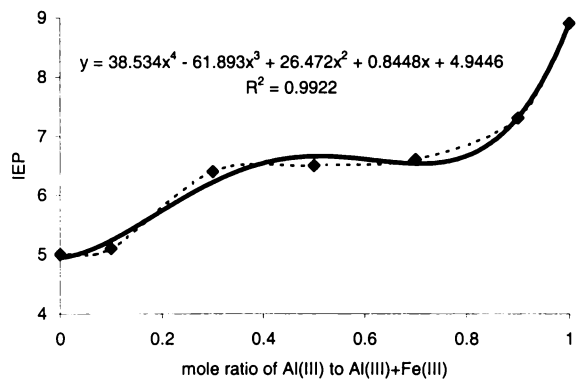

Figure 6.2 The trend of the IEP versus Al(III) mole ratio. The dashed is the experimental data and the solid line is the polynomial fit of the data.

X- ray studies

X-ray diffraction of the bulk phase materials was performed using a Philips X'Pert-XRD system.

X-ray diffraction data for the precipitates formed by neutralising the Al(III)/Fe(III) solutions are summarised in Figure 6.3. The precipitates were largely amorphous. Crystallinity increased as the Al(III) content increased but even at the highest Al(III) content the lines were broad, of low intensity and did not correspond to any known crystalline phase.

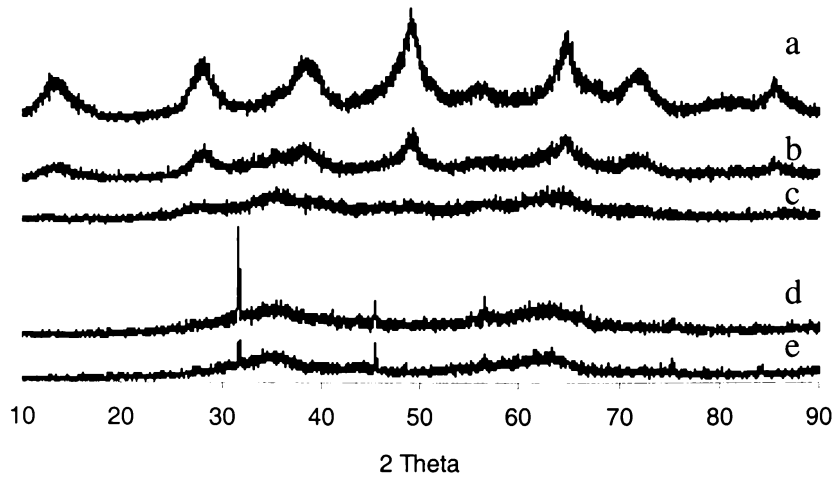

Figure 6.3 XRD pattern of hydroxide Al(III)/Fe(III) in various mole ratios (a) 9:1 (b) 7:3 (c) 5:5 (d) 3:7 (e) 1:9.

Curves d and e display varying amounts of a highly crystalline material. The lines correspond to those of NaCl. It is believed that small amounts of NaCl were carried over from the rinsing step.

6.1.1 Preparation of Al(III)/Fe(III)/Fe(II) mixed hydrous oxide

Al(III)/Fe(III)/Fe(II) mixed hydrous oxide precursor solutions (AFF) were prepared by neutralization of Al(III), Fe(III) and Fe(II) solutions in the mole ratios of 0:2:1,1:2:1, 2:2:1, 4:2:1 and 6:2:1, respectively. All solutions were thoroughly deaerated with nitrogen, which was continuously bubbled during the preparation. Ammonia solution was then slowly added into AFF solutions with vigorous stirring. Care was taken to exclude oxygen during all stages of the preparation. The reaction solutions were sealed with an airtight plastic film for 30 min and the supernatant was withdrawn under N_2 using a pipette. The solid was rinsed in the reaction flask with degassed distilled water introduced under N_2, and separated again. This process was repeated twice. The colloid was then oven dried in air at 100^0C for 24 hrs. The crystal morphology of Al(III)/Fe(III)/F(II) = 2:1:2 is shown in Appendix 6.1 (b).

Isoelectric point and magnetic properties

The electrokinetic and magnetic properties of the pure precipitates of Al(III)/Fe(III)/Fe(II) are summarised in Table 6.2. The magnetic properties of the product formed depended on the amount of Al(III) involved. More Al(III) results in weaker magnetic features, but higher cationic potential. IEP and the magnetic properties versus the mole % total Fe are shown in Figure 6.4.

Table 6.2 The IEP and magnetic properties of pure precipitates of the magnetic Al(III)/Fe(III)/Fe(II)

Molar ratio Al(III)/Fe(III)/Fe(II)	IEP ± 0.06	Mass (m) ± 0.001 (g)	Weight increase (Δ) ± 0.001 (g)	Δ/m ± 0.002 (g)	Magnetic effect $(\Delta/m)/(\Delta/m)_{Fe3O4}$ (%)± 0.3%
Fe_3O_4*	4.90	0.541	10.610	19.612	100
0:2:1	4.90	0.376	5.350	14.244	72.6
1:2:1	5.41	0.624	7.279	11.670	59.5
2:2:1	7.13	0.596	5.666	9.508	48.5
4:2:1	8.92	0.386	0.483	1.251	6.4
6:2:1	9.00	0.439	0.041	0.093	0.5
$Al(OH)_3$	8.90	-	-	-	-

*Pure magnetite (Fe_3O_4, 99%, Alfa Aesar)

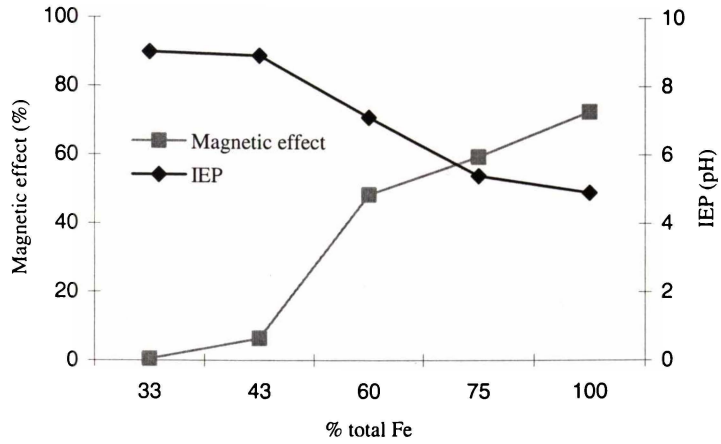

Figure 6.4 The effect of Fe content (%) on the IEP and magnetic effect of oven dried Al(III)/Fe(III)/Fe(II) hydroxide precipitates.

The data show that to achieve an IEP of approximately 6, an Fe(III) content of approximately 70% is required. At this Fe(III) content, the product still has useful magnetic properties (approximated 58% of that of Fe_3O_4).

X-ray studies

X-ray diffraction data for the precipitates formed by neutralising the Al(III)/Fe(III)/Fe(II) solutions are summarised in Figure 6.5. These materials were more highly crystalline than the Al(III)/Fe(III) systems. All but the two systems of lowest iron content had strong diffraction lines. Comparison of d-spacing data for these lines with published data (JCPDS) indicated the presence of magnetite (see Table 6.3). In addition, the black colour and magnetic properties that increased with Fe(II) content, distinguished these products from those containing Al(III) and Fe(III) alone.

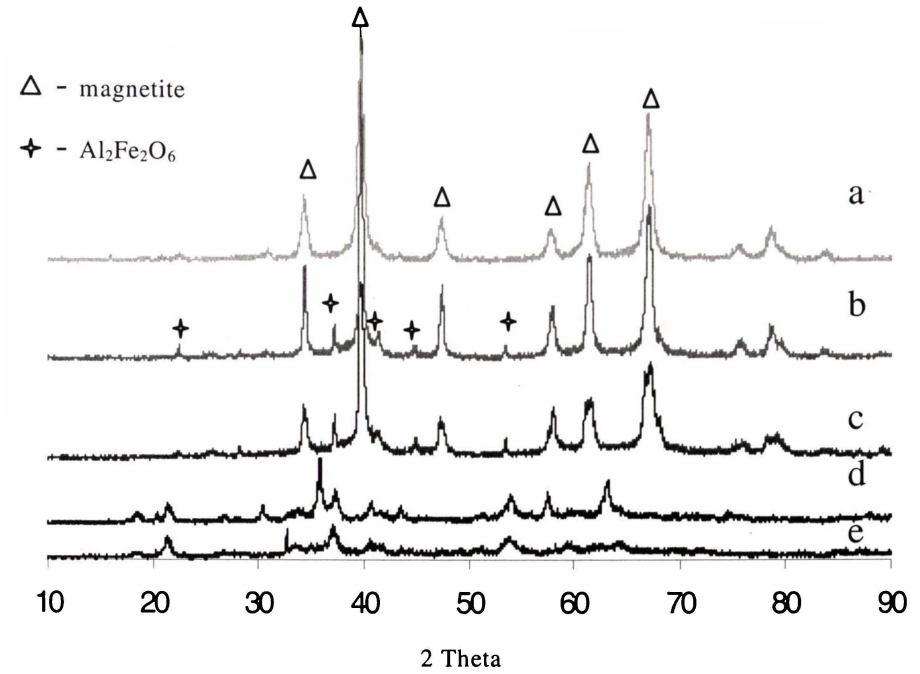

Figure 6.5 XRD pattern of magnetic materials Al(III)/Fe(III)/Fe(II) in mole ratios of (a) 0:2:1 (b) 1:2:1 (c) 2:2:1 (d) 4:2:1 (e) 6:2:1

Crystallographic data are summarised in Table 6.3. The six peaks in Figure 6.5 (a) correspond to magnetite Miller indices {hkl} of {220}, {311}, {400}, {422}, {511} and {440}, respectively (JCPDS 11-0614). There is some evidence of small amounts of hercynite ($Al_2Fe_2O_6$) also being present in all systems containing some aluminium. The published d-spacing data for synthetic hercynite (JCPDS 11-0562) are compared with the products formed in this work in Table 6.4. The d-spacing values correspond to Miler indices {hkl} value of {003},{310},{113}, {104}, {331}, {323}, {403}, {242} and {423}respectively.

Table 6.3 Comparison of d-spacings of magnetite and synthetic materials

Crystal plane {hkl}	220	311	400	422	511	440
Magnetite*	2.9660	2.5300	2.0960	1.7120	1.6140	1.4830
S_{021}	2.9623	2.5256	2.0868	1.7048	1.6120	1.4776
S_{121}	2.9518	2.5226	2.0868	1.7003	1.6108	1.4796
S_{221}	2.9628	2.5295	2.0958	1.7122	1.6162	1.4852
S_{421}	2.9452	2.5093	2.0814	1.7819	1.6053	1.4740
S_{621}	-	2.5686	2.0800	1.7047	-	1.4955

* JCPDS – (11-0614)

Table 6.4 Comparison of d-spacing of Hercynite ($Al_2Fe_2O_6$) and synthetic Al(III)/Fe(III)/Fe(II) materials

Crystal plane {hkl}	003	310	113	104	331	323	403	242	423
$Al_2Fe_2O_6$*	2.4800	2.2150	2.1650	1.7960	1.5330	1.4910	1.4310	1.3450	1.3030
S_{621}	2.4210	2.2228	2.1724	1.7840	1.5548	1.4918	1.4495	1.3516	1.3055
S_{421}	2.4100	2.2163	2.1629	1.7819	1.5543	1.4740	-	1.3896	1.3896
S_{221}	2.4977	2.2088	-	1.7122	1.5966	1.4852	1.4506	1.3136	1.3104
S_{121}	2.5051	2.2067	-	1.8402	1.5999	1.4759	1.4513	1.3219	1.3106

* JCPDS – (11-0562)

The XRD data analysis show that the products of Al(III)/Fe(III)/Fe(II) systems are mixed two phase materials. Magnetite content decreased with Al(III) content.

6.2 Modification of ARSS by treatment with Al(III)/Fe(III) solutions

6.2.1 Materials and method

In this study the stock Al(III)/Fe(III) precursor solutions used to form the Al(III)/Fe(III) films were prepared by the method of Section 6.1. The ARSS media used in this study was prepared as described in Section 2.2.2.

The following procedure was followed:

- The desired amount of ARSS was place in a Buchner flask and evacuated with a venturi aerator until all air had been excluded. Stock solutions of $AlCl_3$ and $FeCl_3$ (total volume of 100 mL at 1 mol/L) in the mole ratios of 1:9; 3:7; 5:5; 7:3 and 9:1, respectively were then drawn into the flask and stirred with the ARSS.

- The mixture was neutralised by drop-wise addition of 100 mL (3 mol/L) sodium hydroxide solution.

- After 30 min of contact, excess solution was drained and the ARSS was oven dried at 100°C for 24 hr.

- The dried samples were then rinsed vigorously with deionised water to remove loose precipitate.

- They were then oven dried at 100°C for a further 24 hr. The samples obtained in this way were named: '$S_{nAl(III)nFe(III)}$' (nAl(III)nFe(III) = 1:9; 3:7; 5:5; 7:3 and 9:1). Where *n* indicates the Al(III) to Fe(III) mole ratios.

- Above steps were repeated to produce samples with 2 coats. The samples were named '$S_{nAl(III)nFe(III)(2)}$', where (2) indicates two coatings.

6.2.2 Results and discussion

Characterisation of coating films

The ICP data and IEP data for untreated and treated ARSS with Al(III)/Fe(III) are summarised in Table 6.5. Untreated ARSS gave 0.006 x 10^{-3} mole/g Al and 0.005 x 10^{-3} mole/g Fe, while treated samples had total Fe and Al values generally in the range 0.822 to 1.682 x 10^{-3} mole/g. The amounts of metal species extracted increased with the number of coating cycles.

The effect of treatment on the IEP of ARSS is apparent from the IEP data summarised in Table 6.5. The IEP of ARSS increased from 4.72 ± 0.06 to 6.68 ± 0.06 with various Al(III)/Fe(III) mole ratios. In general the IEP of the treated ARSS increased with Al(III) content of the treatment solution and the final film formed. A second contact cycle increased the total amount of material deposited in the film but had little effect on film composition or IEP.

Table 6.5 Properties of ARSS coated with A(III)/Fe(III)

Sample	Al(III)/Fe(III) mole ratio	Al x 10^3 ±0.001 (mole/g)	Fe x 10^3 ±0.001 (mole/g)	(Al+Fe) x 10^3±0.001 (mole/g)	Al/(Al+Fe) mole ratio (%)	IEP ±0.06	Coating cycles
ARSS	-	0.006	0.005	0.012	-	4.10	
Al(III)*	-	-	-	-	-	8.90	1
Fe(III)*	-	-	-	-	-	5.81	1
$S_{1:9}$	1:9	0.128	0.747	0.875	14.6	4.72	1
$S_{3:7}$	3:7	0.273	0.549	0.822	33.2	5.90	1
$S_{5:5}$	5:5	0.523	0.506	1.029	50.8	6.25	1
$S_{7:3}$	7:3	0.598	0.348	0.946	63.2	6.57	1
$S_{9:1}$	9:1	0.848	0.134	0.981	86.5	6.68	1
$S_{1:9(2)}$	1:9	0.166	1.144	1.310	12.7	4.90	2
$S_{5:5(2)}$	5:5	0.785	0.897	1.682	46.7	5.91	2
$S_{9:1(2)}$	9:1	1.134	0.229	1.364	83.2	6.52	2

* Pure $Al(OH)_3$ & $Fe(OH)_3$ precipitates

6.3 *Modification of ARSS by treatment with Al(III)/Fe(III)/Fe(II) solutions*

6.3.1 Materials and method

The preparation of stock precursor solutions of Al(III)/Fe(III)/Fe(II) used to form mixed hydrous oxide iron/iron films was described in Section 6.1.1.

The coating procedure was similar to that described in Section 5.5.2. The products obtained in this way were named: '$S_{nAl(III)nFe(III)nFe(II)}$' (nAl(III)nFe(III)nFe(II) = 121; 221; 421 and 621), where *n* indicates the Al(III), Fe(III) and Fe(II) mole ratios.

6.3.2 Results and discussion

Characterisation of coating films

The ICP analysis data and IEP data are summarised in Table 6.6. The presence of Al(III) in the treatment systems generally led to higher IEP values. This was most pronounced for the Al(III)/Fe(III)/Fe(II): 4:2:1 and 6:2:1 systems where IEPs of 8.51 ± 0.06 and 8.72 ± 0.06 were observed.

At low Fe(III)/Fe(II), little or no magnetite was observed in the bulk phases. In systems containing low concentrations of Fe(III)/Fe(II) and where magnetite was not apparent in the bulk phases (Figure 6.5 d-e), IEPs similar to those for the pure Al(III) systems were observed. The broad and low intensity XRD peaks for the bulk phases of these systems did not correspond to any known crystalline phase and the pattern was quite different from those obtained for the bulk phases formed from the Al(III)/Fe(III) systems.

Table 6.6 Properties of ARSS coated with Al(III)/Fe(III)/Fe(II)

Sample	Al(III)/Fe(III)/Fe(II) mole ratio	Al x 10^3 ±0.001 (mole/g)	Fe x 10^3 ±0.001 (mole/g)	(Al+Fe) x 10^3 ±0.001 (mole/g)	Al / (Al+Fe) mole ratio (%)	IEP ±0.06
ARSS	-	0.006	0.005	0.012	-	4.10
S_{mag-1}	0:2:1	0.016	0.871	0.887	-	4.52
S_{121}	1:2:1	0.165	0.551	0.716	23.0	5.41
S_{221}	2:2:1	0.206	0.443	0.649	31.7	7.10
S_{421}	4:2:1	0.231	0.352	0.583	39.7	8.51
S_{621}	6:2:1	0.466	0.257	0.723	64.5	8.72

Magnetic and surface charge properties

The magnetic properties of the modified ARSS were examined by measuring the extent the samples were attracted or repelled by an applied magnetic field. The weight change when applying a magnetic field (Gouy Method) was used.

The magnetic properties of the modified media are shown in Table 6.7. Pure magnetite (Fe_3O_4, 99%, Alfa Aesar) and TM ($Fe_{3-x}Ti_xO_4$, provided by BHP New Zealand Steel Ltd) are presented for comparison. TM produced a magnetic effect that was 80.5% of that observed for pure magnetite. The magnetic properties of the bulk synthetic phases decreased with Al content (Table 6.2). They ranged from 72.6% of the magnetite value with no Al addition to 0.5% of the magnetite value when the Al(III) to total Fe mole ratio was 6. ARSS modified by a Fe(III)/Fe(II) coating containing no Al had a magnetic effect that was 7.0% of the effect observed for pure magnetite. The effect decreased sharply when Al was incorporated into the coating film.

Table 6.7 Magnetic properties of ARSS treated with Al(III)/Fe(III)/Fe(II)

Sample	Al(III)/Fe(III)/Fe(II) mole ratio	Mass (m) ± 0.001 (g)	Weight increase (Δ) ± 0.001 (g)	(Δ)/m ± 0.002	(Δ/m)/ $(\Delta/m)_{Fe3O4}$ (%)± 0.3%
Fe_3O_4	-	0.541	10.610	19.612	100
Natural TM	-	1.122	17.720	15.790	80.5
ARSS	-	0.213	-0.005	-0.023	-0.1
S_{mag-1}	0:2:1	0.242	0.330	1.364	7.0
S_{121}	1:2:1	0.258	0.069	0.267	1.4
S_{221}	2:2:1	0.244	0.440	0.180	0.9
S_{421}	4:2:1	0.236	0.023	0.099	0.5
S_{621}	6:2:1	0.239	0.012	0.050	0.3

The variations of the magnetite effect and IEP of the modified ARSS with total Fe content are shown in Figure 6.6. Generally, the coated ARSS had the IEP values similar to the bulk precipitate phases, but showed very weak magnetic properties.

XRD studies detected some magnetite deposited onto the surface of ARSS. The d-spacing data of for the coated samples are presented together with published magnetite data in Table 6.8. The peaks obtained for the treated systems were of very weak intensity indicating the presences of only small amounts of crystalline material.

Table 6.8 Comparison of d-spacings of Fe_3O_4 and coated sample

Crystal plane {hkl}	220	311	400	422	511	440
Fe_3O_4 (Magnetite)	2.9660	2.5300	2.0960	1.7120	1.6140	1.4830
Coated sample	2.9442	2.5154	-	1.7465	1.6042	1.4792

The magnetite effect is decreased and the IEP value is increased with decreases in total Fe content. However the effect, particularly the magnetic effect, is non linear suggesting that factors other than the total amount of Fe deposited are important.

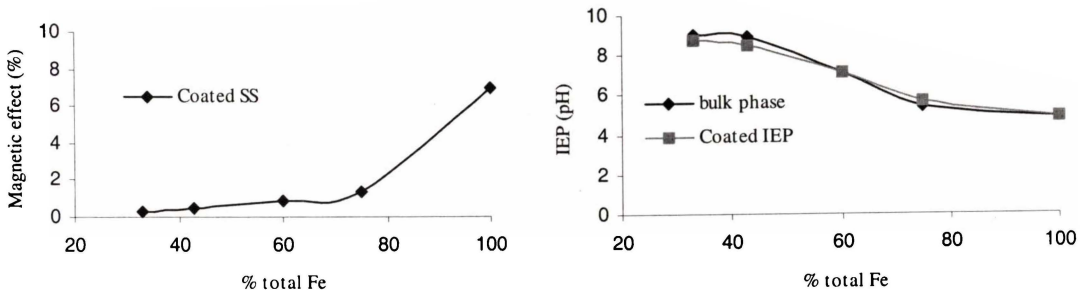

Figure 6.6 IEP and magnetic effect versus % total Fe

6.4 Summary

The principal findings of the research described in this chapter are summarised below:

- The IEP of synthetic Al(III)/Fe(III) oxides can be controlled by the mole ratio of Al(III) to Fe(III).

- Using appropriate mole ratios of A(III)/Fe(III)/Fe(II) it is possible to prepare bulk phases with useful magnetic properties and controlled IEP.

- The IEP of treated ARSS increases with increasing Al(III) content of the treatment solutions for both the Al(III)/Fe(III) and Al(III)/Fe(III)/Fe(II) solutions.

- Treatment of ARSS with Al(III)/Fe(III)/Fe(II) solutions produces modified ARSS with very weak magnetic properties. Only for the system prepared from Fe(III)/Fe(II) alone was a useful magnetic property obtained. This system showed clear evidence for magnetite in the XRD trace. It appears that the presence of Al inhibits the formation of magnetite in the ARSS pores.

Chapter Seven: Filtration by Modified Silicon Sponge

7.1 Introduction

In previous chapters it has been shown that it is possible to modify the charge characteristics of SS by pre-treatment with Al(III), Fe(III) and mixtures of Al(III) and Fe(III). Treatment by pure Al(III) yielded a product of highest isoelectric point. This was considered likely to be the most useful for the filtration of negatively charged colloids. In this chapter the filtration efficiency of Al(III) coated SS is described. The effects of ARSS particle size and bed depth for both Al treated and untreated systems were also investigated.

It has also been demonstrated (See Section 5.5.3 and 6.3.2) that appropriate treatment of SS with Fe(II)/Fe(III) mixed solutions, imparted magnetic properties to the SS. Since it was expected that the use of SS of small particle size, while giving better filtration efficiency, would also lead to lower hydraulic conductivities, the use of magnetically conditioned beds of fine ARSS was envisaged. Magnetic ARSS was prepared following the procedure outlined in Chapter 6. Hydraulic conductivity and filtration using magnetically condition beds of fine magnetically conditioned ARSS will be described.

7.2 Filtration properties of ARSS

7.2.1 Effect of ARSS particle size on hydraulic conductivity

The effect of particle size on hydraulic conductivities of ARSS of various particle sizes was investigated using the apparatus shown in Figure 4.11 (a). Measurements were performed under constant total head and head loss across the bed. Particle size fractions of 125-250 μm, 250-500 μm, 500-600 μm and 710-

1000 μm were chosen. Data for hydraulic conductivity of naturally packed ARSS are summarised in Table 7.1.

Table 7.1 Hydraulic conductivity of naturally packed ARSS

Particle size (μm)	125-250	250-500	500-600	600-710	710-1000
Hydraulic conductivity, K x10^4 (m/s)	6.50	31.7	33.5	64.1	85.6

As anticipated, the hydraulic conductivity of ARSS increased with particles size. For the particle size range of 125-250 μm, hydraulic conductivity of ARSS was 6.5 x 10^{-4} (m/s). This is significantly higher than value obtained (3.2 x 10^{-4} m/s) for ARTM of the same particle size (Section 4.3.3). It is likely that the difference was due to the closer packing of the denser and regularly shaped TM grains. According to the Kozeny Equation (Section 4.1.1, Equation 4.3), closer packing will decrease the porosity, consequently, the hydraulic conductivity *K* will decrease.

7.2.2 Effect of ARSS particle size on filtration efficiency

The effect of ARSS particle size on filter performance was studied using the three size fractions investigated above (125-250 μm, 500-600 μm and 710-1000 μm). Filter bed depths were 200 mm. The kaolin sample used in these studies was prepared according to the method of outlined in Section 2.2.3. It had an initial turbidity of 42 NTU and a concentration of 35.68 mg/L. The pH of the suspension was 5.7 and the filter flow rate was maintained at 4.5 m/hr. The results of turbidity removal for the three filter medium sizes are shown in Figure 7.1.

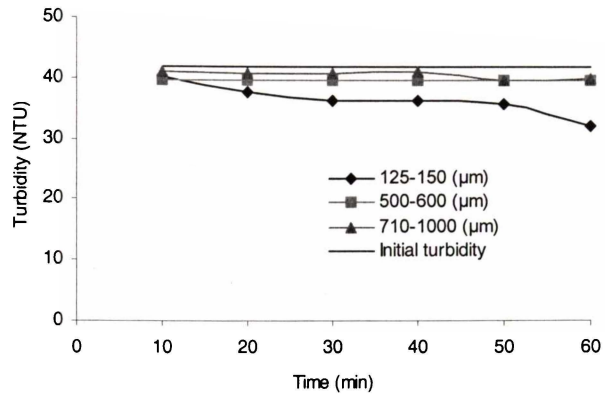

Figure 7.1 Effect of ARSS size on turbidity removal (bed depth 200 mm, pH 5.7)

The filtration results show that all the media gave poor turbidity reductions. The finest medium (size range of 125-250 μm) performed only slightly better than the others. It appears that under the conditions of the filtration experimental (pH 5.7), charge effects dominate the filtration process. Both suspended kaolin colloid and ARSS media will have negatively charged surfaces.

7.3 Filtration properties of treated SS

7.3.1 Effect of aluminium pre-treatment and ARSS particle size on filtration efficiency

The effect of medium surface pre-treatment on filtration efficiency was studied using aluminium coated ARSS. The coating procedure of Section 5.3.1 was followed. Medium particle size and other conditions were as described in Section 7.2.2. The results for turbidity removal for the three filter particle sizes are shown in Figure 7.2.

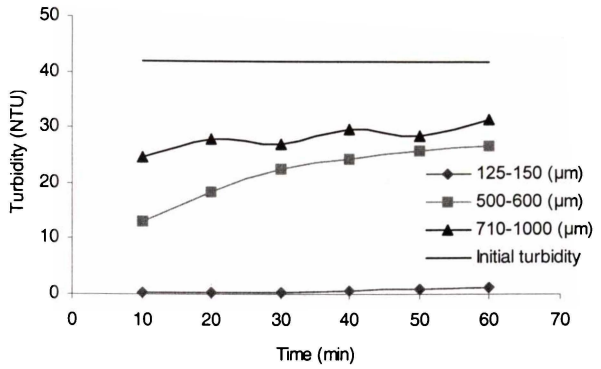

Figure 7.2 The effect of particle size on turbidity removal by coated ARSS (bed depth 200 mm, pH 5.7)

The aluminium treated ARSS of 125-150 μm particle size shows high turbidity removal and achieved 99% turbidity reduction. The coated ARSS of 500-600 μm particle size achieved about 42% turbidity reduction and the 710-1000 μm particle size treated ARSS achieved only 22% turbidity reduction. Comparison with the data of Figure 7.1 shows that all treated ARSS media produced improved turbidity removal which was most pronounced for the fine medium.

7.3.2 Effect of pH on filtration efficiency by aluminium treated ARSS

The effect of pH on Al(III) coated ARSS (particle size 710 – 1000 μm) filtration efficiency was investigated. The filter bed depth was 400 mm and a filtration velocity of 6.5 m/hr was maintained by adjusting an outlet valve. The filtration experiments were carried out under various pH conditions: 3.5, 5.7 and 9.5. The pH was adjusted using 0.1 mol/L HCl and NaOH.

The filtration experimental was as described in Section 4.2.2. The treated ARSS had an IEP of 7.25 ± 0.06 and the untreated ARSS had an IEP of 4.10 ± 0.06. The kaolin sample for filtration was prepared according to the method of outlined in Section 2.2.3.

The filtration results at pH 3.5 are shown in Figure 7.3.

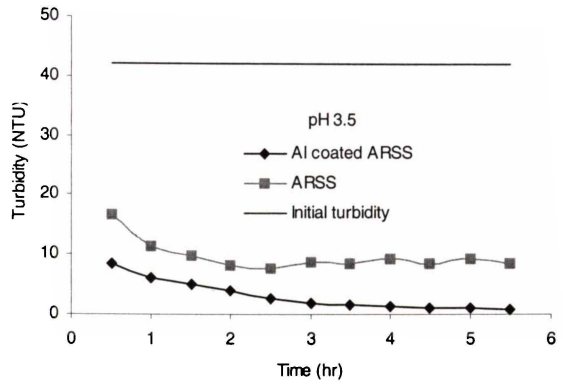

Figure 7.3 Turbidity reduction using modified ARSS and ARSS at pH 3.5 (particle size 710-1000 μm, bed depth 400 mm)

Both media showed significant colloid removal. The treated ARSS produced a turbidity reduction of 94% while the untreated ARSS gave about 72% turbidity reduction. At this pH condition both treated ARSS and untreated ARSS would have a positively charged surface. On the other hand the kaolin colloids would be negatively charged. As anticipated, the electrostatic interaction improved the filtration efficiency for both media but the improvement was greater for treated SS.

The filtration results at pH 5.7 are shown in Figure 7.4.

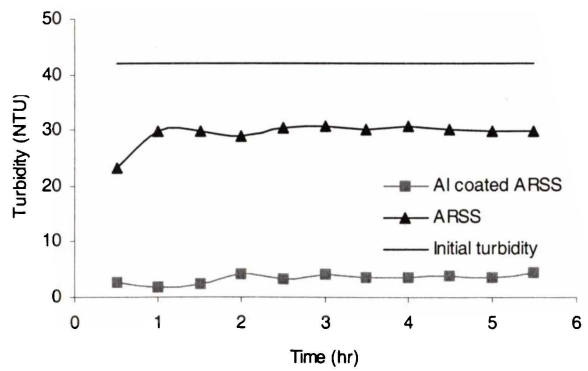

Figure 7.4 Turbidity reduction using modified ARSS and ARSS at pH 5.7 (particle size 710-1000 μm, bed depth 400 mm)

7.4 Magnetic conditioning of magnetite treated SS filtration beds

7.4.1 The effect of magnetic field

SS modified by a Fe(III)/Fe(II) coating was found (see Section 5.5.2) to have a magnetic effect that was 7.0% of the effect observed for Fe_3O_4. Al containing samples had much lower magnetic effects ranging from 1.4% to 0.3% of the values obtained for Fe_3O_4 (see Table 6.7).

The effect of magnetic field strength on magnetic conditioning of the magnetite treated ARSS was investigated using the procedure described in Section 4.3.2. The coated 125-250 μm ARSS, $S_{mag\text{-}1}$ (see Section5.5.3), was used in a bed with an initial bed depth of 45 mm. In order to achieve higher field strengths, a 10 A 30V (Model: TPS-2000) DC power supply was used. Data for settled bed volumes at various vertical field strengths are summarised in Table 7.2.

Table 7.2 Bed depth of settled ARSS, $S_{mag\text{-}1}$, for various field conditions.

Field strength		Vertical Field	
i (A)	H (T)	Bed depth (mm)	Bed expansion (%)
6	0.018	48.0	6.6
4	0.012	46.5	3.3
2	0.006	45.0	0

The results show that a vertical field at the maximum field strength obtainable (0.018 T) produced a bed expansion of approximately 7%. No effect was observed when a horizontal field was used.

7.4.2 Measurement of hydraulic conductivity of magnetically conditioned beds

The effect of magnetic conditioning of a $S_{mag\text{-}1}$ bed on hydraulic conductivity was investigated following the procedure described in Section 4.3.3. The $S_{mag\text{-}1}$ bed was expanded by controlled backwash flows. A vertical field of 0.018 T was

achieved. After backwash flow was stopped and the bed had settled to its magnetically conditioned volume, hydraulic conductivity measurements were performed under constant total head and head loss across the bed. Data are summarised in Table 7.3.

Table 7.3 Effect of magnetic conditioning on hydraulic conductivity of $S_{mag\text{-}1}$.

Sample	Magnetic conditioning	Bed expansion (%)	K x 10^4 ± 0.1 (m /s)
$S_{msg\text{-}1}$	Vertical field 0.018 (T)	6.6	10.5
$S_{msg\text{-}1}$	Horizontal field 0.018 (T)	0	7.4
$S_{msg\text{-}1}$	Unconditioned	0	7.3
ARSS	Unconditioned	0	6.5

The data show that under a vertical magnetic field, the hydraulic conductivity of the $S_{mag\text{-}1}$(10.5 x 10^{-4} m/s) was significantly higher than that of the unconditioned bed (7.3 x10^{-4} m/s) even though the bed expansion was slight. In addition, the data for hydraulic conductivity of $S_{mag\text{-}1}$ was higher than the value obtained for untreated ARSS (6.5 x 10^{-4} m/s) of the same particle size (Section 7.2.1) in a naturally packed bed. This suggests that some magnetic alignment of the particles may be occurring even when no field is applied.

For a horizontally applied field at maximum field strength, no bed expansion was observed and no significant effect on hydraulic conductivity was recorded.

7.4.3 Filtration study

The effects of medium surface charge and magnetic conditioning of the filtration bed were studied using ARSS and $S_{mag\text{-}1}$. The coating procedure of Section 6.4.1 was followed. Medium particle size was in the range 125 – 250 μm. Filter bed depths were 120 mm. The kaolin sample for filtration was prepared according to

the method of outlined in Section 2.2.3. Filtration at two pH conditions was investigated.

Filtration at pH 6.8

Figure 7.6 shows the filtration of a kaolin suspension at pH 6.8 by ARSS and $S_{mag\text{-}1}$. The ARSS was used in naturally settled bed whereas the $S_{mag\text{-}1}$ was used in both a settled bed and a magnetically conditioned bed (vertical field, 0.018 T). The pH 6.8 was chosen to be higher than the IEP of ARSS, $S_{mag\text{-}1}$ and kaolin.

Filtration at pH 4.5

The experiment described above was repeated at pH 4.5. Results are summarised in Figure 7.7. The pH 4.5 was chosen so that the pH was intermediate between the IEP of ARSS and $S_{mag\text{-}1}$ and above that of kaolin.

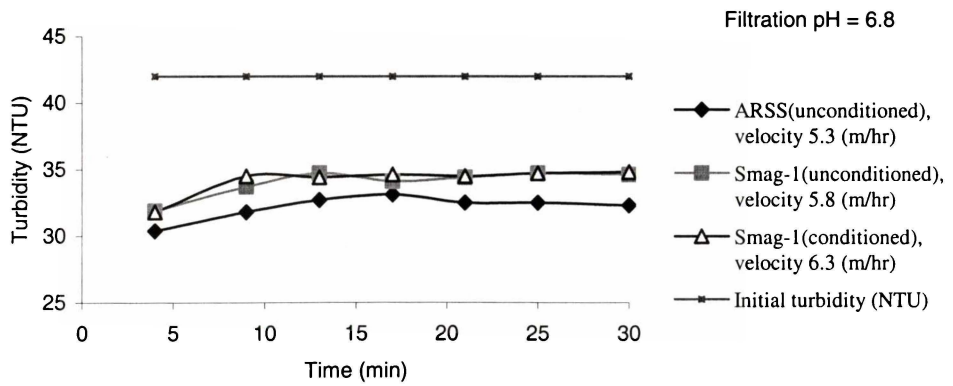

Figure 7.6 Turbidity reduction of ARSS and $S_{mag\text{-}1}$ in unconditioned and magnetically conditioned beds at pH 6.8.

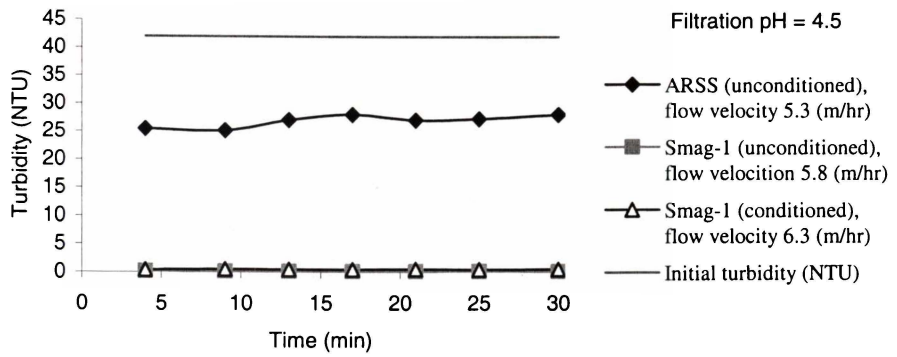

Figure 7.7 Turbidity reduction by ARSS and $S_{mag\text{-}1}$ in unconditioned and magnetically conditioned beds at pH 4.5.

At pH 6.8, both the treated and untreated media and the kaolin would be negatively charged. It is clear that neither modified ARSS nor untreated ARSS were able to effectively remove the negatively charged colloids. ARSS achieved colloid removal to about 21% turbidity reduction at a filtration flow rate of 5.3 m/hr. $S_{mag\text{-}1}$, achieved turbidity reduction of about 17% with a filtration flow rate of 5.8 m/hr for an unconditioned bed and 6.3 m/hr for a vertically conditioned bed. The slightly lower turbidity reduction achieved for magnetically conditioned $S_{mag\text{-}1}$ may have been the result of the slightly higher flow rate observed.

At pH 4.5, ARSS and the suspended colloids would both be negatively charged, whereas the $S_{mag\text{-}1}$, would be positively charged. Thus electrostatically enhanced filtration can be expected. Turbidity reduction greater than 99% for both magnetically conditioning and unconditioned beds was observed. On the other hand, the untreated ARSS achieved only 41% turbidity reductions at this pH.

7.5 Summary

The principal findings of the research reported in this chapter are summarised below:

- The effect of particle size on ARSS hydraulic conduction was as predicted by the Kozeny equation. In the size range 710-1000 μm, the value obtained ($85.6 \pm 0.1 \times 10^{-4}$ m/s) is similar to the value reported for silica sand (90×10^{-4} m/s) of similar particle size (Zhang, *et al.*, 1997).

- Particle size of untreated ARSS media, at least for a 200 mm bed, had little effect of filtration efficiency. However when pre-treated with aluminium, the finer material showed much improved filtration efficiency at pH 5.0. Improved performance of the larger particle size material was achieved when the bed depth was increased to 400 mm.

- The effect of pH on filtration efficiency for aluminium pre-treated ARSS supported the conclusion that optimum filtration efficiency was achieved when suspended particles and medium surface are of opposite sign.

- The magnetite coated ARSS, $S_{mag\text{-}1}$, had a magnetic effect that was approximately 7% of that of magnetite. When conditioned with a vertically aligned field bed expansions of approximately 6.6% and hydraulic conductivities that increased by approximately 40% were observed. Some increase, relative to ARSS, in hydraulic conductivity was observed for $S_{mag\text{-}1}$, even when no field was applied. This was interpreted to indicate some magnetic alignment of the particles of the bed even in the absence of a field.

- With a horizontally aligned magnetic field, little conditioning of the bed was observed and hydraulic conductivity was not affected.

7.6 Reference

Zhang, Z. J., Kuninori, O., Takemasa, I. 1997. Environmental Influence of land Use in Northern and Northeastern China. http://www-cger.nies.go.jp/lugec/zhangzj-E.htm, (last access: 8 Aug. 2000).

Chapter Eight: General Discussion and Conclusion

8.1 Summary of principal findings

The research presented in this thesis had the general aim of determining for TM and SS, how particle size, surface charge and packing (of magnetic particles under various fields) affected hydraulic conductivity and filtration efficiency. A central idea motivating the work was that chemicals might be more effectively used to treat the media rather than to treat the water. The principal findings from the research are set out in the sections below.

8.1.1 Filtration by fine TM

As was expected, the filtration efficiency of TM increased as particle size decreased. Excellent turbidity removal was achieved by 55 mm beds of 32-45 μm TM. However hydraulic conductivities were so low, that even for the shallow bed used, filtration flow velocities were lower than achieved in conventional rapid gravity filters. Conditioning the bed in an expanded state using a vertically aligned magnetic field dramatically increased hydraulic conductivity. For example a 28% increase in the bed volume produced a 140% increase in hydraulic conductivity. However the filtration efficiency of the magnetically conditioned bed fell by approximately 9%.

A key to improving removal of negatively charged colloidal particles from water by filtration is to make the medium surface more electropositive. This will enhance electrostatic interactions. Natural and synthetic TMs have IEPs in the range 3.6 to 3.9. In the pH range from the IEP of water impurities to pH 3.6, the TM and the impurities will be of opposite charge. The adjustment of the pH to 3.5 produced 99% removal of kaolin turbidity in a magnetically conditioned bed that gave a flow velocity of 6.3 m/hr.

8.1.2 Surface modification by treatment with Fe(III) and Al(III)

Attempts to raise the IEP of TM by surface treatment with aluminium and iron polycation solutions were unsuccessful. However, treatment of the porous ARSS with the polycation solutions was more successful. ARSS has IEP of 4.10 ± 0.06. This can be raised in a controlled way by surface treatment with appropriate iron and aluminium polycation solutions.

Aluminium treatments raised the IEP of ARSS to within the range 5.73 ± 0.06 to 8.52 ± 0.06 depending on treatment conditions. The IEP of freshly prepared pure precipitates of $Al(OH)_3$ was found to be 8.90 ± 0.06

Iron treatments raised the IEP of ARSS to 5.27 ± 0.06. The IEP of freshly prepared pure precipitate of $Fe(OH)_3$ was found to be 5.82 ± 0.06

When the iron treatment used Fe(II) and Fe(III) in the mole ratio of 1:2, the treated medium exhibited magnetic properties. The magnetic effect appeared to be related to the amount of magnetite deposited into the pores of the ARSS.

Surface treatment of ARSS with Al(III)/Fe(III)/Fe(II) solutions produced a series of materials with IEP and magnetic effects pre-determined by the iron to aluminium ratios. The IEP increased with Al(III) content and the magnetic effect decreased with Al(III) content. While magnetic media with high IEPs could not be produced by a single treatment, a two step treatment involving initial Fe(II)/Fe(III) treatment to impart magnetic properties followed by treatment with Al(III) polycations to raise the IEP should be effective.

The challenge of devising a treatment procedure to raise the IEP of TM remains. On the basis of the results obtain in the present work, treatment with appropriate aluminium, iron or other positively charged colloidal or polymer systems at pHs intermediate between the IEP of the colloid/polymer and the TM appears to be the best strategy for achieving this aim.

It has been demonstrated that modification of filtration media by appropriate surface treatment can achieve improved efficiency for colloid removal. The permanence of the effects achieved in prolonged use and after repeated backwash

cycles remains to be assessed. An advantage of the treated porous ARSS systems is that the hydrous oxide material is not limited to an exterior surface film. Greater durability of the effect can be anticipated.

8.1.3 Backwashing of magnetically conditioned beds

Higher interstitial flow velocity for backwashing can be achieved in magnetically conditioned beds. In the case of magnetically conditioned TM, a significant enhancement of backwash efficiency (i.e. a lower requirement of backwash water) resulted.

8.2 Applications to practical filtration systems

8.2.1 TM

Conventional municipal rapid gravity water treatment filters operate with a bed depth of approximately 500 mm, a total head of between 2-3 m, a head loss across the bed of about 1 m and produce filtration flow velocities of 6-12 m/hr (Harrison Grierson, 2002). The use of 150-180 μm TM under the same conditions would yield flow velocities of 0.4 m/hr and water production would be correspondingly less. Shallower beds may be enable flow to be increased but under current operational regimes there is a limit to how shallow the bed can be made and still ensure formation of a uniform bed after backwashing. The filtration efficiency for kaolin suspensions when using the 150-180 μm TM was only about 60%. Bed depth beyond 55 mm brought about only slight improvement. Filtration efficiencies of 90% and higher were not obtained until the particle size was reduced 32-45 μm and hydraulic conductivities were further reduced. It is unlikely therefore than TM will find application in conventional single media rapid gravity filters.

Two alternative applications are possible. A thinner bed of TM could be used as a bottom polishing layer in multi-media filtration systems. Its small particle size would serve to remove small suspended solids and its high density would help fluidisation at the base of the filter. Two potential problems would need to be

overcome. These include the likelihood that the fine media would become mixed with coarser overlays due to the lower flow velocity required for fluidisation (Blattler, 2002) and the underfloor system would have to be capable of retaining the fine TM particles. Alternatively TM might find application in pressure filtration systems. For a bed depth of 500 mm, a head of 20-30 m would be required. The only realistic way of achieving this pressure would be in a pressurised filtration system.

The possibility of using TM in smaller scale systems shows more promise. For example, water supplies for rural homes and farms are usually equipped with pressure systems. The installation of pressure filters into such supplies could be achieved relatively easily. Such systems would lend themselves more readily to allowing application of magnetic stabilisation with permanent magnets, particularly for backwashing. A robust water treatment facility that could remove fine particulates without the use of chemicals and which could be designed to operate automatically has attractive features. If ways could be found to raise the IEP of TM, the fine particle size range would be less necessary and the usefulness of the system would be increased.

8.2.2 Modified SS.

In contrast to TM, the Al(III) and Fe (III) treated SS media should find application in existing filter systems. The hydraulic conductivity is little affected by the pre-treatment so the hydraulic performance of the medium would not be significantly affected. The pre-treatment does bring about dramatic improvement in filtration efficiency for the 710-1000 μm SS providing the bed depth was sufficient (400 mm or greater). In dual media filters where the SS is used in combination with silica sand, the SS layer is usually about 200 mm (Steven, 1997). To achieve an optimum result it would be necessary to replace all the media with the modified SS.

The use of flocculant dosed beds is not new. The dosing of filter bed with Fe(III) or Al(III) has been used to by-pass a separate clarification step. However such dosing is usually required after each backwash (Jamieson, 2002). A potential

advantage of the conditioned SS developed in the present work is that the surface films are distributed over the internal vesicular pore surfaces as well as exterior surfaces and so will be less easily dislodged during backwashing. Other workers who have used preconditioned media have observed that the effectiveness of the conditioning decreases with time (Chen, *et al.*, 1998).

8.3 Options for water treatment with less reliance on the use of chemicals

The usual approaches to water treatment technologies that place less reliance on chemical generally involve membrane filtration. Improved membrane performance and reliability now means that is possible to remove particulates with sizes below 1 μm at the high volume flow rates needed for water supply systems. The present work has followed the alternative option of developing more efficient media that will allow particulates to be removed by the combination of interactions that operate in granular filtration. The two main strategies investigated were reduction of particle size to increase the effect of straining and surface modification to increase the role of adsorption. In addition the TM medium included in the study allowed investigation of magnetic conditioning as an aid in the management of filtration by fine media beds.

One of the potential benefits of lower chemical consumption is reduced cost. For example, the Hamilton City Council currently spends approximately $300 000 a year on flocculation chemicals (Steven, 1997)

8.4 Summary of conclusions

The principal conclusion drawn from the studies reported in this thesis are summarised below:

- The IEP of natural TM thoroughly washed with deionised water and then rinsed with HCl solution (ARTM) was 3.64 ± 0.06. The value obtained for synthetic TMs ranged between 3.59 to 3.90. High filtration efficiency was

achieved by adjusting the pH to 3.5, which is below the IEP of TM, but above the IEP of the kaolin model suspension.

- The hydrodynamic properties of magnetic media such as TM can be usefully modified by magnetic conditioning. Hydraulic conductivity was increased and backwash efficiency was enhanced by application of a vertical field.

- Surface coating with Fe(III) and Al(III) allowed the IEP of SS to be adjusted. The highest IEP value obtained for the Al(III) treated SS was 8.52 ± 0.06.

- Magnetic properties can be imparted to SS by surface coating with Al(III)/Fe(III)/Fe(II). The IEP of the treated SS increased with Al(III) content while the magnetic effect decreased with Al(III) content.

- The development of filtration systems based upon the media developed in this work, offers the possibility of efficient filtration with less reliance on chemical flocculants.

8.5 Recommendations for future work

During the progress of the work a number of aspects requiring further investigation were identified. These include:

- The Development of an effective way of modifying the electrokinetic properties of natural TM. Treatment by appropriate colloidal or polymer systems is suggested.

- The stability of Al(III) and Fe(III) coated ARSS media needs to be tested in prolonged pilot filtration trials. The effectiveness of these media in removing microbes is a priority.

- Investigations of two step treatments with Fe(II)/Fe(III) followed by Al(III) to produce magnetic ARSS systems with high IEP are required.

- Further work to optimise magnetic conditioning to achieve optimum backwash efficiency would be useful.

A motivating factor for the work described in the this thesis was a desire to gain the information needed to develop new options for granular water filtration systems that placed less reliance on the use of chemicals. Modified SS, providing pilot plant trials demonstrated adequate in service life, could eliminate or reduce the need for flocculation in some filtration systems. While fine media are unlikely to find application in large scale filters, their use in small systems is more promising. One possible application of the fine high IEP magnetic pumice media developed is in small polishing filters for domestic supplies. Installed in line and conditioned by permanent magnets, these filters would find application in untreated farm water supplies and as a protection against particulate and microbial contamination of treated municipal supplies. Work in this area is continuing.

8.6 References

Blattler, A. 2002. *Application of Granular Medium Filtration to Wastewater Treatment.* PhD thesis, University of Waikato.

Chen, J.; Truesdail, S.; Lu, F.; Zhan, G.; Belvin, C.; Koopman, B.; Farrah, S. Shah, D. 1998. Long-term evaluation of aluminium hydroxide-coated sand for removal of bacterial from wastewater. *Water. Res.* 32(7): 2171-2179.

Harrison Grierson. 2002. *Water Treatment Plant Filter Testing.* Harrison Grierson.

Jamieson, G. 2002. Personal communication. Works Filter Systems, Hamilton.

Steven, B. 1997. *Hamilton City Water Treatment Station Milestone Development Plan.* Hamilton City Council.

Appendix 2.1:

Kaolin particle size distribution in various pH

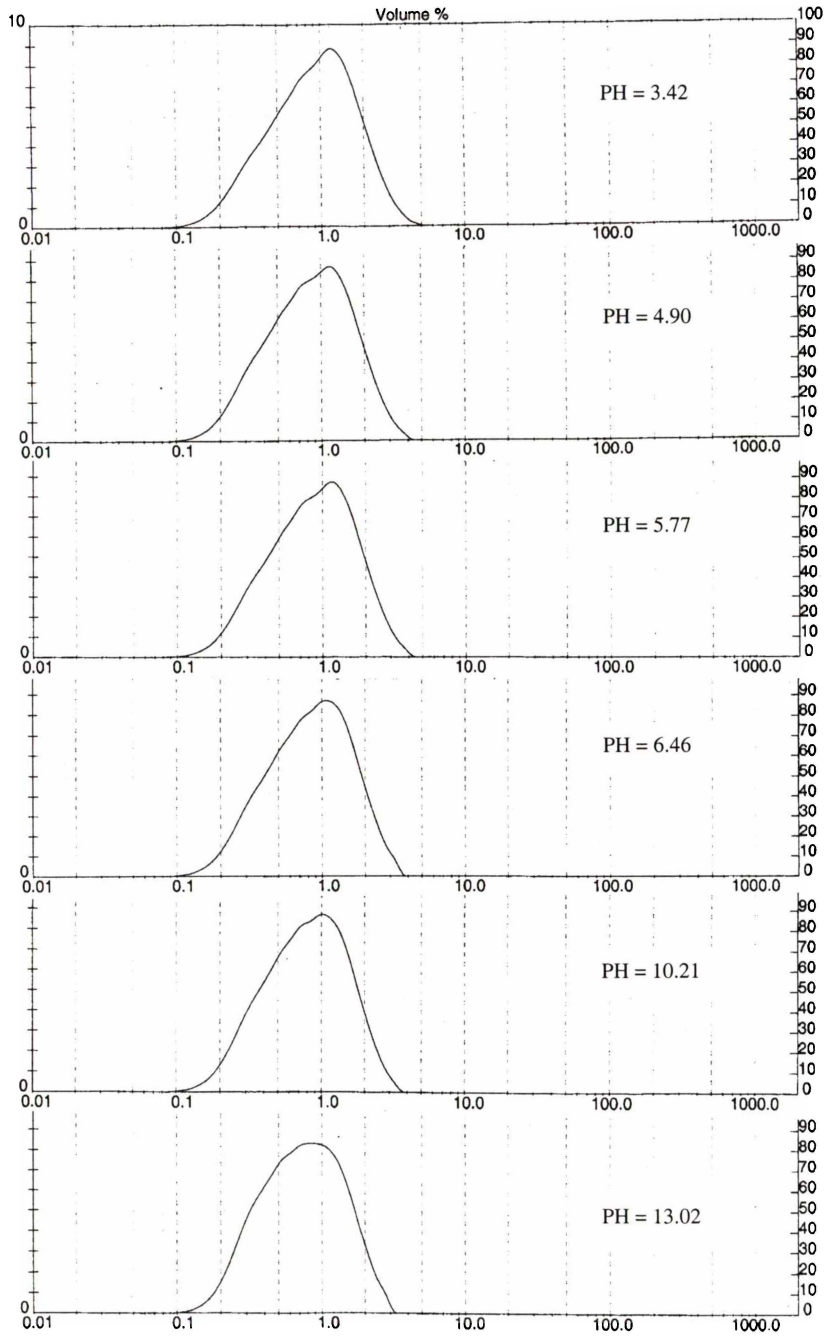

Appendix 2.2:

Crystal systems and Bravais lattices

System	*Axial lengths & angles*	*Brvais lattice*	*Lattice symbol*	
Cubic	Three equal axes at right angles a=b=c, $\alpha=\beta=\gamma=90^0$	Simple body-centred face-centred	P I F	P- simple; I- body-centered F- face-centered; C- base-centered; R- rhombohedral.
Tetragonal	Three axes at right angles, two equal a=b≠c, $\alpha=\beta=\gamma=90^0$	Simple body-centred	P I	
Orthorhombic	Three unequal axes at right angles a≠b≠c, $\alpha=\beta=\gamma=90^0$	Simple body-centred Base-centred face-centred	P I C F	
Rhombohedral	Two equal axes, equally inclined a=b=c, $\alpha=\beta=\gamma=90^0$	Simple	R	
Hexagonal	Two equal coplanar axes at 120^0, third axis at right angles a=b≠c, $\alpha=\beta=90^0, \gamma=120^0$	Simple body-centred face-centred	P	
Monoclinic	Three unequal axes, one pair not at right angles a≠b≠c, $\alpha=\gamma=90^0\neq\beta$	Simple Base-centred	P C	
Triclinic	Three unequal axes, unequally inclined and none at right angles a≠b≠c, $\alpha\neq\beta\neq\gamma\neq90^0$	Simple	P	

Appendix 3.1:

XRD data of natural TM

```
          DI file name: TITAN3.DI
        Input file name: TITAN3

      Start angle [°2θ]: 1.010
        End angle [°2θ]: 99.990
   Maximum d-value  [Å]: 87.39478
   Minimum d-value  [Å]: 1.00560
Maximum number of counts: 1421

         Anode material: Cu
      α1 Wavelength  [Å]: 1.54056
      α2 Wavelength  [Å]: 1.54439

Intensity measured with FIXED slit
```

D I F F R A C T I O N L I N E S:

Angle [°2θ]	d-value α1 [Å]	d-value α2 [Å]	T.width [°2θ]	Height [counts]	Backgr. [counts]	Rel.int. [%]	Signific
1.410	62.60270	62.75834	0.280	1421	23	100.0	3.37
10.725	8.24211	8.26260	0.060	100	10	7.0	1.38
18.450	4.80488	4.81683	0.140	58	10	4.1	3.66
22.110	4.01708	4.02707	0.480	5	9	0.3	1.42
24.290	3.66126	3.67036	0.120	14	9	1.0	2.08
26.795	3.32439	3.33266	0.100	15	9	1.1	1.03
27.780	3.20872	3.21669	0.080	35	9	2.4	1.33
28.225	3.15913	3.16698	0.120	17	9	1.2	0.98
30.255	2.95163	2.95897	0.120	174	9	12.3	3.79
32.015	2.79327	2.80021	0.120	6	9	0.4	0.92
33.250	2.69228	2.69898	0.240	31	9	2.2	3.76
35.580	2.52113	2.52740	0.140	576	9	40.5	12.58
37.210	2.41435	2.42036	0.100	29	9	2.1	1.09
37.935	2.36986	2.37575	0.240	3	9	0.2	0.83
39.355	2.28756	2.29325	0.100	4	10	0.3	0.78
40.965	2.20130	2.20677	0.200	8	10	0.6	1.46
42.125	2.14332	2.14865	0.120	7	10	0.5	1.09
43.190	2.09291	2.09811	0.120	207	10	14.6	4.59
43.435	2.08167	2.08684	0.040	119	10	8.4	3.81
43.550	2.07644	2.08160	0.040	53	10	3.7	2.87
44.770	2.02264	2.02767	0.400	3	10	0.2	0.83
49.575	1.83726	1.84183	0.240	5	9	0.4	0.95
52.340	1.74652	1.75087	0.120	6	10	0.4	1.06
53.585	1.70884	1.71309	0.140	62	10	4.4	4.88
53.725	1.70472	1.70896	0.080	38	10	2.7	1.04
54.015	1.69625	1.70047	0.120	12	10	0.9	0.77
57.015	1.61392	1.61793	0.120	114	11	8.1	2.39
57.225	1.60849	1.61249	0.060	146	11	10.3	2.96
59.860	1.54383	1.54767	0.120	4	10	0.3	0.94
62.735	1.47981	1.48349	0.080	117	10	8.2	0.76
64.095	1.45165	1.45526	0.280	7	10	0.5	1.84
65.905	1.41610	1.41962	0.240	4	10	0.3	2.45
71.065	1.32541	1.32870	0.080	11	10	0.8	0.80
71.290	1.32178	1.32506	0.160	10	10	0.7	0.79
74.065	1.27897	1.28215	0.100	25	11	1.8	1.37
74.290	1.27565	1.27882	0.100	17	11	1.2	1.16
75.015	1.26511	1.26825	0.080	13	11	0.9	0.91
75.235	1.26195	1.26509	0.120	12	11	0.9	1.04
78.985	1.21118	1.21419	0.120	9	10	0.6	1.64
81.970	1.17446	1.17738	0.400	2	10	0.1	0.93
85.070	1.13940	1.14223	0.480	1	10	0.1	1.50
86.790	1.12118	1.12397	0.160	10	11	0.7	1.33
89.740	1.09182	1.09453	0.040	40	11	2.8	1.17
90.030	1.08906	1.09176	0.080	30	11	2.1	0.97
92.305	1.06807	1.07073	0.100	4	12	0.3	0.80
94.510	1.04888	1.05149	0.080	30	12	2.1	1.16
94.820	1.04627	1.04887	0.120	18	12	1.3	0.81

Appendix 3.2:

XRD data of (Fe, Mg)(Al, Cr, Fe, Ti)$_2O_4$, (JCPDS, 25-1376)

25-1376 Wavelength= 1.54056

(Fe,Mg)(Al,Cr,Fe,Ti)2O4

Magnesium Iron Aluminum Chromium Oxide

Magnetite

Rad.: Cu λ: 1.5405 Filter: d-sp:

Cut off: Int.: I/Icor.:

Ref:

Sys.: Cubic S.G.: F

a: 8.330 b: c: A: C:

α: β: γ: Z: 8 mp:

Ref: Ibid.

Dx: Dm: SS/FOM: F_{10}=7(.069, 22)

PSC: cF56. Volume[CD]: 576.01.

d Å	Int	h	k	l
4.82000	40	1	1	1
2.95000	75	2	2	0
2.51000	100	3	1	1
2.41000	30	2	2	2
2.08000	65	4	0	0
1.70000	20	4	2	2
1.60000	80	5	1	1
1.47000	40	4	4	0
1.27000	20	5	3	3
1.09000	10			
1.04000	10	8	0	0
.855000	30			

Appendix 3.3: IEP of water rinsed natural TM *(see Section 3.3.1)*

	Run 1		Run 2		Run 3		Run 4		Run 5	
	pH	Potential (mV)	pH	Potential (mV)	pH	Potential (mV)	pH	Potential (mV)	pH	Potential (mV)
	3.52	-180	3.65	-244	3.41	-158	3.64	-209	3.52	-180
	3.42	-162	3.36	-185	3.18	-97	3.40	-176	3.12	-86
	3.30	-150	3.17	-102	3.10	-63	3.12	-60	3.02	-56
	3.30	-142	3.09	-78	3.00	-14	3.00	-19	2.92	-34
	2.96	-102	2.97	-17	2.88	45	2.88	9	2.87	-14
	2.87	-48	2.88	7	2.78	69	2.77	27	2.81	0
	2.71	13	2.78	50	2.69	115	2.67	52	2.79	3
	2.63	43	2.73	61	2.67	128	2.59	79	2.74	18
	2.46	120	2.70	77	2.52	136	2.46	86	2.66	43
	2.35	140	2.50	83	2.31	147	2.30	122	2.60	76
IEP	2.74		2.95		2.92		2.94		2.81	
σ	0.09									
IEP	2.87 ± 0.09									

Appendix: 3.4

IEP of TM pre-treated with alkali *(see Section 3.3.4)*

IEP of TM pre-treated with 1.0 mole/L NaOH

	PH	0.5 (hr)	PH	1.5(hr)	PH	3(hr)	PH	4.5(hr)	PH	7.5(hr)	pH	25(hr)	pH	3(day)	pH	17(day)
	3.2	-139	3.75	-244	3.41	-158	3.64	-209	3.77	-204	3.3	-151	3.37	-170	3.37	-98
	2.99	-94	3.36	-185	3.18	-97	3.4	-176	3.54	-142	3.1	-88	2.99	-51	3.27	-63
	2.87	-45	3.17	-102	3.1	-63	3.12	-60	3.29	-80	3	-60	2.85	-1	3.21	-50
	2.76	15	3.09	-78	3	-14	3	-19	3.15	-6	2.89	-32	2.82	4	3.17	-35
	2.66	48	2.97	-17	2.88	45	2.88	9	3.08	14	2.83	-12	2.66	46	3.1	0
	2.43	118	2.88	7	2.78	69	2.77	27	3.05	63	2.79	0	2.75	29	3.07	8
	2.31	139	2.78	50	2.69	115	2.67	52	2.92	82	2.77	5			3.06	19
			2.73	61	2.67	128	2.59	79	2.85	102	2.72	20			3.02	32
			2.7	77							2.64	45			2.99	47
											2.58	70			2.86	95
IEP	2.81		2.93		2.95		2.94		3.10		2.81		2.83		3.14	
σ	0.13															
IEP	2.94 ± 0.13															

IEP of TM pre-treated with 0.1 mole/L NaOH

	pH	0.5(hr)	pH	1.5(hr)	pH	3.0(hr)	pH	4.5(hr)	pH	7.5(hr)	pH	25(hr)	pH	3(day)	pH	17(day)
	4.23	-210	3.56	-206	3.48	-189	3.87	-269	3.69	-129	3.36	-102	3.28	-138	3.18	-165
	4.12	-174	3.48	-169	3.27	-106	3.37	-58	3.52	-109	3.16	-37	3.11	-73	3.08	-116
	3.56	-58	3.27	-74	3.2	-92	3.27	-35	3.47	-86	3.04	-2	3.03	-46	3.01	-84
	3.21	-22	3.11	-5	3.1	-50	3.19	-14	3.38	-47	2.98	0	2.91	-20	2.95	-44
	3.03	15	3.03	6	3.03	-9	3.09	14	3.19	8	2.94	6	2.89	-8	2.9	-19
	2.94	27	3.01	16	2.97	22	3	42	3.14	20	2.89	15	2.85	8	2.86	0
	2.79	84	2.83	70	2.86	67	2.98	82	2.88	125	2.83	40	2.77	25	2.84	14
			2.72	109	2.7	117	2.83	125			2.77	50	2.72	50	2.81	40
					2.62	128					2.71	78	2.59	81	2.76	66
															2.73	88
IEP	3.18		3.07		3.00		3.10		3.21		2.98		2.87		2.86	
σ	0.13															
IEP	3.03 ± 0.13															

IEP of TM pre-treated with 0.01 mole/L NaOH

	pH	0.5(hr)	pH	1.5(hr)	pH	3(hr)	pH	4.5(hr)	pH	7.5(hr)	pH	25(hr)	pH	3(day)	pH	17(day)
	3.91	-278	4.32	-197	3.73	-140	3.72	-124	3.9	-88	3.62	-82	3.75	-131	3.09	-94
	3.72	-162	3.82	-102	3.58	-83	3.57	-74	3.28	-39	3.46	-47	3.53	-66	3.02	-69
	3.56	-98	3.52	-47	3.37	-25	3.44	-33	3.22	-17	3.27	-18	3.18	-25	2.97	-27
	3.34	-1	3.37	-9	3.35	-1	3.35	-12	3.21	-3	3.2	-2	3.16	22	2.92	-3
	3.32	11	3.29	0	3.3	15	3.3	12	3.19	0	3.16	5	3.05	61	2.89	8
	3.23	47	3.26	11	3.06	92	3.12	67	3.15	10	3.09	25	2.92	95	2.87	49
	3.1	115	3.04	73	3	106	3.04	86	3.03	29	3.04	49			2.79	82
	2.86	151	2.83	119	3.1	112	2.9	135	3	57	2.99	76				
IEP	3.33		3.29		3.35		3.34		3.19		3.18		3.17		2.91	
σ	0.15															
IEP	3.22±0.15															

Appendix: 3.5

IEP of TM pre-treated with acid *(see Section 3.3.4)*

IEP of TM pre-treated with 1.0 mole/L HCl

	pH	0.5(hr)	pH	1.5(hr)	pH	3(hr)	pH	4.5(hr)	pH	7.5(hr)	pH	25(hr)	pH	3(day)	pH	10(day)	pH	17(day)
	4.54	-216	4.45	-235	4.57	-192	4.28	-155	4.87	-100	4.57	-86	4.67	-104	6.19	-71	3.08	-76
	4.33	-152	4.22	-159	4.22	-72	3.99	-80	4.75	-75	4.38	-54	4.61	-76	6.13	-53	3.02	-43
	4.14	-100	3.9	-93	3.97	-22	3.8	-18	4.73	-59	4.15	-28	4.56	-62	6.07	-32	2.95	-9
	3.91	-39	3.7	-23	3.9	10	3.72	13	4.33	5	3.94	4	4.43	-29	5.98	-6	2.92	3
	3.85	-4	3.56	1	3.87	20	3.6	49	4.02	22	3.81	17	4.27	4	5.91	2	2.87	37
	3.72	17	3.4	62	3.74	73	3.48	94	3.82	50	3.62	38	4.13	47	5.8	19	2.81	75
	3.63	57	3.34	91	3.64	167	3.32	141	3.62	67	3.47	66	4.1	60	5.68	63	2.79	98
	3.52	93	3.3	134	3.33	197			3.07	170	3.23	126	3.93	92				
	3.41	184							2.86	219	3.11	169	3.94	120				
	3.21	275																
IEP	3.79		3.57		3.94		3.76		4.58		4.02		4.39		5.96		2.94	
σ	0.50																	
IEP	3.87 ± 0.50																	

IEP of TM pre-treated with 0.1 mole/L HCl

	pH	0.5(hr)	pH	1.5(hr)	pH	3(hr)	pH	4.5(hr)	pH	7.5(hr)	pH	25(hr)	pH	3(day)	pH	10(day)	pH	17(day)
	3.78	-231	3.79	-114	4	-173	4.02	-162	4.02	-162	3.43	-116	3.61	-118	4.45	-156	3.04	-94
	3.62	-108	3.64	-75	3.65	-34	3.73	-64	3.81	-78	3.31	-75	2.94	-79	4.21	-87	2.97	-46
	3.5	-72	3.45	-28	3.63	-20	3.66	-42	3.69	-25	3.23	-56	2.79	-27	4.07	-42	2.89	-5
	3.44	-13	3.47	5	3.6	-8	3.55	13	3.54	0	3.12	-3	2.76	-19	4.01	-13	2.83	23
	3.37	-2	3.49	15	3.46	1	3.49	40	3.5	18	3.07	1	2.72	0	3.95	6	2.78	55
	3.35	7	3.45	67	3.51	18	3.31	93	3.45	58	3.02	17	2.71	4	3.91	18	2.71	92
	3.32	27	3.33	88	3.48	42	3.24	124	3.38	107	3	34	2.66	13	3.68	72	2.66	108
	3.27	54	3.29	107	3.31	118			3.28	133	2.93	72	2.6	25	3.6	93		
	3.2	88	3.2	212	3.25	126					2.82	112	2.59	57	3.54	108		
	3.16	108											2.54	64				
	3	182																
IEP	3.36		3.46		3.47		3.61		3.54		3.08		2.72		3.97		2.85	
σ	0.36																	
IEP	3.32 ± 0.36																	

IEP of TM pre-treated with 0.01 mole/L HCl

	pH	0.5hr	pH	1.5hr	pH	3hr	pH	4.5hr	pH	7.5hr	pH	25hr	pH	3day	pH	10day	pH	17day
	3.67	-245	3.99	-201	3.78	-135	3.78	-156	3.6	-145	3.35	-108	3.34	-82	4	-97	2.98	-78
	3.57	-181	3.97	-124	3.67	-93	3.7	-100	3.55	-89	3.25	-73	3.2	-53	3.92	-71	2.92	-33
	3.41	-80	3.74	-53	3.57	-51	3.52	-46	3.52	-37	3.2	-39	3.1	-17	3.75	-11	2.88	-6
	3.32	-39	3.64	-17	3.45	-12	3.47	-15	3.44	-4	3.18	-12	3.04	2	3.65	11	2.85	14
	3.31	-12	3.59	-5	3.37	-1	3.46	-2	3.35	31	3.09	8	2.95	23	3.4	66	2.78	52
	3.25	2	3.51	12	3.33	13	3.38	15	3.28	67	3.04	19	2.98	50	3.39	94	2.74	79
	3.21	17	3.38	42	3.26	50	3.33	50	3.22	101	3.01	47	2.87	82	3.3	109		
	3.11	83	3.14	150	3.11	95	3.18	120	3.18	122	2.94	78	2.79	104				
	3.05	110	2.96	169	3.01	121	3.05	164			2.83	110						
	2.91	180																
IEP	3.29		3.54		3.36		3.46		3.40		3.12		3.07		3.70		3.86	
σ	0.25																	
IEP	3.39 ± 0.25																	

Appendix 3.5:

Crystal morphology of Al_{13} and Fe polymer

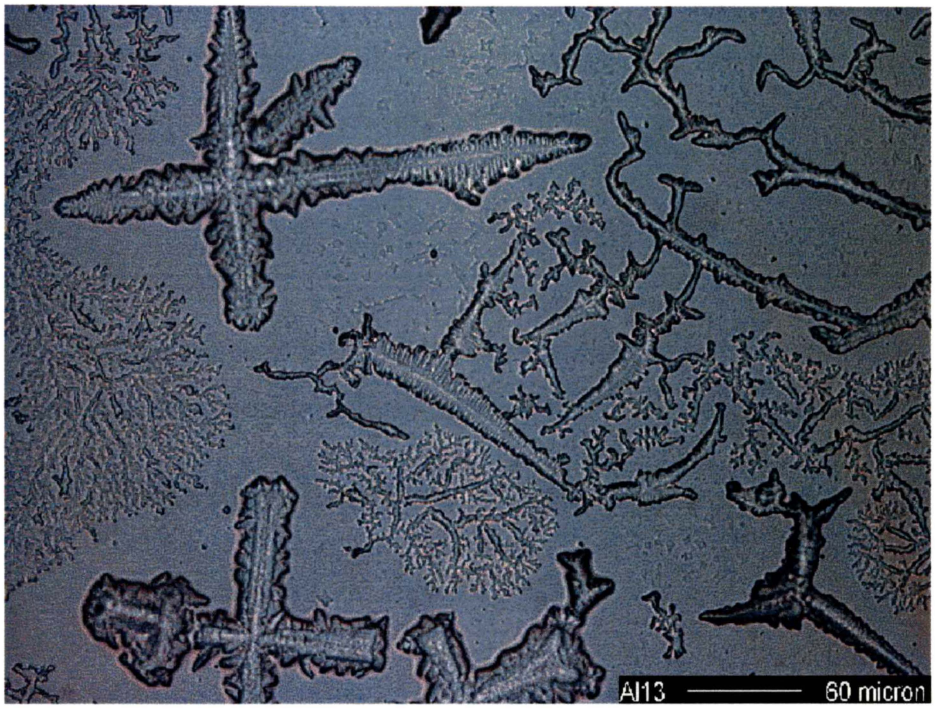

(a) Optical micrographs of crystalline phase of Al_{13}

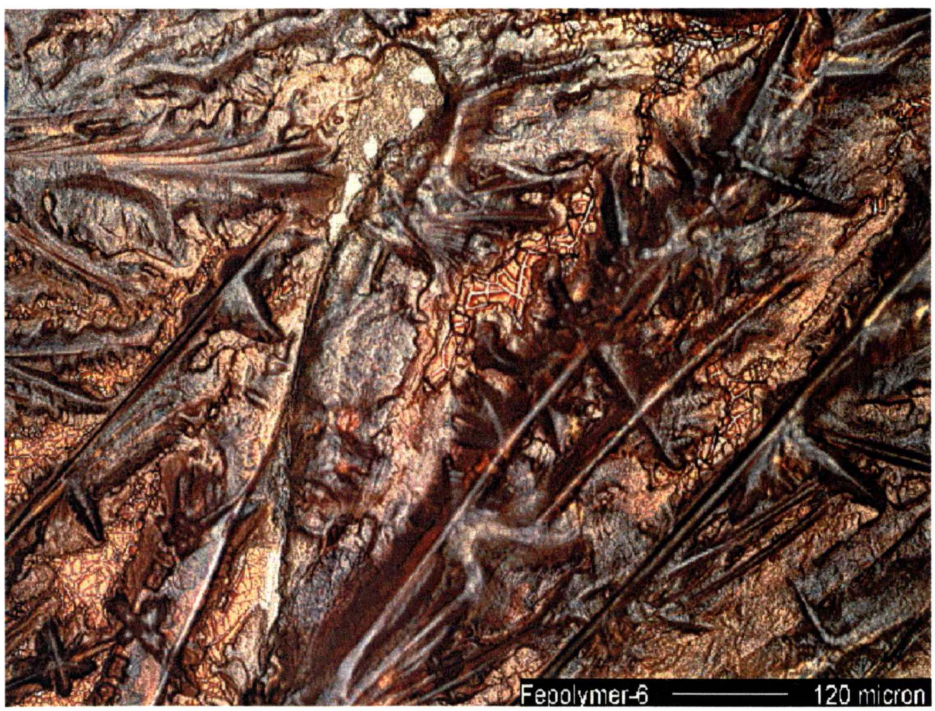

(b) Optical micrographs of crystalline phase of Fe polymer

Appendix 4.1

Hydraulic conductivity of expanded beds predicted by Kozeny equation

When a magnetic field was applied, the bed was expanded and the porosity was increased. For the naturally packed bed, porosity n:

$$n = \frac{U_{\exp} - U_b}{U_b} = 0.5$$

where U_{exp} is the volume of the bed; U_b is bulk volume of the medium, U_b = weight of sample/true density = 38.85/3.81 = 10.10 (cm^3) (see Section 2.9).

From Kozeny's equation (4.8) and (4.2), hydraulic conductivity is given by:

$$K = kg / v = \tfrac{1}{9} c_o T.[n^3 / (1-n)^2] r^2 g / v$$

or

$$K = C[n_0{}^3 / (1-n_o)^2],$$

where $C = \tfrac{1}{9} c_o T r^2 g / v$.

For naturally packed TM (0% bed expansion), the value of C = 6.40 was obtained allowing calculation of K value from Equation (4.8). Data are summarised in Table A4.1.

Table A4.1 Comparison of experimental and calculated (Kozeny Equation) hydraulic conductivity for vertical and horizontal magnetically conditioned TM beds (see Section 4.3.3).

Vertical field					Horizontal field				
Bed expansion %	U_{exp} x10^6 (m^3)	n	Kx10^4 (m/s)	K_{cal} x10^4 (m/s)	Bed expansion %	U_{exp} x10^6 (m^3)	n	Kx10^4 (m/s)	K_{cal} x10^4 (m/s)
0	20.34	0.50	3.2	3.2	0	20.34	0.50	3.2	3.20
7	21.70	0.53	4.6	4.3	2	20.80	0.51	3.4	3.52
12	22.60	0.55	5.3	5.3	4	21.25	0.52	3.4	3.90
15	23.50	0.57	6.2	6.4	6	21.70	0.53	3.5	4.29
17	23.96	0.58	6.7	7.1	13	23.06	0.56	3.5	5.82
24	25.31	0.60	6.9	8.6	18	23.96	0.58	3.6	7.10
28	26.22	0.61	7.7	9.5					

Appendix 5.1:

XRD data for β-Al(OH)$_3$ and SiO$_2$

12-0457 — Wavelength= 1.5418

β-Al(OH)3

Aluminum Hydroxide

Bayerite

Rad.: CuKa λ: 1.5418 Filter: Ni Beta.M d-sp: Diffractometer

Cut off: Int.: Diffract. I/Icor.:

Ref: Stumpf, H., Research Laboratories, Aluminum Co. of America, New Kensington, PA, USA, Private Communication

Sys.: Hexagonal S.G.:

a: 5.01 b: c: 4.69 A: C: 0.9361

α: β: γ: Z: 2 mp: 150

Ref: Ibid.

Dx: 2.541 Dm: 2.530 SS/FOM: F_{14}=9(.105, 15)

Color: Colorless
Sample precipitated from sodium aluminate solution at 40 C by saturating the solution with C 02. Reference reports: a=5.04, c=4.72, Dx=2.49. Deleted by Revision. Mwt: 78.00. Volume[CD]: 101.95.

d Å	Int	h	k	l
4.72000	100	0	0	1
4.36000	70	1	0	0
3.19000	25	1	0	1
3.08000	2			
2.69000	4			
2.45000	4			
2.34000	6	0	0	2
2.28000	4			
2.21000	65	1	1	1
2.14000	4			
2.06000	2	1	0	2
1.97000	4	2	0	1
1.91000	2			
1.83000	2			
1.76000	2			
1.71000	25	1	1	2
1.68000	2			
1.64000	2	2	1	0
1.59000	4	2	0	2
1.56000	2	0	0	3
1.55000	4	2	1	1
1.52000	2			
1.48000	2	1	0	3
1.47000	2			
1.45000	8	3	0	0

39-1425 — Wavelength= 1.5405981

SiO2

Silicon Oxide

Cristobalite, syn

Rad.: CuKa1 λ: 1.5405 Filter: Graph Mono. d-sp: Diffractometer

Cut off: 17.7 Int.: Diffract. I/Icor.:

Ref: Wong-Ng, W., McMurdie, H., Paretzkin, B., Hubbard, C., Dragoo, A., NBS (USA), ICDD Grant-in-Aid, (1988)

Sys.: Tetragonal S.G.: $P4_12_12$ (92)

a: 4.9732(4) b: c: 6.9236(8) A: C: 1.3922

α: β: γ: Z: 4 mp:

Ref: Wong-Ng, W et al., Powder Diffraction, 3, 253 (1988)

Dx: 2.331 Dm: SS/FOM: F_{30}=84(.0100, 36)

Color: Colorless
The temperature was ~25 C. Cristobalite was prepared by the Trans Tech Company using Berkeley 5 micron MIN-U-SIL(R). A two kilogram sample was heated at 1600 C for eight hours. The sample was then air quenched, treated with 6N HCl and then jet-milled. The +325 mesh fraction was then removed by sieving. There are a number of other forms of Si 02. The structure was determined by Peacor (1). 02 Si type. Tungsten, fluorophlogopite used as an internal stands. PSC: tP12. To replace 11-695 and validated by calculated pattern. Mwt: 60.08. Volume[CD]: 171.24.

d Å	Int	h	k	l	d Å	Int	h	k	l
4.03974	100	1	0	1	1.22375	<1	4	0	1
3.51470	<1	1	1	0	1.20599	1	4	1	0
3.13592	8	1	1	1	1.18427	1	3	2	3
2.84116	9	1	0	2	1.17576	<1	2	1	5
2.48740	13	2	0	0	1.16384	<1	3	1	4
2.46750	4	1	1	2	1.15546	<1	3	3	1
2.34170	<1	2	0	1	1.11050	<1	3	3	2
2.11791	2	2	1	1	1.09783	1	4	2	1
2.01957	2	2	0	2	1.09628	1	1	1	6
1.92935	4	1	1	3					
1.87147	4	2	1	2					
1.75907	<1	2	2	0					
1.73033	<1	0	0	4					
1.69221	2	2	0	3					
1.63488	<1	1	0	4					
1.61217	3	3	0	1					
1.60131	1	2	1	3					
1.57207	<1	3	1	0					
1.56745	<1	2	2	2					
1.53356	2	3	1	1					
1.49520	2	3	0	2					
1.43165	2	3	1	2					
1.42102	1	2	0	4					
1.39908	1	2	2	3					
1.36560	2	2	1	4					
1.35277	<1	3	2	1					
1.34650	<1	3	0	3					
1.33398	1	1	0	5					
1.29976	1	3	1	3					
1.28133	1	3	2	2					
1.23318	<1	2	2	4					

Appendix 5.2:

XRD data for FeO(OH) and Fe_3O_4

34-1266 — Wavelength= 1.7902

FeO(OH)

Iron Oxide Hydroxide

Akaganeite-M, syn

Rad.: CoKa λ: 1.7902 Filter: Graph Mono. d-sp: Diffractometer

Cut off: Int.: Diffract. I/Icor.:

Ref: Murad, E., Clay Miner., 14, 273 (1979)

Sys.: Tetragonal S.G.: I4/m (87)

a: 10.535 b: c: 3.030 A: C: 0.2876

α: β: γ: Z: 8 mp:

Ref: Ibid.

Dx: 3.510 Dm: SS/FOM: F_{24}=47(.0196, 26)

A 0.1M Fe Cl3 solution was heated to 60 C for 8 days. The precipitate was separated by centrifuging, washed with H2 O and dried at 40 C. Cryptomelane group, tetragonal subgroup. PSC: tI32. To replace 13-157. Mwt: 88.85. Volume[CD]: 336.29.

d Å	Int	h	k	l
7.46700	40	1	1	0
5.27600	30	2	0	0
3.72800	5	2	2	0
3.33300	100	3	1	0
2.63440	25	4	0	0
2.55020	55	2	1	1
2.48300	2	3	3	0
2.35590	9	4	2	0
2.29520	35	3	0	1
2.10380	7	3	2	1
2.06660	7	5	1	0
1.95400	20	4	1	1
1.86240	4	4	4	0
1.80720	<1	5	3	0
1.75570	15	6	0	0
1.72990	3	4	3	1
1.66580	<1	6	2	0
1.64340	35	5	2	1
1.51550	9	0	0	2
1.50340	5	6	1	1
1.48960	3	7	1	0
1.48520	3	1	1	2
1.45770	1	2	0	2
1.44560	15	5	4	1

11-0614 — Wavelength= 1.7902

Fe3O4

Iron Oxide

Magnetite

Rad.: CoKa λ: 1.7902 Filter: Fe Beta.M d-sp: 114.6

Cut off: Int.: Estimation I/Icor.:

Ref: Basta, Mineral. Mag., 31, 431 (1957)

Sys.: Cubic S.G.: Fd3m (227)

a: 8.3963 b: c: A: C:

α: β: γ: Z: 8 mp:

Ref: Ibid.

Dx: 5.196 Dm: SS/FOM: F_{21}=11(.071, 27)

εα: nωβ: 2.42 εγ: Sign: 2V:

Ref: Ibid.

Color: Black
Pattern taken at 18 C. Specimen from Bisperg, Sater, Sweden.
PSC: cF56. Deleted by 19-629. Mwt: 231.54. Volume[CD]:
591.92.

d Å	Int	h	k	l
4.85000	40	1	1	1
2.96600	70	2	2	0
2.53000	100	3	1	1
2.41900	10	2	2	2
2.09600	70	4	0	0
1.71200	60	4	2	2
1.61400	85	5	1	1
1.48300	85	4	4	0
1.32700	20	6	2	0
1.27900	30	5	3	3
1.26400	10	6	2	2
1.21120	20	4	4	4
1.12140	30	6	4	2
1.09220	60	7	3	1
1.04890	40	8	0	0
.989000	10	6	6	0
.969200	40	7	5	1
.938600	30	8	4	0
.879400	40	9	3	1
.856500	50	8	4	4
.811300	40	9	5	1

Appendix 5.3:

3 point BET of ARSS for coated with aluminium

Materials	Target relative pressure (P/P_0)	Actual relative pressure (P/P_0)	Total volume adsorbed (cc/g)	BET transform $1/(w[P_0/P-1])$	Specific surface area m^2/g)
ARSS	0.10	0.09	0.97	88.56	3.93
	0.20	0.21	1.15	181.53	
	0.30	0.31	1.30	277.14	
S_{al-1}	0.10	0.10	0.69	129.11	2.72
	0.20	0.20	0.79	259.13	
	0.30	0.31	0.90	394.78	
S_{al-3}	0.10	0.10	0.71	125.33	2.87
	0.20	0.21	0.83	249.37	
	0.30	0.31	0.95	376.16	
S_{al-5}	0.10	0.09	0.71	118.46	2.89
	0.20	0.20	0.83	241.23	
	0.30	0.30	0.94	364.74	
S_{al-7}	0.10	0.09	0.83	100.03	3.41
	0.20	0.20	0.98	207.95	
	0.30	0.31	1.11	315.94	
S_{al-9}	0.10	0.09	1.51	55.54	6.03
	0.20	0.19	1.74	112.53	
	0.30	0.29	1.96	171.61	
$S_{Al-pH-5.37}$	0.10	0.09	0.36	227.92	1.55
	0.20	0.19	0.43	458.60	
	0.30	0.29	0.49	681.42	
$S_{Al-pH-6.33}$	0.10	0.10	0.50	179.54	2.14
	0.20	0.21	0.60	348.33	
	0.30	0.31	0.70	516.33	
$S_{Al-pH-7.44}$	0.10	0.10	0.53	169.61	2.25
	0.20	0.21	0.63	330.05	
	0.30	0.31	0.73	490.17	
$S_{Al-pH-8.13}$	0.10	0.09	0.81	106.05	3.37
	0.20	0.21	0.96	218.16	
	0.30	0.31	1.11	329.44	
$S_{Al-pH-9.11}$	0.10	0.10	0.61	145.90	2.46
	0.20	0.21	0.71	291.46	
	0.30	0.31	0.81	442.01	

BJH pore size distribution and total pore volume

Materials	Pore radios (angstrom)	Pore volume (cc/g)	Pore area (m^2/g)	Total volume adsorbed (cc/g)
ARSS	12.59 9.96	6.95 E-04 7.53 E-04	1.10 E+00 1.52 E+00	1.30
S_{al-1}	12.54 9.99	4.69 E-04 4.62 E-04	7.48 E-01 9.24 E-01	0.90
S_{al-3}	12.53 9.98	5.32 E-04 5.19 E-04	8.48 E-01 1.04 E+00	0.94
S_{al-5}	12.37 9.86	5.12 E-04 5.38 E-04	8.27 E-01 1.09 E+00	0.94
S_{al-7}	12.49 9.89	6.15 E-04 6.67 E-04	9.85 E-01 1.35 E+00	1.11
S_{al-9}	12.27 9.81	1.00 E-03 1.06 E-03	1.63 E+00 2.17 E+00	1.96
$S_{Al-pH-5.37}$	12.30 9.82	2.97 E-04 3.08 E-04	4.83 E-01 6.28 E-01	0.49
$S_{Al-pH-6.33}$	12.61 10.03	4.38 E-04 4.27 E-04	6.95 E-01 8.51 E-01	0.70
$S_{Al-pH-7.44}$	12.62 10.03	4.59 E-04 4.45 E-04	7.27 E-01 8.87 E-01	0.73
$S_{Al-pH-8.13}$	12.67 9.98	6.48 E-04 7.00 E-04	1.02 E+00 1.40 E+00	1.11
$S_{Al-pH-9.11}$	12.59 10.01	4.42 E-04 4.60 E-04	7.02 E-01 9.20 E-01	0.81

Appendix 6.1

Crystal morphology of Fe(III)/Al(III)=1:9 and Al(III)/Fe(III)/Fe(II)=2:2:1

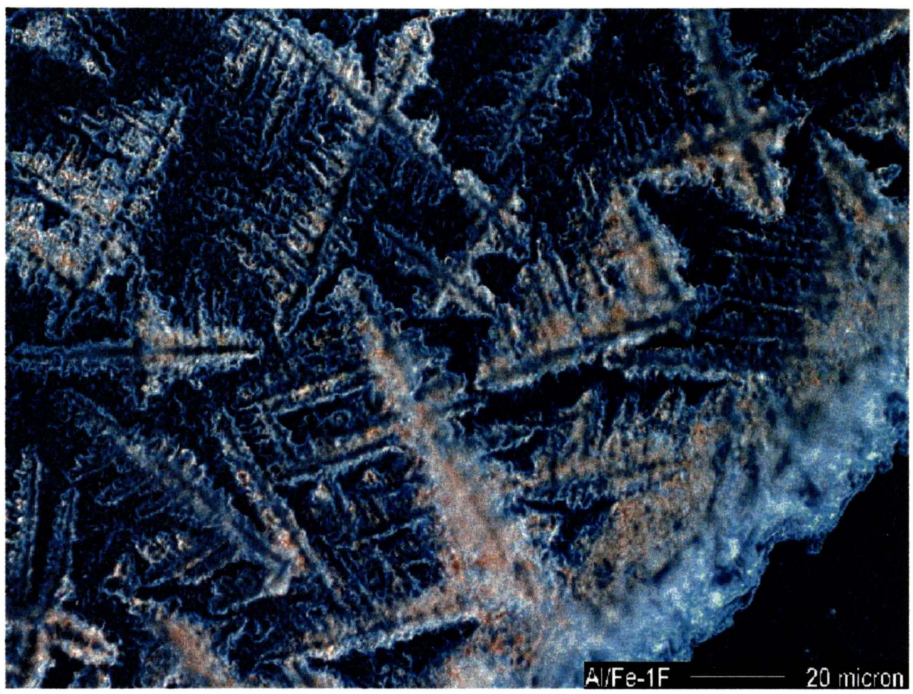

(a) Optical micrographs of crystalline phase of Fe(III)/Al(III) = 1:9

(b) Optical micrographs of crystalline phase of Al(III)/Fe(III)/Fe(II) = 2:2:1